Università degli Studi di Cagliari

DOTTORATO DI RICERCA

In Ingegneria Elettronica ed informatica

Ciclo XXVI

TITOLO TESI

PRINTED LOG-PERIODIC FEEDS FOR RADAR APPLICATIONS

Settore/i scientifico disciplinari di afferenza

ING-INF/02 Campi Elettromagnetici

Presentata da: Paolo Maxia

Coordinatore Dottorato Prof. Fabio Roli

Tutor/Relatore Prof. G. Andrea Casula.

Esame finale anno accademico 2012 – 2013


Ph. D. in Electronic Engineering and Computer Science
Dept. of Electrical and Electronic Engineering
University of Cagliari, Sardinia, Italy

Printed Log periodic Feeds for RADAR Applications.

Paolo Maxia

Advisor: Prof. G. Andrea Casula.
Curriculum: ING-INF/02 Campi Elettromagnetici.

XXVI Cycle.
April 2014.

To the memory of my parents,
Giuseppe and Marina,
and my uncles Piero and Piera.


Acknowledgment

Special thanks to Sardinia Regional Government for the financial support of my PhD scholarship (P.O.R. Sardegna F.S.E. Operational Programme of the Autonomous Region of Sardinia, European Social Fund 2007-2013 - Axis IV Human Resources, Objective l.3, Line of Activity l.3.1.)".

I apologize if the remainig row are in italian, but i prefer to thank everyone in their native language so...procediamo con ordine e permettetemi prima di tutto, di ringraziare (e anche se glielo dico sempre...ora lo scrivo pure, perchè, come dicevano i latini "scripta manent") il mio tutor Andrea, che in questi tre anni è stato prodigo di consigli e di suggerimenti e che mi è stato vicino tutte le volte che c'è stato bisogno della sua esperienza e competenza: GRAZIE DI CUORE! Grazie per l'opportunità che mi è stata concessa, grazie perchè se cinque anni fa qualcuno mi avesse detto che avrei scritto una tesi di dottorato...gli avrei dato del pazzo furioso. Ma, si sa, il "sacro fuoco della ricerca" è una malattia contagiosa...e io ne sono diventato un malato cronico fin da quando ne ho mostrato i primi sintomi (durante la stesura della tesi di laurea, nel lontano 2009). Non dimenticherò mai questi 3 anni e i nostri colloqui di lavoro, che, inevitabilmente finivano, dopo aver tracciato il "cosa" fare e soprattutto il "come" fare, in risate. Grazie perchè ad ogni conferenza, dopo ogni presentazione effettuata, puntualmente squillava il telefono e dall'altra parte della cornetta si sentiva la rassicurante frase "beh? come è andata? Fatto?".

Grazie a Giuseppe per tutte le volte (infinite...non ricordo quante) che l'ho disturbato (anche agli orari più improponibili, tipicamente...all'ora di pranzo) chiedendogli una mano per la risoluzione di questioni spinose: 5 minuti a colloquio con lui sono assimilabili a una settimana di studio matto e disperatissimo...con la differenza che nell'ultimo caso, non sempre si riesce ad arrivare ad una soluzione del problema.

Grazie a Giorgio, ricorderò sempre il suo rigore scientifico e i suoi rimproveri per tutte le volte che (a ragione) le cose non erano fatte nel giusto modo.

Grazie ad Alessandro, collega di stanza, sempre disponibile per qualsiasi cosa: se ho imparato a destreggiarmi con la burocrazia che, ahimè, affligge anche il mondo della ricerca, lo devo a lui. In questi tre anni abbiamo parlato di tutto e ci siamo tenuti compagnia durante le lunghe, lunghissime giornate in attesa di un responso da parte del simulatore...finendo poi a lanciarci palline di carta (con buona pace degli esterrefatti tesisti presenti).

Grazie a Luisa, che mi è stata vicina durante le mie prime uscite internazionali, rincuorandomi ed incoraggiandomi riguardo i miei timori sulla lingua inglese.

UN GRAZIE ENORME a Francesco Gaudiomonte dell'osservatorio astronomico di Cagliari: grazie a lui ho imparato la profonda differenza tra il mondo delle simulazioni ed il mondo reale...non dimenticherò mai le cose apprese "sul campo" discorrendo con lui, e non dimenticherò mai la passeggiata sullo specchio primario del riflettore del Sardinian Radio Telescope di San Basilio, che è stata possibile grazie al suo interessamento.

Grazie infine a Gianluca, Fabrizio e a tutta la mia famiglia, in particolare mia Zia Piera, che purtroppo non potrà leggere queste righe, per tutte le volte che mi sono stati vicini in questi tre anni nei momenti di bisogno e di sconforto.

Grazie ancora a tutti...

Paolo Maxia.

Abstract.

Radar systems are well known since the end of world war II and are widespread.

The basic concept of radar is relatively simple: the system uses the propagation characteristics of electromagnetic waves and works by radiating electromagnetic energy in the space and detecting the echo reflected by the objects (named “target”). The information related to the target is available in the echo signal: the range, or distance, to the target is found from the time it takes for the radiated energy to travel to the target and back; the angular location is detected using narrow beam width directive antennas (i.e. reflector antennas). The ability to discern about the nature and size of the target depends on the radar resolution which is related to the bandwidth and to the electrical size of the antenna.

The physical principles of radar are suitable also to the weather radars, used to detect the precipitations at long distance, where the "object of interest” (the target) are the particles of rain and clouds. The detection of these objects involves radar operating at multiple frequencies located in S and C bands, where the wavelength (from 15 to 3.75 centimeters) is comparable to the size of hydrometeors.

Radar systems use directive antennas, such as mechanically steered parabolic reflector antennas and planar phased arrays. Aim of these antennas is to concentrate the energy in a narrow beam width of about 1° or 2°. This characteristic not only concentrates the energy on the target itself, but also permits a measure of its direction.

In this work we have studied the substitution of reflector horn feeds with printed log-periodic planar feeds in order to obtain the same performance of the horn antennas, but with considerable advantages in terms of weight and cost. The design of log-periodic feeds has been focused on the feed antenna network, and their possible improvements with respect to the state-of-the-art.

In the first chapter, a general description of radar systems is given, introducing the Probert-Jones equation for meteorological target. The second and third chapter provide a brief description of antennas concepts and an introduction to reflector antennas.

The chapter four is fully dedicated to reflector horn antennas and printed microstrip feed with a brief description of the state-of-art.

Finally, in chapter five, three printed log-periodic feed for reflector antennas are presented. The first structure is a printed log-periodic array (LPDA) operating over the C, X and Ku bands. The antenna feeding structure consist of two coaxial cables, in order to realize an infinite balun which provides the required broadband input matching. The second coaxial cable mirrors the first one, connected to

the antenna input, and is capable of both stabilizing the antenna phase center and improving the radiation pattern. Both the simulated and measured results have show that the LPDA can be successfully user as a wide band feed for reflector antennas.

The second feed consists of a LPDA operating between 3 and 6 GHz, and fed with a coplanar waveguide. The structure has been designed starting from Carrel's theory, optimized using CST MICROWAVE STUDIO 2012 and then realized. The comparison between simulated and measured results shows that the proposed antenna can be used as feed for reflector broadband applications in the whole operating frequency band, with a very good input matching and a satisfactory endfire radiation pattern.

The results obtained with these two printed LPDA provided the starting point for the design of a high gain "V-shaped" log-periodic feed for weather radar applications, operating in S and C band and fed by the dual coaxial cable configuration. The developed feed provides very good input matching and a symmetric radiation pattern both in E-plane and H-plane, with a reasonable gain over the whole operating bandwidth. This feed may be recommended for usage in weather radar systems having a transmitting power less than 400 KW, allowing a discrete operational range.

Contents

Chapter 1.

Radar Systems

1.1 Introduction [3].

The basic concept of radar is relatively simple: the system uses the propagation characteristics of electromagnetic waves and works by radiating electromagnetic energy in the space and detecting the echo reflected by the objects (named "target").

The information related to the target is available in the echo signal: the range, or distance, to the target is found from the time it takes for the radiated energy to travel to the target and back; the angular location is detected using narrow beam width directive antennas. The ability to discern about the nature and size of the target depends by the radar resolution which is related to the bandwidth and to the electrical size of the antenna. The radar is an active device, able to detect electrically small objects at near or far distances, and, unlike the optical and infrared sensors, it does not depends on the weather conditions.

From an historic point of view, the first radar types were bi-static devices with two different antennas: one transmitting the signal in the surrounding space and the other one receiving the echo from the target. The distinction between receiving and transmitting antenna was overcome with the mono-static radars, where the same antenna works both in transmitting and receiving mode: for this reason, the mono-static radar system is equipped with a decoupling and protection system which processes the received and transmitted signals.

The various parts of a radar system are shown in figure 1.1: the duplexer is the device which allows to employ a single antenna both in transmission and reception. The emitted radar signal is usually a repetitive train of short pulses radiated into surrounding space by the antenna.

Reflecting objects (the targets) intercept and re-radiate a portion of the radar signal, a small amount of which is returned in the direction of the transmitting

station. The returned echo signal is collected by the radar antenna and amplified by the receiver, that allows also to “clean” the received signal by the noise. Afterwards, the output of the receiver is electronically processed in order to automatically recognize the presence of targets.

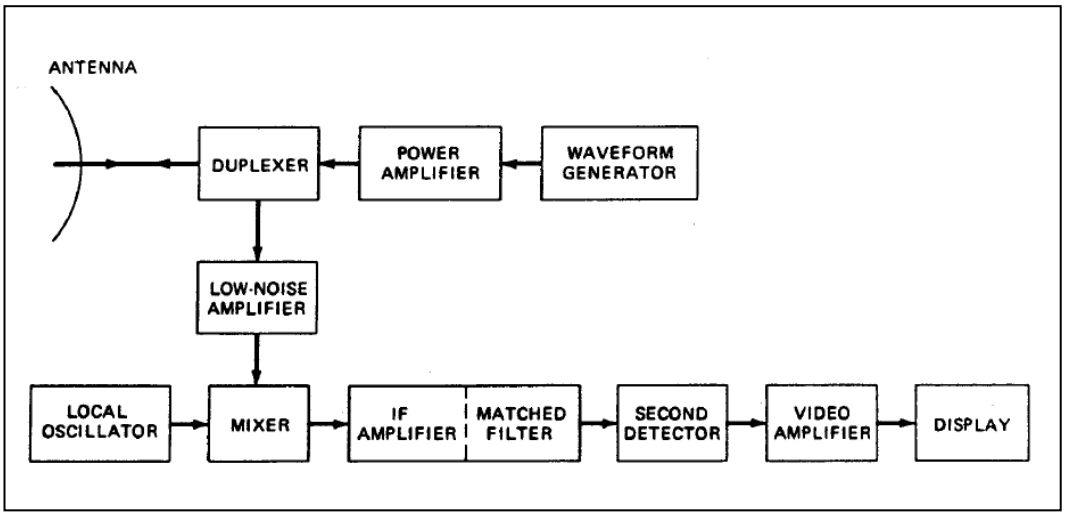

Figure 1.1. *Radar block diagram. [3]*

A radar generally determines the location of a target in range and angle (2D radars), and the echo signal can provide information about the nature of the target.

The output power coming from the transmitter is radiated into space by a directive antenna: mechanically steered parabolic reflector antennas and planar phased arrays both find wide application in radar systems. Aim of the antenna is to concentrate the energy in a narrow beam width of about 1° or 2°. This characteristic not only concentrates the energy on the target itself, but also permits a measure of its direction.

The shape of the radiated beam (figure 1.2) depends on the type of radar: tracking radars are characterized by a pencil beam, air surveillance radars have instead a fan-shaped beam generated by mechanically rotating reflector antennas.

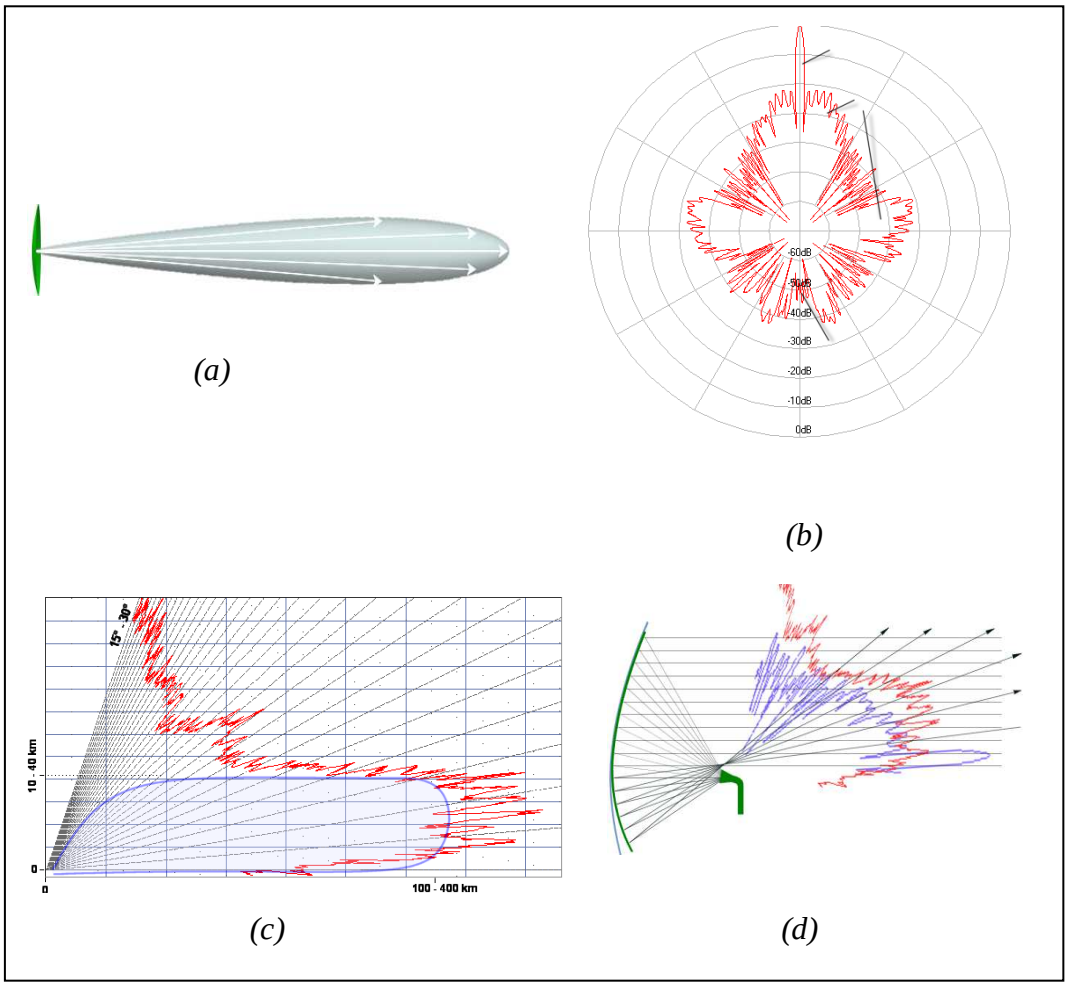

Figure 1.2*. (a) Parabolic antenna radiation pattern, (b) Horizontal cross section of a real measured radiation pattern of a parabolic antenna in logarithmic scale, (c) Air surveillance radar radiation pattern, (d) reflector antenna for air surveillance radar [5].*

Although it is possible to employ antennas with mechanical movement both in elevation and rotation, most of widespread civilian air surveillance radars (primary radars) can detect the azimuth and range coordinates only. The acquisition of the target's height (elevation angle) is performed by a secondary system (named "secondary surveillance radar") which operates jointly with the primary radar and involves the active cooperation of the target transponder.

In early radar systems, separate height finding antennas with mechanical rocking motion in elevation were used to determine the third coordinate: more recent three-dimensional (3D) military radars use a single antenna to detect all three coordinates (figure 1.3).

(a) *(b)*

***Figure 1.3**. (a) ASC-Signal 2D S-Band air surveillance radar, (b) BAE-Thales S1850M L-Band 3D air surveillance radar.*

The size of a radar antenna depends both on the frequency and on its location (on the ground or on a moving vehicle): at low frequencies, physically large antennas are easy to produce because the mechanical and electrical tolerances are proportional to the wavelength. In the UHF band, the dimensions of a large antenna may be of 30.5 meters or more, whereas in the upper frequencies (such as X band) an antenna of 3 or 6 meters is considered large.

Although there have been microwave antennas with beam widths as small as 0.05°, radar antennas rarely have beam widths less than about 0.2°.

1.2.Radar equation [1][3][8].

The performance of radar systems can be described by the radar equation: this expression allows to compute the range of a radar in terms of target characteristics, involved power levels, and antenna gain (for a more accurate description of the antenna parameters, see chapter 2).

Let us consider now a generic bi-static radar system: if P_T is the transmitting power and G_T is the gain of the transmitting antenna, the Poynting vector incident on a generic object, placed at distance R_T, is given by:

$$S_{object} = \frac{P_T G_T}{4\pi \cdot R_T^2} = S_O \tag{1.1}$$

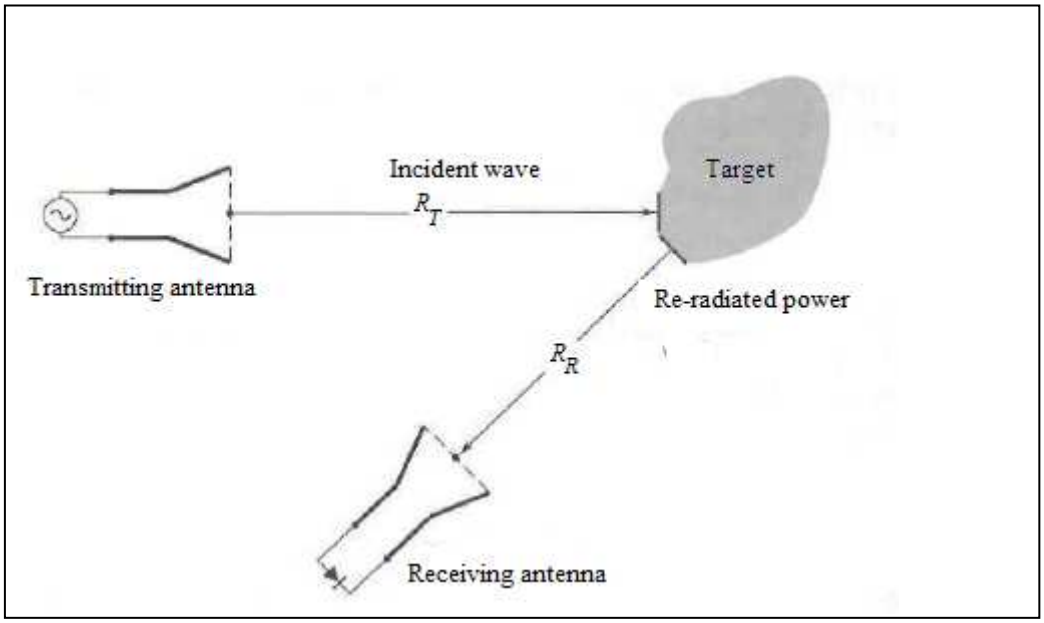

Figure 1.4*. Determination of radar equation [1].*

If the object is able to absorb and re-radiate the power in the surrounding space, using the expression (1.1) we have:

$$\begin{aligned} P_O &= A_O \cdot S_O \\ P_{OT} &= \eta_O \cdot P_O \end{aligned} \tag{1.2}$$

Where A_O is the effective area of the object, P_{OT} is the re-radiated power and η_O take into account the losses due to the power absorption by the object. If we consider a receiving antenna with effective area A_R placed at distance R_R from the object, the received power will be:

$$P_R = \frac{G_O P_{OT}}{4\pi \cdot R_R^2} \cdot A_R \tag{1.3}$$

Where G_O is the gain of the re-transmitting object.
In order to take into account the effects due to de-polarization of the receiving and transmitting antennas, the previous expressions (1.2) can be rewritten as:

$$\begin{aligned} P_O &= A_o^{p_T} \cdot S_O \\ P_R &= \frac{G_O^{p_R} \cdot P_{OT}}{4\pi \cdot R_R^2} \cdot A_R \end{aligned} \tag{1.4}$$

Where $A_o^{p_T}$ is the effective area of object related to the polarization of transmitting antenna, and $G_o^{p_R}$ is related to the fraction of the power transmitted by the object in the polarization of the receiving antenna.
By substituting equations (1.4) into equation (1.3) we get:

$$P_R = P_T G_T \frac{1}{4\pi \cdot R_T^2} \cdot A_R \cdot \frac{1}{4\pi \cdot R_R^2} \cdot \underbrace{G_O^{p_R} \eta_o A_O^{p_T}}_{\alpha} \tag{1.5}$$

The term α is named “radar cross section” of the target and is strictly related to physical and electromagnetic properties of the object:

$$\sigma = G_O^{p_R} \eta_O A_O^{p_T} \tag{1.6}$$

Using the equation (1.6), the expression (1.5) becomes:

$$P_R = \frac{P_T G_T A_R}{4\pi \cdot R_T^2 R_R^2} \cdot \sigma \tag{1.7}$$

In the mono-static radar, where a single antenna works both in transmission and reception, taking into account the relations:

$$R_T = R_R = R$$
$$G_T = G_R = G$$
$$A_T = A_R = A$$

and $A=(\lambda^2/4\pi)G$, equation (1.7) can be rewritten as:

$$P_R = \frac{P_T G^2 \lambda^2}{(4\pi)^3 \cdot R^4} \cdot \sigma = \frac{P_T A^2}{4\pi \cdot \lambda^2 R^4} \cdot \sigma \tag{1.8}$$

From this equation, it is possible to compute the maximum radar range R_{MAX} as:

$$R_{MAX}^4 = \frac{P_T G^2 \lambda^2 \cdot \sigma}{(4\pi)^3 \cdot S_{MIN}} = \frac{P_T A^2 \cdot \sigma}{4\pi\lambda^2 \cdot S_{MIN}} \tag{1.9}$$

Where S_{MIN} is the receiver minimum detectable signal.

Despite these equations are simple to calculate once know the radar equation, the determination of the maximum range R_{MAX} is not immediate: as a matter of fact, expressions (1.9) are useful for a rough computation of the range performance and do not give realistic results. There are at least two major reasons why the simple

form of the radar equation does not predict with enough accuracy the range of actual radars: first, it does not include the various losses that can occur in a radar; second, the target radar cross section σ and the minimum detectable signal S_{MIN} are statistical in nature.

For present purposes, we will consider only the characteristics of S_{MIN}, which is a statistical quantity, and, to be reliably detected by the system, it must be 10 or 20 dB larger than noise. The minimum detectable signal can also be expressed as the signal-to-noise ratio required for reliable detection times the receiver noise which is related to the thermal noise produced by an ideal receiver.

In general, the thermal noise can be expressed as $K \cdot T \cdot B$, where K is the Boltzmann's constant, T is the temperature and B is the receiver bandwidth; taking into account these considerations, it is possible to express the receiver noise as the product of the thermal noise by the receiver noise figure F_N relative to a reference room temperature $T_0=290K$: at this temperature the product $K \cdot T_0$ is equal to $4*10^{-21}$ W/Hz. Therefore, the minimum detectable signal S_{MIN} can be written as:

$$S_{MIN} = KT_0 \cdot B \cdot F_n \cdot \frac{S}{N} \tag{1.10}$$

Sometimes, the factor T_0F_n is replaced with T_S, the system noise temperature. A more precise expression of (1.10) allow to express S_{MIN} as a function of the signal-to-noise energy ratio E/N_0. For a rectangular pulse of width τ, the signal power is E/τ, and the noise power is N_0B, where N_0 is the noise energy, and B is the receiver bandwidth. With these assumptions equation (1.10) becomes:

$$S_{MIN} = KT_0 \cdot F_n \cdot \frac{E}{N_0} \cdot \frac{1}{\tau} \tag{1.11}$$

By substituting into equation (1.9) we obtain:

$$R_{MAX}^4 = \frac{E_T G \cdot A \cdot \sigma}{(4\pi)^2 K T_0 F_n (E / N_0)} \tag{1.12}$$

Where $E_T = P_T \cdot \tau$ is the energy contained in the transmitted signal waveform. Equation (1.12) allow then to calculate the maximum range of a radar equipped with *A* effective area antenna illuminating a target with σ radar cross section.

In radar applications, where the tracking is the primary function, the previous equation becomes:

$$R_{MAX}^4 = \frac{P_{AV} t_0 \cdot G \cdot A \cdot \sigma}{(4\pi)^2 K T_0 F_n (E / N_0)} \tag{1.13}$$

In this expression t_0 is the interval of time where the radar tracks continuously the target, and $P_{AV} = E_T / t_0$ is the average power employed by the system.

Thus, a long range tracking radar requires high values of average power P_{AV}, high values of t_0 (time on target), and, independently of system frequency that does not enter explicitly in the determination of equation (1.13), the radar antenna must have both large electrical and physical size.

Since it is easier to mechanically move a small antenna than a large one, the tracking radars usually operate at high frequencies, in order to utilize small aperture antennas with high gain and adequate $G \cdot A$ product. Tracking radars are usually designed to obtain a good angular accuracy, which is achieved with antennas having a high gain G (narrow beam widths), and high values of ratio E / N_0 (large effective areas A).

1.3. Radar frequency bands [3].

According with the assertions of the previous paragraphs, any device which employs the electromagnetic energy to locate a target using the reflected echo can be considered a radar. From a generic point of view, there are no limitations regarding the operating frequency bands: historically, radar devices have been developed to operate at frequencies from a few megahertz up to a dozen of gigahertz.

The basic operating principles are the same at any frequency, even though the system implementation is widely different and depends on the frequency itself.

In table 1.1 a subdivision of electromagnetic spectrum according with the *standard radar frequency letter band nomenclature* is shown:

Band designation	Nominal frequency range	Specific frequency ranges for radar based on ITU assignments for Region 2
HF	3 MHz–30 MHz	
VHF	30 MHz–300 MHz	138 MHz–144 MHz
		216 MHz–225 MHz
UHF	300 MHz–1000 MHz	420 MHz–450 MHz
		890 MHz–942 MHz
L	1000 MHz–2000 MHz	1215 MHz–1400 MHz
S	2000 MHz–4000 MHz	2300 MHz–2500 MHz
		2700 MHz–3700 MHz
C	4000 MHz–8000 MHz	5250 MHz–5925 MHz
X	8000 MHz–12,000 MHz	8500 MHz–10,680 MHz
K_u	12.0 GHz–18 GHz	13.4 GHz–14.0 GHz
		15.7 GHz–17.7 GHz
K	18 GHz–27 GHz	24.05 GHz–24.25 GHz
K_a	27 GHz–40 GHz	33.4 GHz–36.0 GHz
V	40 GHz–75 GHz	59 GHz–64 GHz
W	75 GHz–110 GHz	76 GHz–81 GHz
		92 GHz–100 GHz
mm	110 GHz–300 GHz	126 GHz–142 GHz
		144 GHz–149 GHz
		231 GHz–235 GHz
		238 GHz–248 GHz

***Table 1.1**: Radar frequency bands. [3]*

This subdivision is universally employed in radar applications and derives from the code letters (P, L, X and K) born during World War II for secrecy purpose.

After the end of war, these designations remained and other letters were added to indicate new regions of the electromagnetic spectrum.

The letters are an useful way to specify the operating radar band without using the exact values of frequencies: this is an important practical feature, particularly in military applications.

In the third column of table 1.1, the specific radar frequencies allowed for ITU Region 2 (North and South America) are shown: as apparent, only a part of various bands is reserved for radar applications. In other ITU Regions (Region 1: Africa, Europe and North Asia; Region3: South Asia and Oceania) the distribution of radar frequencies is virtually the same.

HF Band (3 to 30 MHz).

Historically it was the first frequency band used in radar applications.

The air surveillance radar grid installed by Great Britain during the World War II operated at these frequencies.

Despite the achieved results, the radars working at HF band have several disadvantages. Since the antenna beam width is directly proportional to the wavelength, and inversely proportional to the size of antenna itself, in order to obtain a narrow radiated beam a HF radar antenna must be very large.

Furthermore, we have at least two other main problems related to HF band: first, the high level of noise due to the back ground affects the target detection capability of the system; second, some objects appear very small compared with the HF wavelength, and, with respect to microwave frequencies, their radar cross section might be reduced.

Currently, this frequency band is used only in the OTH (Over The Horizon) Radar: as a matter of fact, at these frequencies the refraction of the electromagnetic waves by the ionosphere allows to obtain ranges from 900 to 3500 kilometers, and to detect aircrafts and other targets beyond the horizon. This property makes of the HF region of spectrum quite attractive for the radar observation of areas not practical with a conventional microwave radar.

VHF Band (30 to 300 MHz).

The radars operating at this frequency band were developed during the years of World War II, and represented the best of first-generation radar systems until the advent of microwave radars.

Similar to shortwave radars (HF), the 30-300 MHz band allows to handling high transmitting power; for this reason, the operating features are similar to those described in HF systems: narrow radiated beam and large antennas.

In this frequency range, the performance is not affected by the reflections from rain and the techniques used to reduce the target radar cross section (stealth techniques) are quite ineffective.

As the HF band, a very interesting feature of these radar operating at relatively low frequencies is the possibility to increase the maximum range of detection up to twice: when a signal is transmitted with horizontal polarization over a good reflecting surface (such as the sea), the constructive interference between the direct and reflected wave from the surface can result in a substantial increase in the maximum range against aircraft.

The VHF band is a good frequency band for cheap radars and for long-range radars, such as those for the detection of satellites, but in spite of its many attractive features, there have not been many applications of radar in this frequency range because its limitations and the high external noise do not always counterbalance its advantages.

UHF band (300 to 1000 MHz).

Many features related to previous radars classes, such as the low impact of rain on the received signal, are suitable in the UHF band.

In these frequency ranges, however, the effects of thermal noise are weaker and it is possible to obtain radiated beam narrower than the VHF band.

The UHF band is useful to realize long distance surveillance radars with sufficiently large antennas, employable to detect extraterrestrial targets, such as spacecrafts and ballistic missiles.

L band (1 to 2 GHz).

The L band is mainly employed for the land-based long-range air surveillances radar (ARSR): at these frequencies, where the external noise is low, it is possible to achieve good range performances (typical ARSR radar have a maximum range of about 400 kilometers), and high power with narrow beam width antennas.

In L band also operate military 3D radars such as the SMART-L, but they also are at S band (such as AN/SPY-1 passive electronically scanned system)

S band (2 to 4 GHz).

In the S band operate some air surveillance radars (figure 1.5) such as the TASR-2020S, but the characteristic of long range is more difficult to achieve than at lower frequencies, because the echo due to the rain can significantly reduce the maximum range.

The S band is also employed in long-range weather radars for an accurate estimate of rainfall rate, and in medium range air surveillance applications, such as the ASR airport surveillance radar found at air terminals. The narrower beam widths at this frequency can provide good angular accuracy and resolution, and make it easier to reduce the effects of hostile main-beam jamming that might be encountered by military radars. Long-range airborne air surveillance radars, such as AWACS (Airborne Warning and Control System) also operate in this band.

***Figure 1.5**. TASR-2020S S-band air surveillance radar*

C band (4 to 8 GHz).

The C-Band can be described as a compromise between the S and X band, though it is difficult to make long air surveillance radars at this or higher frequencies. The C-band is used to design long-range precision instrumentation radars for missiles accurate tracking, and to design both multifunction phased array air defense radars and medium-range weather radars (figure 1.6).

Figure 1.6. *ASC SIGNAL C-band weather radar.*

X band (8 to 12.5 GHz).

In the X-Band operate military weapon control radar systems and devices for civil applications. Other equipments working at these frequencies are shipboard navigation radars, Doppler Navigation radars and devices employed by the police to detect the speed of cars.

X-Band radars are characterized by convenient size, and are thus of interest for applications where mobility and light weight are important, and long-range is not such as high resolution radars: as a matter of fact, at these frequencies it is possible to achieve narrow beam widths with relatively small-size antennas.

Ku, K, Ka bands (12.5 to 40 GHz).

Not many radar applications work at these frequencies, because we have limitations due to rain clutter and high attenuation by the atmosphere. However, even if it's difficult to generate and radiate power in this region of the electromagnetic spectrum, these frequencies are of interest because of the wide bandwidths and narrow beam widths that can be achieved with small apertures: an example of device operating in this band are the Ku band high resolution radars for the location and control of ground traffic at the airports.

Millimeters Wavelenghts (above 40 Ghz).

This band is characterized by high attenuation and by high clutter due to the rain. The exceptionally high attenuation caused by the atmospheric oxygen absorption line at 60 GHz precludes serious applications in the vicinity of this frequency within the atmosphere. Therefore, the 94 GHz frequency region (3 millimeters wavelength) is generally what is thought of as a "typical" frequency representative of millimeter radar: an example is the "mini-radar" developed in the 2001 for the ground traffic control at airports.

The millimeter-wave region is more likely to be of interest for operation in space, where there is no atmospheric attenuation, and for short-range applications within the atmosphere, where the total attenuation is not large and can be tolerated.

1.4. A brief summary on some radar systems [3][4][5].

The various radar systems may be classified into several types according with their use.

A very important category is the air traffic control radar used in civilian and military applications. Depending on their operating distance we can distinguish:

- The “en-route” radars operating in L band for the long-distance control of aircraft (the maximum range achievable by these radars is up to 450 kilometers).
- The Air Surveillance Radars (ASR) used for the identification and the determination of aircraft approach sequence by the air traffic security operators.
- The Precision Approach Radars (PAR) employed to guide the aircraft to safe landing in zero visibility approaching condition (figure 1.7).
- The Surface Movement Radars (SMR) operating in the land traffic control in the airport surface.

Figure 1.7. *TC-Z precision approach radar RP-5 GI.*

Common military radar systems are all the devices mounted aboard of the military ships such as: surface search radars, air search radars, height finding radars and various fire control radars.

The primary function of a surface radar is the detection and determination of accurate range and bearings of surface targets and low flying aircraft, while maintaining a 360° search for all target within line-of-sight distance from the radar antenna.

The purpose of the air search radar (figure 1.8) is nearly the same of the previous type: its main function is exclusively the determination of range and bearings of aircraft targets; jointly with the air search radar, the height finding radar, which calculate more accurately all the space coordinates of target, is typically used.

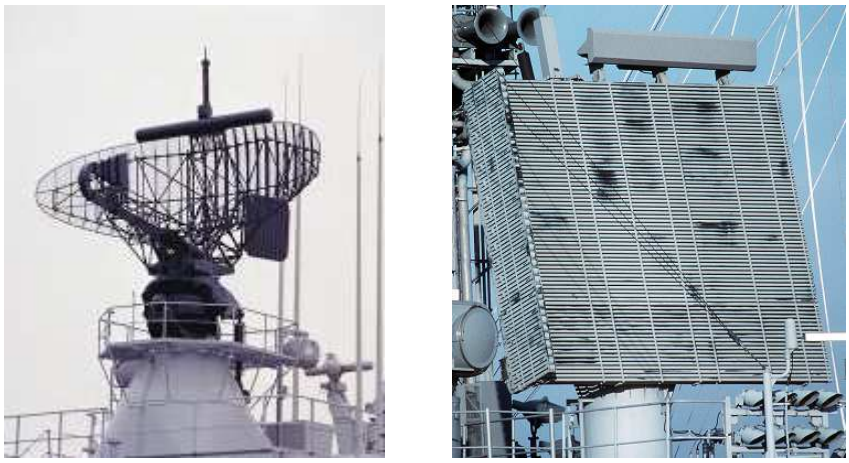

(a) *(b)*

Figure 1.8. *(a) THALES LW-08 surface surveillance radar, (b) ITT EXELIS AN/SPS 48 3D air search radar.*

The main difference between these two systems is the higher operating frequency of height finding radar in addition to the higher power output and much narrower vertical beam width.

Finally, the fire control radars (missile and gun control radar) provide information used to guide the weapons of a ship to a target. These radars work at a higher operating frequency, and employ a dish-shaped antenna to produce circular

beams (figure 1.9). In most recent military ships, their task is achieved (especially with regard the missiles control) by modern multifunction radar, such as the EMPAR.

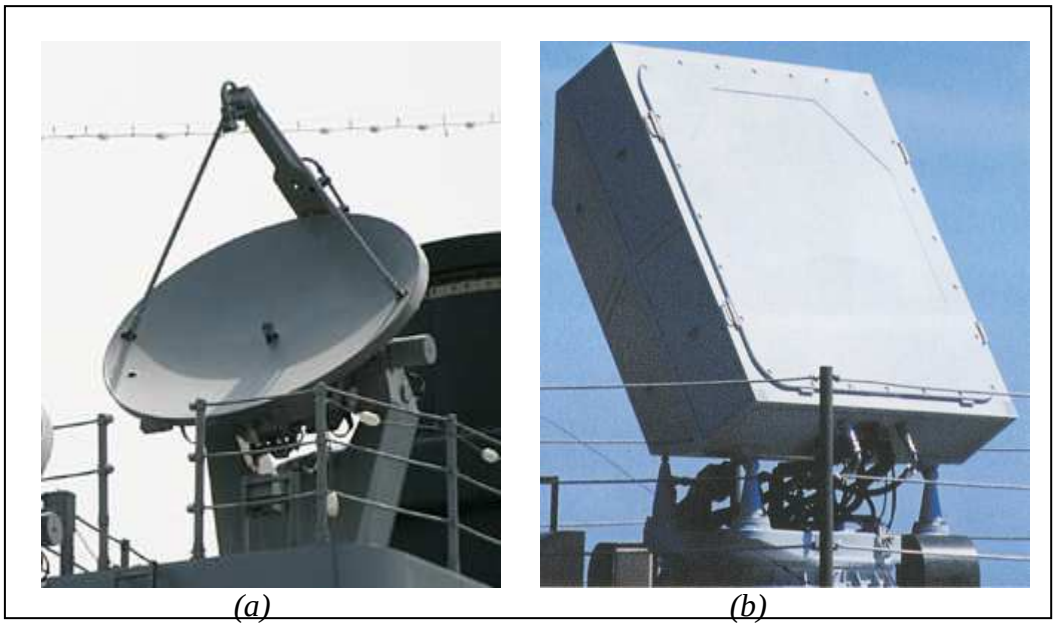

(a) *(b)*

Figure 1.9. *(a) AN/SPG-62 fire control radar, (b) EMPAR multifunction radar.*

The technical features of surveillance radar are suitable to another class of radar systems: the weather radars. The main difference consists in the characteristics of the observed target: in navigation and air surveillance radars, the target can be a ship, a plane or a more generic flying object. Once detected, the target is completely described by its range, speed, angular position and physical characteristics related to its radar cross section.

In the weather radar, the shape of "object of interest" is considerably different: the particles of rain and clouds are much fluid than a generic moving target and their velocity is normally considerably lower with respect to a plane or other flying machine.

The detection of snow, particles of rain and clouds involves weather radar operating at multiple frequencies located in S and C bands, where the wavelength (from 15 to 3.75 centimeters) is comparable to the size of hydrometeors. Since the attenuation increases with decreasing wavelength, the S band radars are the most

suitable for tropical regions and areas where hurricanes, tornadoes and cyclones are more likely. The S-band radar, however, are related with structural problems: the antenna size is proportional to the wavelength, and it follows that, to obtain a narrow beam width, large reflectors are necessary.

To achieve a high maximum range (more than 600 kilometers), radar weather system ground based are required to handle high transmitted power (up to 800-900 kilowatts). Nevertheless, high sensitive receivers are required to detect and identify the atmospheric disturbance, because the received echo due to rain particles is weak with respect to macroscopic objects.

Figure 1.10. *DWSR-8500S S-band weather radar*

Weather radar operating at smaller wavelengths (K or X band) designed for different purposes are also used in meteorological applications: good results in clouds detections could be achieve by radar working in K band. In most cases, however, at these frequencies the atmospheric absorption can significantly reduce the system performances.

1.5. The radar equation for meteorological targets [3][5] .

In the weather radar electromagnetic description, the received power backscattered from distributed targets (the hydrometeors) can be derived from the general radar equation:

$$P_R = \frac{P_T G^2 \lambda^2}{(4\pi)^3 \cdot R^4} \cdot \sigma = \frac{\beta}{R^4} \cdot \sigma \tag{1.14}$$

Where β is a constant related to radar system parameters (transmitting power, antenna gain, operating wavelength), R is the range and σ is the radar cross section.

In the determination of the radar cross section for meteorological targets, the equation (1.14) differs from the one used for point targets. A more generic expression of σ can be obtained using the radar reflectivity in units of cross-sectional area per unit volume:

$$\sigma = \eta \cdot V = \left(\sum_{i=1}^{N} \sigma_i \right) \cdot V \tag{1.15}$$

In equation (1.15), N is the number of scatterers per unit volume, and σ_i is the backscattering cross section of the *i*th scatterer: in the characterization of weather phenomena, these scatterers can take a variety of form such as water droplets, ice crystals, hail and snow.

If we consider the backscattered energy from a generic spherical drop, using the Rayleigh approximation [6], an expression of the *i*th scatterer can be written as:

$$\sigma_i = \frac{\pi^5}{\lambda^4} |K|^2 \cdot D_i^6 \tag{1.16}$$

Where D_i is the diameter of the *i*th drop and K is a quantity related to the drop complex index of refraction. From L to X radar bands $|K|^2$, is equal to about 0.93 for water particles and 0.2 for ice.

Using (1.16), from (1.15) we have:

$$\eta = \sum_{i=1}^{N} \frac{\pi^5}{\lambda^4} |K|^2 \cdot D_i^6 \tag{1.17}$$

Introducing the *radar reflectivity factor*, defined as:

$$Z = \sum_{i=1}^{N} D_i^6 \tag{1.18}$$

equation (1.17) becomes:

$$\eta = \frac{\pi^5}{\lambda^4} |K|^2 \cdot Z \tag{1.19}$$

Now, if the scatterers fill the radar beam, an approximation of the sample volume V is given by [6]:

$$V \cong \frac{\pi \phi \theta \cdot R^2 c \cdot \tau}{8} \tag{1.20}$$

Where θ and φ are the azimuth and elevation beam widths, c is the light velocity and τ is the radar pulse width.

Substituting equations (1.20), (1.15) and (1.16) into equation (1.14), we obtain:

$$P_R = \frac{\beta \pi}{R^4} \cdot \frac{\phi \theta \cdot R^2 c \cdot \tau}{8} \cdot \frac{\pi^5}{\lambda^4} |K|^2 \sum_{i=1}^{N} D_i^6 = \underbrace{\frac{\beta \pi^6 \phi \theta \cdot c \cdot \tau |K|^2}{8 \lambda^4 R^2}}_{\beta'} \cdot Z = \frac{\beta' Z}{R^2} \tag{1.21}$$

The term β' expresses the dependence of the received power by radar system parameters. From the previous equation, the received power P_R is proportional to Z (radar reflectivity factor), and inversely proportional to R^2.

In applications, however, the use of equation (1.21) for the calculation of Z can lead to errors due to a not uniform antenna gain over the bandwidth. To avoid this

problem, we can assume a Gaussian shape for the antenna beam, and, introducing a correction factor, we can write the received power as [7]:

$$P_R = \frac{P_T G^2 \lambda^2 \phi\theta \cdot c\tau}{512(2\ln 2)\pi R^2} \cdot \sum_{i=1}^{N} \sigma_i \qquad (1.22)$$

This equation can be rewritten as:

$$P_R = \frac{P_T G^2 \phi\theta \cdot c\tau \cdot \pi^3 |K|^2 Z}{512(2\ln 2) R^2 \lambda^2} \qquad (1.23)$$

Expression (1.23) allows to measure the reflectivity factor *Z* when the assumption of Rayleigh approximation is valid, and the scatterers are in either ice or water phase.

Due to high values of *Z* factor, often a logarithmic scale is introduced:

$$dBZ = 10\log_{10} Z$$

Typical values of Z in non precipitating clouds are less than -40 *dBZ*. In case of rain Z may range from about 20 *dBZ* to as much as 60 *dBZ*, with values of 55 or 60 *dBZ* in case of thunderstorms. Severe hailstorms may produce *Z* values higher than 70 dBZ.

Operational radars are generally designed to detect *Z* values ranging from 10 to 60 dBZ, while research applications usually aim for the maximum possible range.

Chapter 2.

Antenna Basic Concepts

2.1. Introduction [1].

An Antenna is commonly defined as a "Device, generally rod-shaped, used for radiating or receiving electromagnetic waves". This definition, however, is generic and influenced by the shape of the first antenna types, which consisted of metal wires or rods. Actually, according with the specific applications, the antennas have different shapes and sizes. A more precise definition (IEEE Standard Definition of Term for Antennas; *IEEE Std. 145-1983*) describes the antenna as "a means for radiating or receiving radio waves": as a matter of fact the antenna is a transducer placed between the free space and a transmission line (a coaxial structure or waveguide) used to carry the electromagnetic energy from the source to the antenna and vice versa.

When an antenna radiates in the space, it is "in transmitting mode"; a typical example of transmitting antennas are the television repeaters. Conversely, if an antenna receives the electromagnetic radiation, it is "in receiving mode": an example of these antennas are the radio telescope large parabolic antennas.

All antennas can be used both in transmission and reception: typical examples are the mono-static RADAR antennas and the mobile phone antennas.

The behavior of antennas in two operating modes is equal, due to reciprocity theorem therefore, in all the theoretical discussions we will consider the antennas "in transmission mode".

From an "electric" point of view, an antenna can be defined through a transmission line Thevenin equivalent scheme (figure 2.1), where Z_C is the characteristic impedance of the transmission line and Z_A is the antenna complex impedance defined as:

$$Z_A = (R_L + R_R) + jX_A \tag{2.1}$$

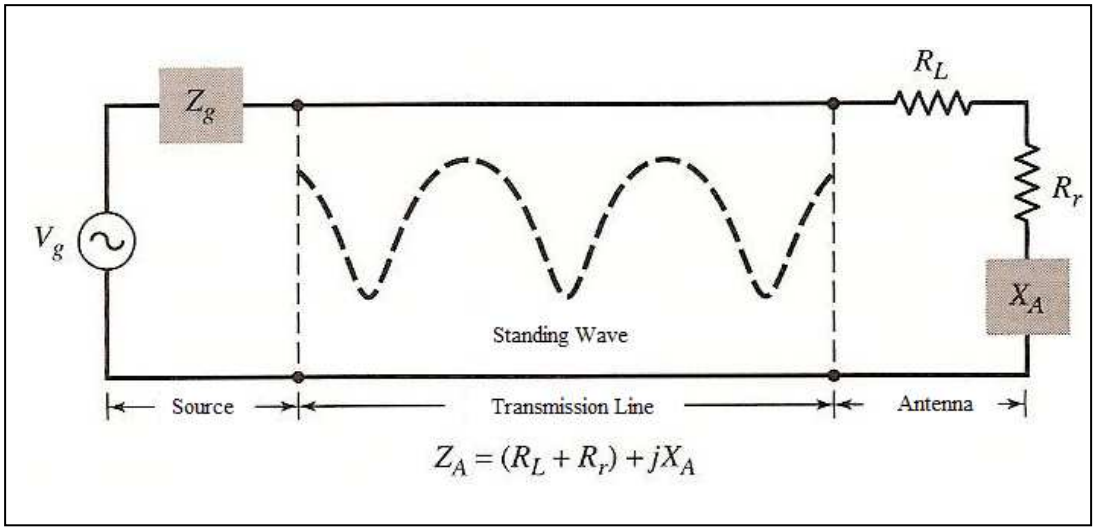

Figure 2.1. *Transmission-line Thevenin equivalent scheme of antenna [1].*

In equation (2.1), R_L is a resistance that identifies the antenna dielectric losses, R_r is the antenna radiation resistance and the imaginary term X_A is the reactance associated with the antenna radiation.

In ideal conditions, where all the devices are without losses, the energy of the generator signal should be transferred to the radiation resistance; in a real system, if we neglect the internal generator impedance and the reflection losses, the maximum power is transferred to the antenna under conjugate matching conditions.

2.2 Antenna Radiated Field and Radiation Pattern [1][3] .

An antenna is, a device able to radiate electromagnetic power in the space; it is therefore useful to introduce an appropriate coordinate system which allows to determine the fields produced by the antenna.

Considering a generic antenna, we will use a spherical coordinates system with origin placed in the center of symmetry of the antenna itself in order to locate a point in the space. A generic point (figure 2.2) is identified by the radius *R* and by angles ϕ (which identifies the elevation plane) and θ (which identifies the azimuth plane). In this coordinates system, a surface element is described by:

$$dA = r^2 \operatorname{sen}\theta \cdot d\theta \cdot d\varphi . \tag{2.2}$$

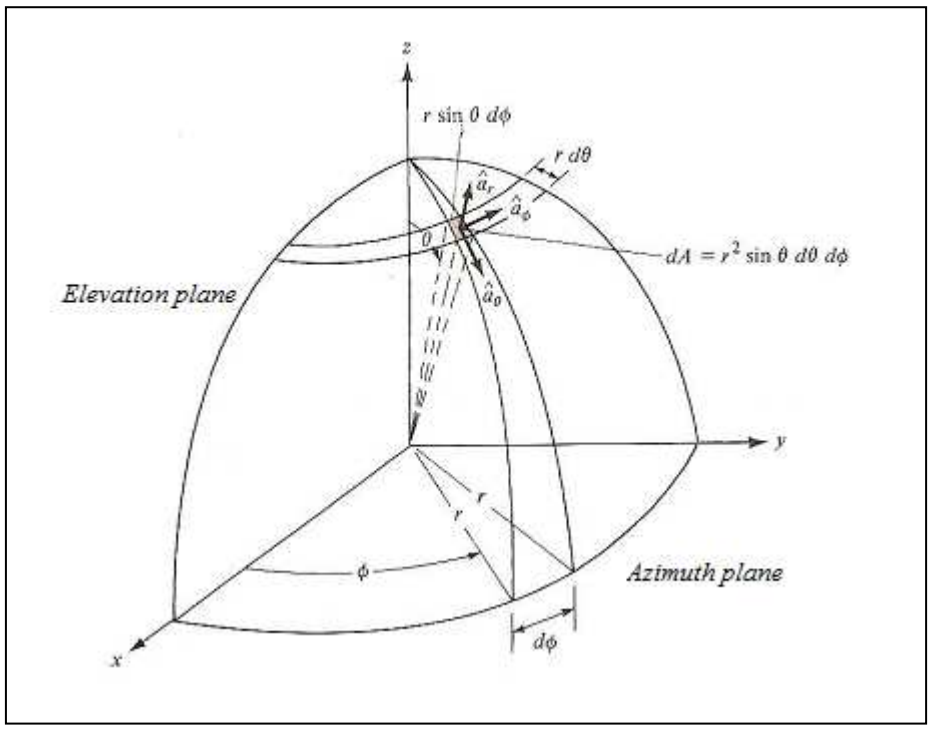

Figure 2.2*. Spherical coordinate system [1].*

In order to determine the electromagnetic field radiated by the antenna, we will consider the antenna as a set of elementary dipoles, and the total field as a sum of each single source contribution.

Let Q be a generic point placed far away by the generic source (figure 2.3), far enough that the phase delay due to any element of antenna can be neglected; the total electric field is given then by the equation:

$$E_{TOT} = j\frac{\xi \cdot I_0}{2\lambda r} \cdot e^{-j\beta r} \left\{ sin\theta \cdot \underline{i}_{\theta} \int_{antenna} \hat{I}(P) \cdot e^{j\beta \underline{i}_r \cdot r'} dz \right\} \qquad (2.3)$$

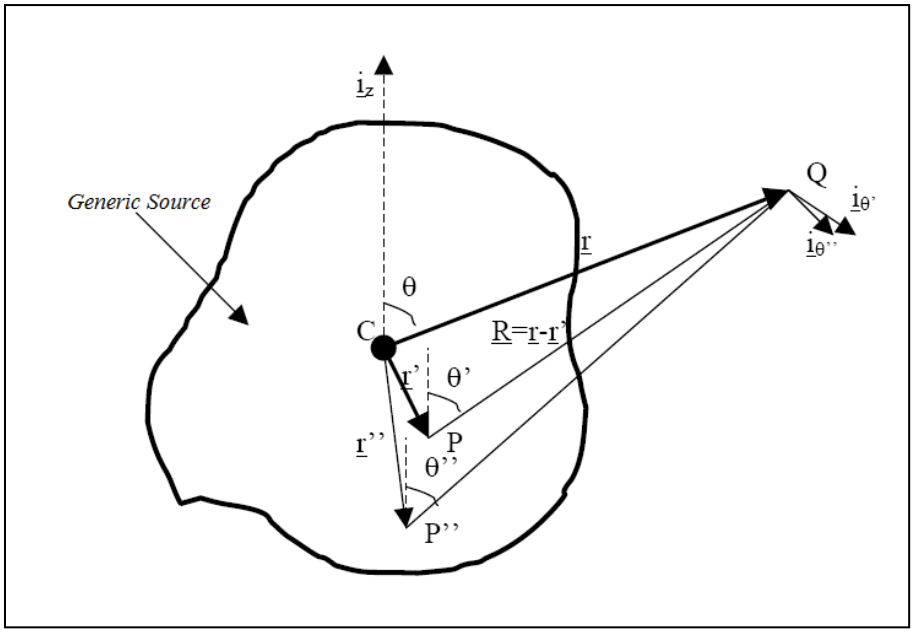

Figure 2.3. *Antenna total field computation*

In the equation (2.3), $I = I_0 \cdot \hat{I}(P)$ is the antenna current distribution, λ is the operating wavelength, and the quantity between brackets is the "*effective height*" of antenna.

Closely related to the determination of the antenna electromagnetic field is the radiation pattern. The antenna radiation pattern (figure 2.4) is a three-dimensional plot of electromagnetic energy radiated in the space by the antenna, and provides a graphical representation, in the selected coordinate system, of field spatial

distribution and of the radiation properties of antenna (power flux density, directivity and field polarization). More frequently two-dimensional plots are employed for a more simple representation: these plots are cuts of the 3D pattern in a given reference axis of antenna.

A more generic pair of orthogonal principal planes is frequently employed: these planes for a generic antenna are called E-Plane (plane of electric field vector $\underline{E}$) and H-plane (plane of magnetic field $\underline{H}$).

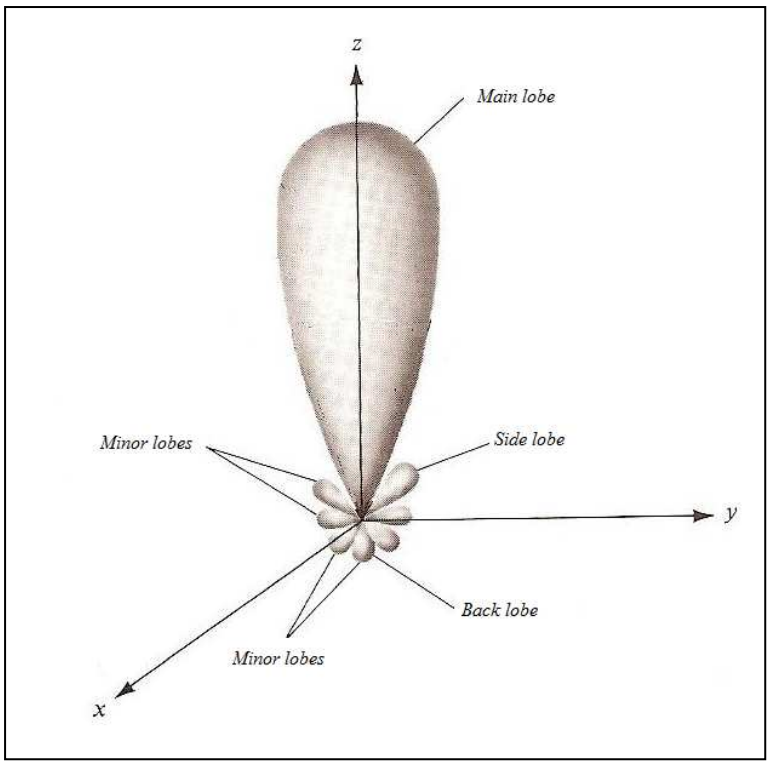

Figure 2.4. *Antenna radiation pattern [1]*.

A radiation pattern can be *isotropic*, *directional* and *omni-directional*. The first term is related to an ideal antenna without losses which radiates in the same way in all directions, the second is referred to a real antenna where the properties of transmission or reception are stronger in some directions than others, while the latter denotes an antenna with a non directional radiation pattern in a given plane of space and directional in any plane horizontal to it.

As shown in figure 2.4, various parts of a radiation pattern are referred to as "*lobes*", which may be sub-classified into *major* (or *main*), *minor*, *side*, and *back* lobes.

The main lobe contains the direction of maximum irradiation: an antenna has one or more main lobes; in the radar antennas the main lobe has circular cross section and we refer to it as "pencil beam". The lobe located at 180° from the main lobe is defined as "*back lobe*".

The main beam angular extent is one of the main features of antenna itself. A quantity related to it is the half-power beamwidth, that occur at 3 dB to maximum and measures the resolution of an antenna: in radar applications, two identical targets having the same range are said to be "*resolved in angle"* if separated by the half power beamwidth.

A large number of *minor lobes* exists outside the main lobe region: the lobes near the main beam are called "*side lobes*", and are commonly expressed by the highest peak level with respect to the maximum of the main lobe. In radar systems, the presence of side lobes in the radiation pattern can be a source of problems because the energy radiated by the antenna aims also in different directions with respect to the main lobe. For example, if a radar antenna is designed to detect low flying aircraft targets, the side lobes can receive strong echoes by the ground (named "clutter") which may blind the weaker echo coming from the target with a low radar cross section.

In order to avoid these problems, the requested side lobes for radar antennas must be as low as possible. The optimum side lobe level depends on specific application, and side lobes level of 20 dB below the maximum are acceptable for most applications: a typical reflector antenna with a horn feed has a first side lobe 23 or 28 dB below the maximum.

2.3. Antennas principal parameters [1].

In this section we will describe some of the quantities used in the analysis and synthesis of antennas.

From a source point of view, an antenna can be considered as a resonator (more or less ideal) where a large part of power dissipated in the resistance of the resonator is radiated into space. In general, once selected the antenna operating frequency, its length (or its spatial dimensions) is determined using a multiple of the wavelength λ: for example, the length of a dipole antenna is usually set equal to $\lambda/2$.

A very important parameter for an antenna is its radiated power. Let us consider the expression of the Poynting vector $\underline{S}$ for a generic point located at great distance from the source:

$$\underline{S} = \frac{1}{2 \cdot \xi} \cdot \left|\underline{E}\right|^2 = \frac{\xi}{2} \cdot \frac{\left|I\right|^2}{4 \cdot \lambda^2 r^2} \cdot \left|h(\theta, \varphi)\right|^2 \cdot \underline{i_r} \qquad (2.4)$$

where $h(\theta,\varphi)$ is the effective height introduced in the equation (2.3); this parameter is characteristic for each antenna and allows to determine both the radiated field and the amplitude of radiated power. Using equation (2.4) we obtain:

$$P_{RAD} = \int \underline{S} \cdot \underline{i_r} \cdot ds = \frac{\xi}{2} \cdot \frac{\left|I\right|^2}{4 \cdot \lambda^2} \int \left|h(\theta, \varphi)\right|^2 d\Omega \qquad (2.5)$$

Where the integration operation is extended to the whole space. Starting from this expression, if we consider that an antenna is an electric circuit, the antenna input power can be expressed by a sum of two terms: the radiated power in the space (calculated by the previous equation) and the power dissipated in the antenna itself:

$$P_{IN} = P_{RAD} + P_D \tag{2.6}$$

For an ideal lossless antenna, the dissipated power P_D is equal to zero and P_D=P_{IN}.

A parameter related to the effective height of antenna is the effective area, given by:

$$A_{eff} = \frac{\xi}{4R_{IN}} |\underline{h}|^2 \tag{2.7}$$

In addition to losses due to dissipated power, it is necessary to consider the reflected power from the antenna itself: a measure of this effect is the reflection coefficient Γ. If Z_A is the input impedance of the antenna and Z_C is the impedance of the feed line, the expression of the reflection coefficient is:

$$\Gamma = \frac{Z_A - Z_C}{Z_A + Z_C} \tag{2.8}$$

The parameter Γ is equal to zero only if the antenna is matched with its feed line.
A parameter related to the reflection coefficient is the *standing wave ratio* (*SWR*), which measures the amplitude of the reflected wave by the antenna. The *SWR* is given by:

$$SWR = \frac{1+|\Gamma|}{1-|\Gamma|} \tag{2.9}$$

The minimum value of *SWR* occurs when $\Gamma=0$ (*SWR=1*).
One of the most relevant parameter of an antennas is the *directivity*. The *directivity*, according with the IEEE Standard definitions of Terms of Antennas,

can be defined as "*the ratio of radiation intensity in a given direction from the antenna to the radiation intensity averaged over all directions. The average radiation intensity is equal to the total power radiated by the antenna divided by 4π. If the direction is not specified, the direction of maximum radiation intensity is implied*".

The directivity is therefore a measure of the capability of an antenna to concentrate the radiated power in a certain direction, and according with the previous definition, its mathematical expression is:

$$D(\theta,\varphi) = \lim_{r\to\infty} \frac{S(\theta,\varphi)}{\frac{1}{4\pi\cdot r^2}\cdot P_{RAD}} \tag{2.9}$$

High values of directivity imply that the antenna radiates principally in a relatively small area of space.

In general, since the radiated power is not easily controllable, in equation (2.10) the parameter normally used to describe the radiation properties of the antenna is the *gain*, obtained by substituting in the equation (2.10) the radiated power P_{RAD} with the input power P_{IN}:

$$G(\theta,\varphi) = \lim_{r\to\infty} \frac{S(\theta,\varphi)}{\frac{1}{4\pi\cdot r^2}\cdot P_{IN}} \tag{2.11}$$

The gain and the directivity of an antenna are related by the expression:

$$G(\theta,\varphi) = \eta\cdot D(\theta,\varphi) \tag{2.12}$$

Where $0\leq\eta\leq 1$ is the antenna efficiency and take in to account the effect of non-ideality of the antenna itself.

If the antenna is without losses, $\eta=1$, and the gain coincides with directivity.

High-gain antennas (with highly directional main beam) are used in RADAR and radio-astronomy applications to focus a large part of radiated power in a given area of space.

A simpler expression of (2.11), which allows to calculate the gain starting from the effective height and the input impedance of an antenna, is:

$$G = \pi \cdot \frac{\xi}{R_{IN}} \left(\frac{h}{\lambda} \right)^2 \tag{2.13}$$

Using (2.7) and (2.13), it is possible to obtain a relation between the gain and the effective area:

$$\frac{A}{G} = \frac{\lambda^2}{4\pi} \Rightarrow G = \frac{4\pi}{\lambda^2} \cdot A \tag{2.14}$$

Another very important parameter that characterizes the antennas is the bandwidth. The bandwidth of an antenna is defined [1] as “the range of frequencies within which the performance of antenna, whith respect to some characteristic, conforms to a specific standard”.

This parameter can be expressed as the range of frequencies (centered on a center frequency which usually is the antenna resonance frequency) where the characteristics, such as input impedance, shape, width and direction of the irradiated beam, polarization , side lobe level, gain and efficiency of irradiation, do not vary significantly with respect to the center frequency. Since the various parameters that characterize an antenna do not necessarily have the same frequency behavior, this definition of bandwidth is not “unique”.

In general, the bandwidth is usually expressed as the ratio between the highest and lowest operating frequency: for example, a bandwidth of 10:1 indicates that the highest frequency of operation is 10 times larger than the lowest one.

2.4. Examples of type of antennas [1].

In this section we describe a brief overview of various types of antennas. The famous and familiar antennas, are undoubtedly the wire antennas. As a matter, wire antennas are widespread: thus are employed in cars, in buildings, in aviation and in many other areas. Wire antennas may assume different configurations such as dipole, loop and helix antennas (figures 2.5): these devices are the easiest radiating elements to fabricate, and their performance depends only by the length and thickness of the wire.

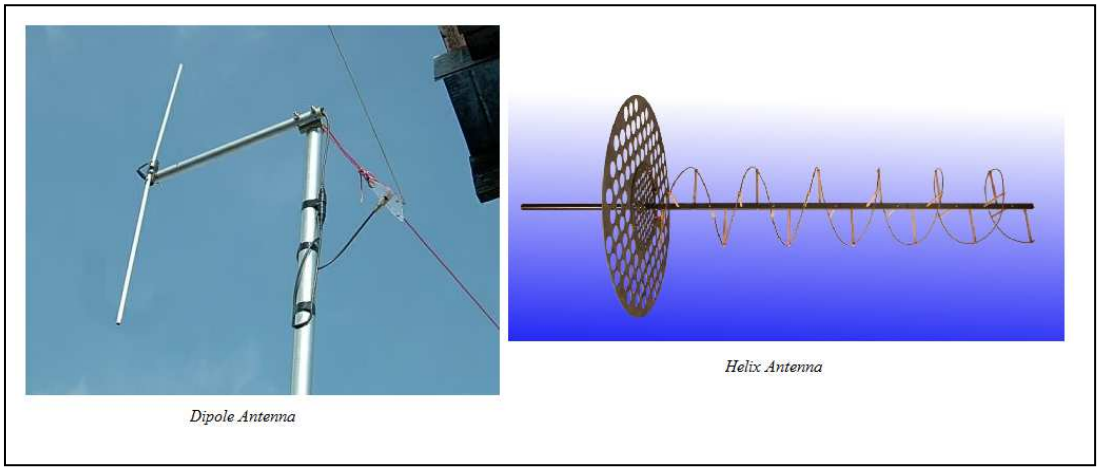

Figure 2.5. *Example of wire antennas* .

In industry and in aerospace applications, aperture antennas are widely used (figure 2.6). These devices, obtained by truncated waveguides, are employed in high frequency bands and they can be covered with dielectric material, in order to protect them by atmospheric agents.

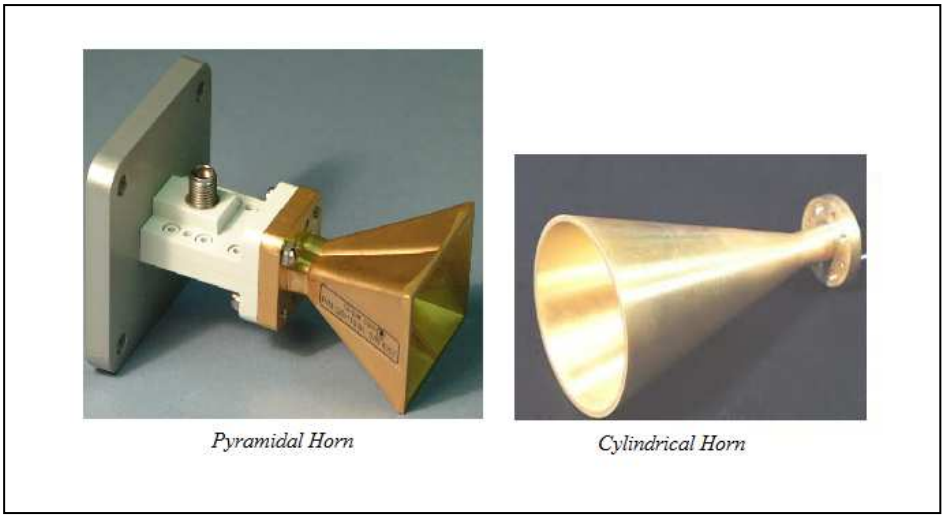

Figure 2.6. *Example of aperture antennas .*

A very important antenna family is the group of microstrip patch antennas (figure 2.7), that may assume many different shapes. This kind of devices became very popular in the 70s, thanks to their widely use in space and astronautic applications.

Today, due to their interesting characteristics of radiation, and to the facility of manufacturing, the patch antennas are employed in a large number of areas, including also aeronautics and mobile communications.

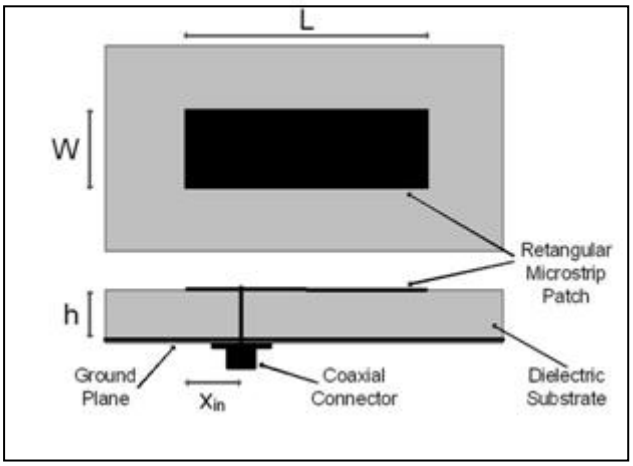

Figure 2.7 *Example of rectangular microstrip patch antennas with coaxial probe.*

In many applications, the request is to obtain high gain and particular characteristics of radiation not achievable with a single radiating element.

A solution to this problem are the arrays: they consist of group of several single antennas (figure 2.8), suitably disposed, and that allow to obtain high gain ad desirable radiating beam shape.

***Figure 2.8**. Example of array antennas*

2.5. Radar antennas examples [3] .

The radar devices are grouped in two main categories: the “search or surveillance radar”, where the coverage of a wide space region is ensured by a quick and rapid rotation of an antenna with a characteristic fan shaped beam (figure 2.9) ; and the “tracking RADAR”, that follows the target once it has been detected.

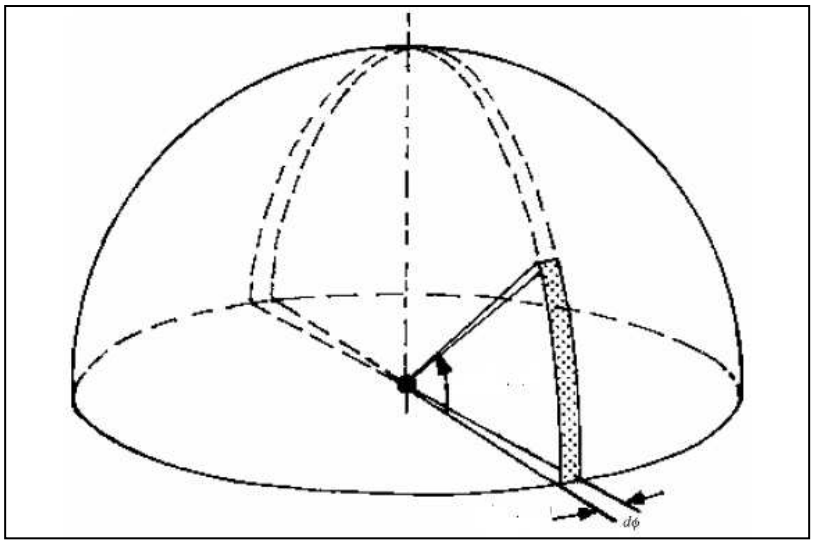

Figure 2.9. *Fan beam example.*

The high gain and the narrow beam width required for radar antennas is achieved by phased arrays and reflector antennas: in the phased arrays the number of elements and their mutual coupling allow to obtain a narrow beam width (figure 2.10). In the surveillance RADAR the coverage of wide angular regions is performed by changing the beam direction using the array feeding network.

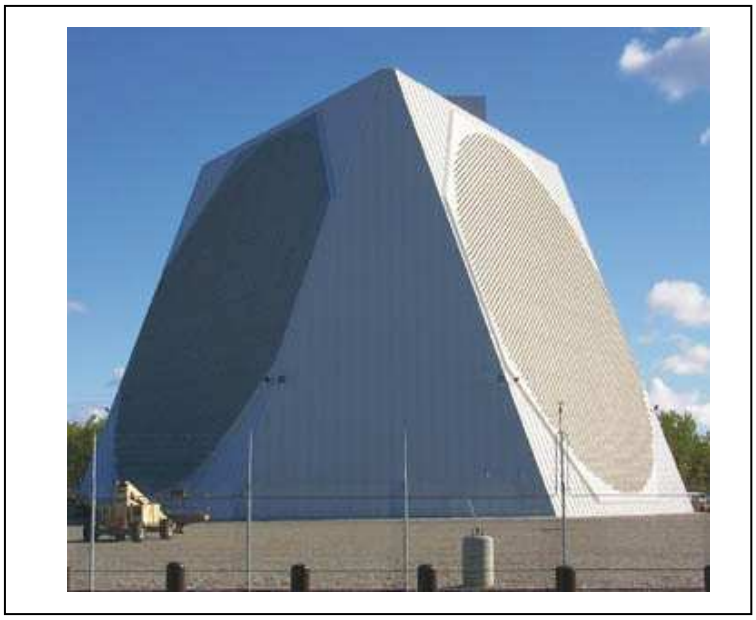

***Figure 2.10**. Phased array radar antenna.*

On the other hands, in the reflector antennas (figure 2.11) the principles of geometrical and ray optics are employed to obtain high gain while the mechanical rotation of the antenna provides the coverage of the space region surrounding the antenna.

***Figure 2.11**. Rotating reflector radar air surveillance antenna.*

Chapter 3.

Reflector Antennas

3.1 Introduction [1][2] .

The reflector antennas may exhibit a wide variety of shapes and feed systems, depending on their applications. Reflector antennas have been employed since the discovery of electromagnetic waves (Hertz, 1888). During the World war II, the birth of RADAR applications for aerial target detection, resulted in a huge progress of reflector design and analysis techniques.

In the '60s, the massive satellite communications and the requirement of high antenna performance and gain, led to achieve many kinds of reflector antennas.

Although many geometrical configurations are possible (i.e. plane reflector, corner reflector), the most popular shape is the family of curved reflectors.

The best known antenna curved reflector consists of a parabolic conducting surface (figure 3.1) with vertex *V* (symmetric point of surface), diameter *d* and focal length *f* , illuminated by a device (the feed) placed in the focus *F*: the feed is usually located in front of the dish, and this configuration is knows as *front fed*.

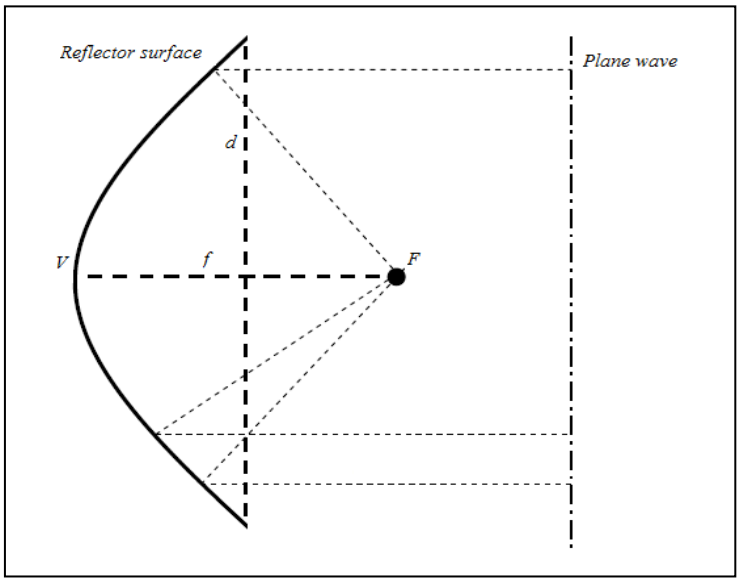

Figure 3.1: *Parabolic front-fed configuration.*

With this configuration, it is possible to achieve radiated fields with high gain and minimum beam width.

If the size of the dish is greater than the operative wavelength, the feed can be considered as a point source for the paraboloid. By geometrical optics considerations, a beam of ray originated by a point source placed in the focus, after reflection from the parabolic surface emerges as a plane wave, identified by a parallel beam with the same direction of the reflection surface axis. We refer to this parallel ray formation as “collimated”. The term “collimation” is also employed to describe the highly directional characteristic of antennas.

However, especially in radar systems, the reflector outline can vary depending on the requirements (figure 3.2): the oblong reflector (named also “orange peel”) is employed if the azimuth and elevation beam width requirements are different (figure 3.2b); the offset configuration (described later) is used to avoid the blockage losses (figure 3.2c). Finally, the corners of most paraboloidal reflectors are rounded (figure 3.2d), mitered (figure 3.2e) or stepped (figure 3.2f) in order to minimize the area of the antenna and the torque required to turn the antenna.

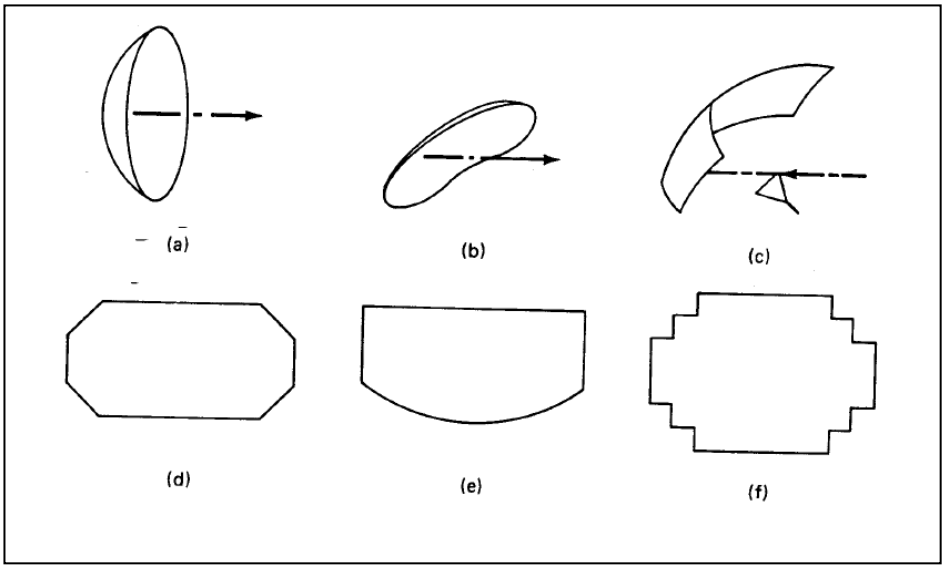

Figure 3.2. *Paraboloidal reflector outline [3].*

3.2 Reflector Analysis: physical optics approximation [1][2] .

In this sections the radiated electric field of a reflector antenna will be calculated using some physical optics considerations. The determination of the radiation characteristics (gain, efficiency, polarization, pattern, etc.) of each reflector antenna requires the evaluation of the current on the reflector surface induced by the feed. Considering a generic conducting surface, the current density, named $\underline{J_s}$, can be expressed by the equation:

$$\underline{J_s} = \underline{i_n} \times \underline{H} = \underline{i_n} \times \left(\underline{H_{inc}} + \underline{H_{ref}} \right) \tag{3.1}$$

where $\underline{H_{inc}}$ and $\underline{H_{ref}}$ are the incident and reflected components of the magnetic field and $\underline{i_n}$ is a unit vector normal to the surface.

If the overall size of the reflector and its radius of curvature are large compared to the wavelength of the incident wave, it is possible to estimate the reflector surface with an infinite plane surface (this condition is locally met for a parabola). Therefore, using the method of images, we have:

$$\underline{i_n} \times \underline{H_{inc}} = \underline{i_n} \times \underline{H_{ref}} \tag{3.2}$$

Thus, replacing in equation (3.1)

$$\underline{J_s} = \underline{i_n} \times \left(\underline{H_{inc}} + \underline{H_{ref}} \right) = 2\underline{i_n} \times \underline{H_{ref}} = 2\underline{i_n} \times \underline{H_{inc}} \tag{3.3}$$

The approximation of physical optics is very accurate at the center of the reflector surface and it is useful in the computation of the main lobe and first side lobes of the antenna radiation pattern.

Let ***R*** be the reflection matrix for a generic plane wave incident on the reflector surface with arbitrary polarization and *(x, y, z)* a set of rectangular coordinates with z axis orthogonal to reflector. The equation (3.3) can be rewritten as:

$$\begin{pmatrix} J_x \\ J_y \end{pmatrix} = 2 \cdot \begin{pmatrix} R_{xx} & R_{xy} \\ R_{yx} & R_{yy} \end{pmatrix} \begin{pmatrix} -H_y \\ H_x \end{pmatrix} = 2\underline{\underline{R}} \cdot \begin{pmatrix} -H_y \\ H_x \end{pmatrix} \tag{3.4}$$

It is possible to define the ***R*** matrix by the product of the surface impedance matrix ***Z***, related to the electric properties of the reflector surface, and the impedance wave matrix ***W*** , that characterizes the incident wave direction:

$$\underline{\underline{R}} = \left(\underline{\underline{W}} + \underline{\underline{Z}}\right)^{-1} \cdot \left(\underline{\underline{W}} + \underline{\underline{Z}}\right) \tag{3.5}$$

If $\underline{S}$ is the Pointing vector of the incident field on the reflector surface, the **W** matrix can be written as:

$$\underline{\underline{W}} = \frac{\xi}{S_z} \cdot \begin{pmatrix} -(1-S_x)^2 & S_x \cdot S_y \\ S_x \cdot S_y & -(1-S_y)^2 \end{pmatrix} \tag{3.6}$$

Generally, the reflector surface is made of conductive material, and this allows to write the **Z** matrix as the null matrix if the material is perfect electric conductor. On the other hand, if the material is a good conductor, the Z matrix is given by:

$$\underline{\underline{Z}} = \sqrt{\frac{K}{2\xi\sigma}}(1+j) \cdot \underline{\underline{I}} \tag{3.7}$$

Where K is related to the incident wave, ξ is the characteristic impedance of air and σ is the material conductivity.

This technique allows to determine accurately the reflector far-field, and is suitable for any reflector shape (even grid reflectors).

Despite its flexibility, the physical optics approximation is computationally heavy; less accurate results, but expressed in analytical form, can be obtained by using the geometric optics approximation.

3.3 Reflector Analysis: geometric optics approximation. [2]

The radiated field of reflector antennas can be evaluated analytically by using geometric optics approximation. This approach is suitable because the reflectors are usually large in terms of wavelength. Taking into account the ray optics theory, it is possible to consider the electromagnetic field locally as a plane wave that travel in straight line inside a homogeneous media. In presence of obstacles the plane wave is reflected or refracted according to Snell's law. It is also possible to consider the power of the electromagnetic wave as flowing in a flux tube where the electric and magnetic fields are mutually orthogonal to the rays. When the wave is reflected by a perfectly conducting plane surface, the power of the reflected and incident wave is the same. The fields $\underline{E}$ and $\underline{H}$ travel inside the flux tube and, in absence of refraction, their polarization and orientation do not change.

Let $g(\vartheta,\varphi)$ be a conical flux tube with origin in the focus of the reflector (figure 3.3). The quantity $g(\vartheta,\varphi)$ (where ϑ is the angle with respect to the normal $\underline{n}$ of the reflector, and φ is the rotation angle around its axis) represents the amplitude of the Poynting vector travelling towards the dish, while the ratio $g(\vartheta,\varphi)/r^2$ is the power per unit area radiated by the feed. The incident power in an angular sector of the reflector can be written as:

$$P(\theta,\varphi) = r^2 \sin\theta \cdot d\theta d\varphi \cdot \frac{g(\theta,\varphi)}{r^2} = g(\theta,\varphi) \cdot \sin\theta \cdot d\theta d\varphi \qquad (3.8)$$

After the reflection over the surface of the dish, the incident rays emerge as a cylindrical flux tube; since the reflected power is equal to the incident power on the reflector surface, starting from equation (3.8) we find that:

$$P(\theta,\varphi) \cdot r \cdot \sin\theta \cdot d\phi d\rho = g(\theta,\phi) \sin\theta \cdot d\theta d\phi$$

Where $d\rho$ is the width of the reflected flux tube on the aperture surface.

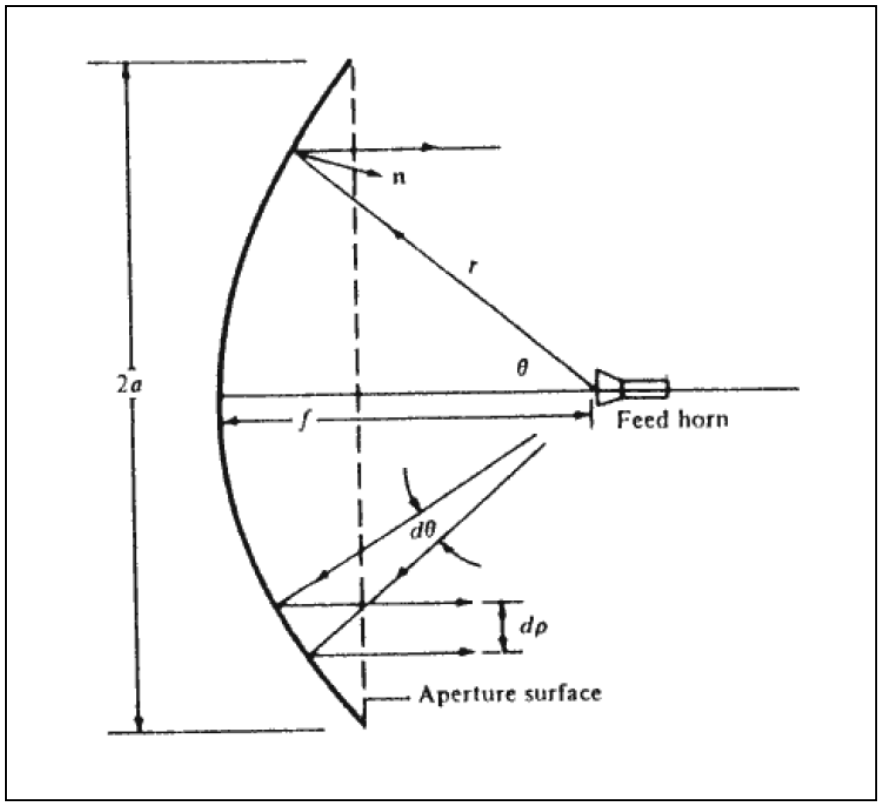

Figure 3.3 *Paraboloidal reflector antenna [2].*

The previous equation can be rewritten as

$$P(\theta,\varphi) = g(\theta,\phi)\frac{1}{r}\cdot\frac{d\theta}{d\rho} \tag{3.9}$$

Eq. (3.9) represents the power density per unit area on the aperture surface.

If f is the reflector focal length, the profile of the dish is described by:

$$r = \frac{2\cdot f}{1+\cos\theta} \tag{3.10}$$

By replacing the expression $\rho = r\sin\vartheta$ in equation (3.10), we obtain:

$$\rho = \frac{2f \cdot \sin\theta}{1+\cos\theta}$$
$$\frac{d\rho}{d\theta} = \frac{2f}{1+\cos\theta} \tag{3.11}$$

And hence:

$$P(\theta,\varphi) = g(\theta,\phi)\frac{1}{r}\cdot\frac{d\theta}{d\rho} = g(\theta,\phi)\frac{(1+\cos\theta)^2}{4f^2} = g(\theta,\phi)\frac{16f^2}{\left(4f^2+\rho^2\right)^2} \tag{3.12}$$

Equation (3.12) shows that the field distribution on the aperture surface depends both on the feed radiation pattern and on geometric considerations. According with the above equations, the directivity of the antenna is maximum when the incident power on the reflector surface $P(\vartheta,\varphi)$ is constant. This implies that $g(\vartheta,\varphi)$ must be proportional to $4\cos^4(\vartheta/2)$.

In order to obtain a uniform illumination for the reflector surface, the feed power pattern should be:

$$g(\theta,\varphi) = \begin{cases} \sec^4\left(\frac{\theta}{2}\right) & 0 \le \theta \le \frac{\psi}{2} \\ 0 & \theta \ge \frac{\psi}{2} \end{cases} \tag{3.13}$$

Where ψ is the overall angular aperture of the reflector (figure 3.4).

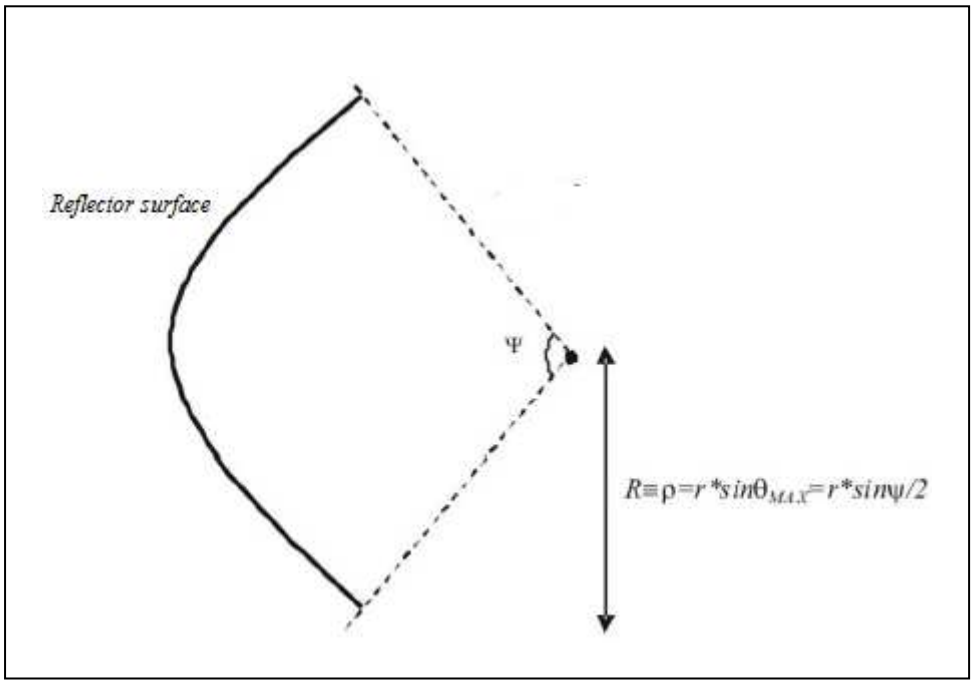

Figure 3.4: *Angular aperture of reflector.*

Equation (3.13) describes an ideal and unfeasible condition, although much effort has been dedicated to design feed with power pattern as similar as possible to these characteristics.

3.4 Reflector analysis: performance and gain losses [2].

In real operating conditions, a part of the radiated field coming from the feed is not intercepted by the reflector. This degradation of the antenna performance, named “spill-over loss”, (figure 3.5) is due to a not-ideal feed radiation pattern, and can be expressed by the efficiency factor η_s:

$$\eta_s = \frac{\int_0^{2\pi\psi/2}\int_0 g(\theta,\varphi)d\Omega}{\int_0^{2\pi\pi/2}\int_0 g(\theta,\varphi)d\Omega} = \frac{D_f}{4\pi}\int_0^{2\pi\psi/2}\int_0 g(\theta,\varphi)d\Omega \qquad (3.14)$$

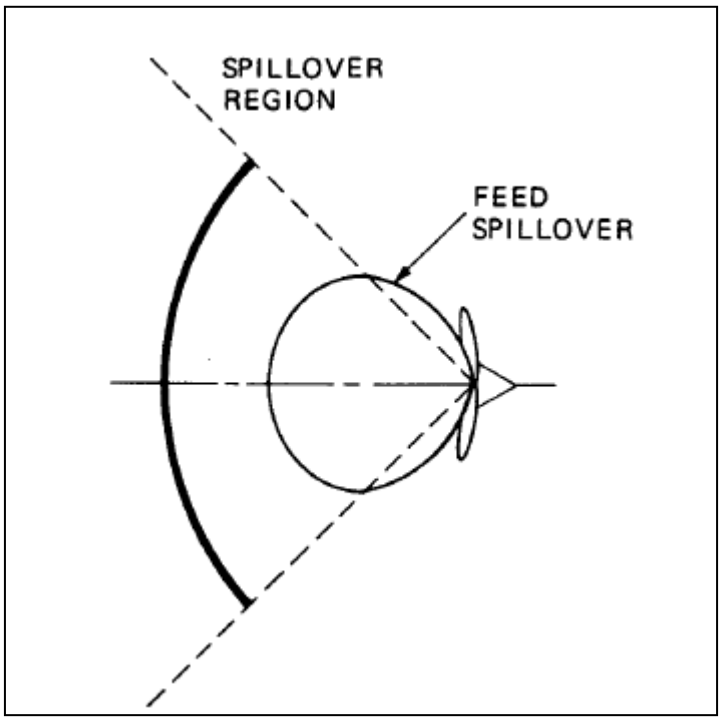

Figure 3.5. *Spill-over loss [3].*

Where D_f is the directivity of the feed.

The spill-over loss can be reduced using reflector having a high angular aperture and a low illumination at its edges.

Another term describing the non-ideality effects is the aperture efficiency:

$$\eta_A = \frac{A_{eff}}{\pi R^2} = \left(\frac{\lambda}{2\pi R}\right)^2 \cdot D \tag{3.15}$$

The aperture efficiency is always smaller than *1* and can be expressed as a product of two terms taking into account the losses due to non uniform illumination of the reflector surface ($1-\eta_i$) and the non constant phase of the aperture field ($1-\eta_p$).
The behavior of the efficiency η_A is dual with respect to η_S efficiency: high values of η_A require reflectors with small values of angular aperture ψ and high illumination at the dish edges. In order to maximize the reflector efficiency, it is therefore necessary a compromise between these two situations, aiming to obtain an optimal distribution of the feed power radiation $g(\vartheta,\varphi)$.
A good approximation of $g(\vartheta,\varphi)$ is given by the following expression:

$$g(\theta,\varphi) = \begin{cases} 2(n+1)\cos^n\theta & 0 \le \theta \le \dfrac{\pi}{2} \\ 0 & \theta \ge \dfrac{\psi}{2} \end{cases} \tag{3.16}$$

Where $n \geq 0$ is an integer number; for high values of n, the feed radiation pattern appears to be very narrow.
In the equation (3-16) the product $2(n+1)$ is a normalization factor chosen to make the total power radiated by the feed equal to 4π. Using this expression of $g(\vartheta,\varphi)$ to calculate the efficiency of the reflector $\eta_A\eta_S$, we obtain that the minimum value of the reflector efficiency is independent of n and is equal to 0.8 (figure 3.6). Regardless the feed employed, the optimal $g(\vartheta,\varphi)$ requires a tapered field pattern with a power level at the edges 10 dB smaller than the one at the center.

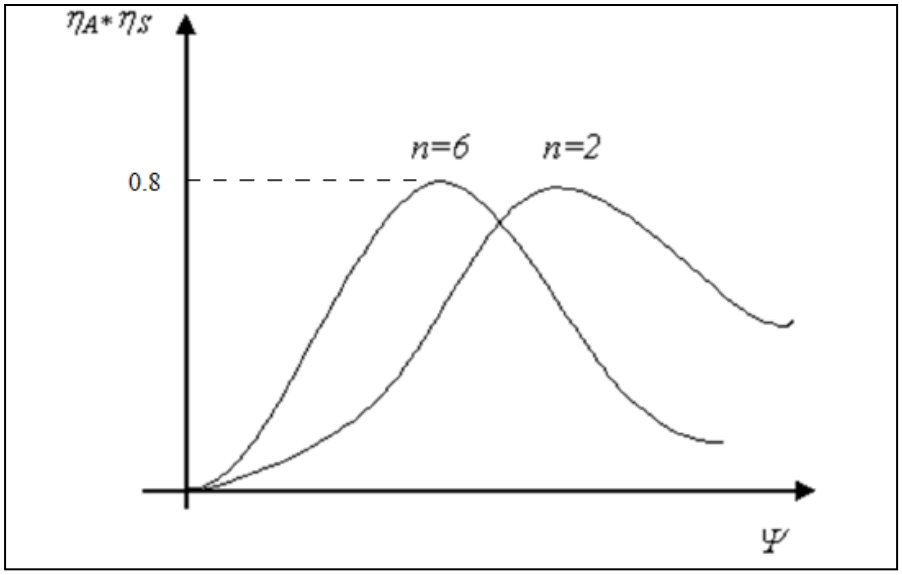

Figure 3.6. *Reflector efficiency [2].*

An additional gain loss factor in the front-fed reflector antenna configuration is the presence of a “shadow zone” (named blockage) in the center of the radiated field area of the reflector, due to the feed position and its supports.

The scattering caused by the presence of the feed involves both the increase of the cross-polar component of the radiated field and side-lobes. Consequently, this phenomenon pulls down the reflector efficiency; this is a critical factor in those systems (i.e radar) designed to have low side-lobes level (less than 30 dB) and reduced cross-polar field component.

Taking into account all the loss factors, the gain of the antenna can be expressed as:

$$G = \eta_X \eta_B \eta_S \eta_A D_M \tag{3.17}$$

Where η_x and η_B are the efficiencies related to the cross-polar component and to the blockage. The D_M term represents the maximum directivity for the structure, obtained when the effective area of the reflector is equal to its physical area:

$$D_M = \frac{4\pi}{\lambda^2} \cdot A_{Phisical} \Rightarrow D = \eta_A D_M = \eta_A \frac{4\pi}{\lambda^2} \cdot \left(\pi R^2\right) \tag{3.18}$$

Using equations (3.17) and (3.18), it is possible to compute the reflector diameter as a function of the desired gain and operating frequency.

The cross-polarization efficiency depends by the feed and its manufacturing processes, while the blockage efficiency can be increased by using the "off-set" configuration (figure 3.7).

In this configuration, only a portion of the paraboloid surface is metalized: a circular section of dish is removed from the reflective surface in order to locate the focus outside of the main lobe of reflector.

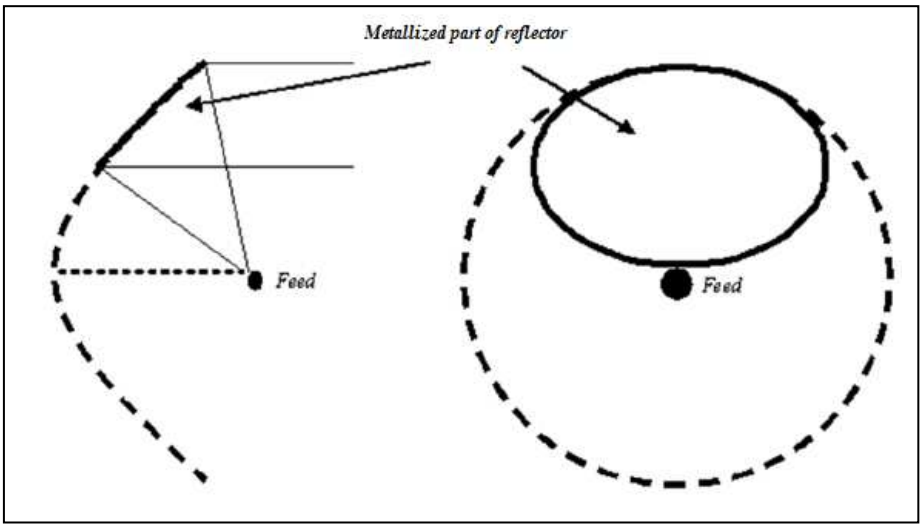

Figure 3.7. *Off-set Configuration.*

This configuration allows an increase of η_B up to 100%, because it avoids the reflected rays to collide with the feed and its supports. In the off-set reflector configuration, in order to keep away losses due to the spill-over, the feed should be directed exclusively toward the metalized area of the dish (figure 3.8).

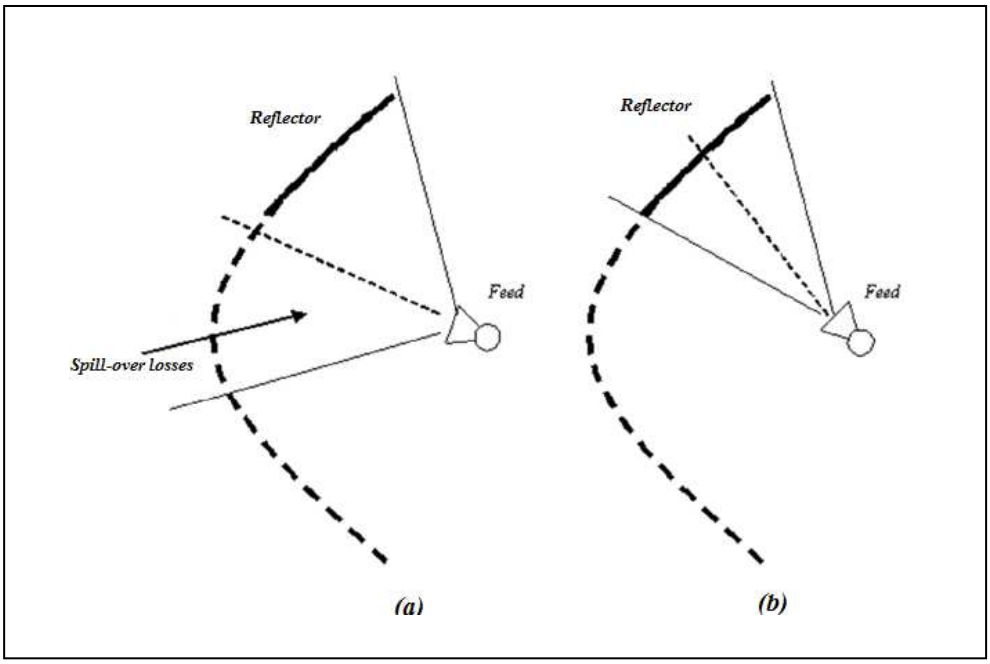

Figure 3.8. *Feed Positioning in the off-set configuration. (a) Incorrect position. (b) Correct position.*

This expedient, therefore, allows to remove the feed and its supports from the maximum irradiation area. The disadvantage is due to the increasing of the cross-polar component of the radiated field: in the off-set systems, this component is around -25 dB, and this value can be too large for some radar applications.

3.5. Dual reflector configurations [2] .

The front-fed configuration has some disadvantages: the transmission line connecting the feed and the receiving/transmitting antenna equipments placed below or behind the dish is typically too long; this may not be tolerable in low-noise applications, where the losses of transmission lines compromise the quality of the received signal.

Typically, in antennas for radio-astronomy and satellite communications, the front-fed configuration is not used. The radiation pattern of large number of feed systems has side lobes that do not go to zero at the edge of the reflector; when the reflector is pointed in the direction of the sky, the feed is pointed in the direction of the ground, receiving also the thermal noise coming from the soil, reducing the system sensitivity.

These problems can be avoided using a configuration known as Cassegrain feed system (figure 3.9). With this configuration, it is possible to obtain a parallel beam of rays by using two reflectors: the first (or main reflector) is a parabola and the latter is a hyperbola, named sub-reflector.

In the Cassegrain system the feed is not placed in the focus of the main reflector but, along its axis, generally near the vertex: providing that the primary and secondary reflectors are respectively a parabola and a hyperbola, the rays reflected by the primary reflector are converted in parallel rays, likely if these rays come from the focal point of the main reflector.

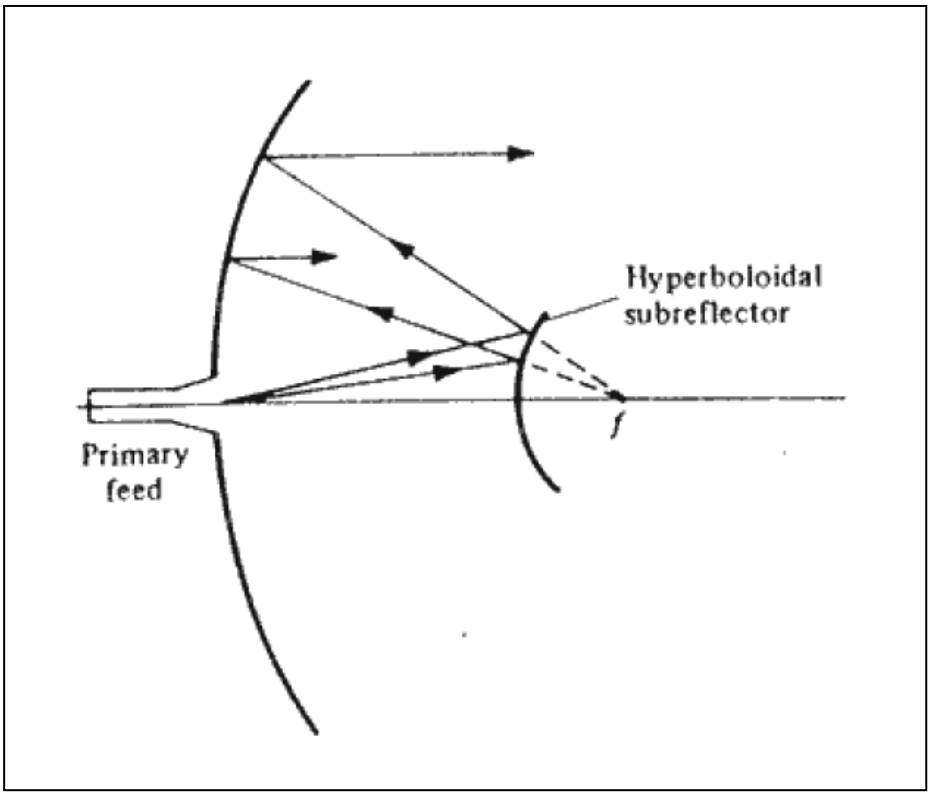

Figure 3.9: *Cassegrain fed system [2]*.

In the Cassegrain configuration the transmitting and receiving equipment can be placed behind the primary reflector, making the system relatively more accessible for maintenance.

In the Gregorian configuration, the sub-reflector is elliptic and placed in such a way that one of the two ellipsoid foci coincides with the focus of the primary reflector (the paraboloid), the feed is instead disposed in the other ellipsoid focus (figure 3.10).

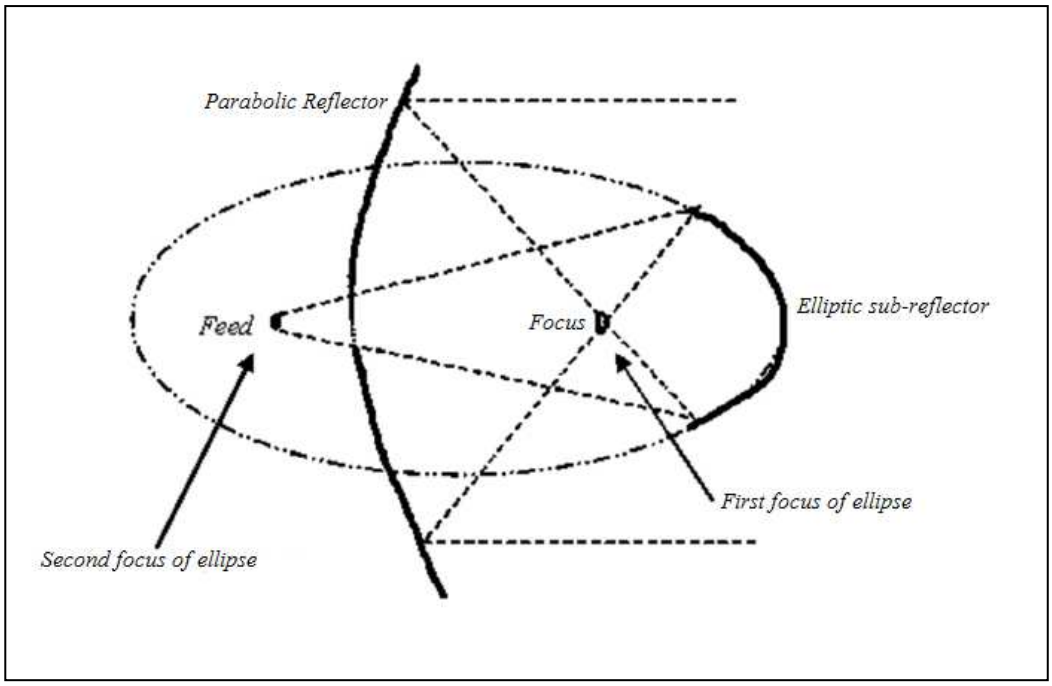

Figure 3.10. *Gregorian fed system.*

In this system the rays reflected by the dish appear to be parallel: as a matter of fact, by conics properties, each ray having origin in the feed and reflected on the sub-elliptic reflector passes through the focus of the main reflector.

The Cassegrain and Gregorian reflector configurations are widely employed in radio astronomy applications and allow therefore to reduce the spill-over losses.

Despite these advantages, the dual reflector configuration show manufacturing problems and also an increment of blockage losses and cross-polar component.

3.6. Short description of shaped beam reflectors [3].

The search rotating RADAR antennas are characterized by a narrow beam in the azimuth plane and by a shaped beam in the elevation plane. These features allow to easily distinguish between two near targets, and to obtain an uniform coverage at constant altitude.

The easiest way to achieve a shaped beam is to employ multiple feeds positioned on the focal plane of the reflector (figure 3.11b) or a single feed locate in a different location from the focus of the reflector (figure 3.11a).

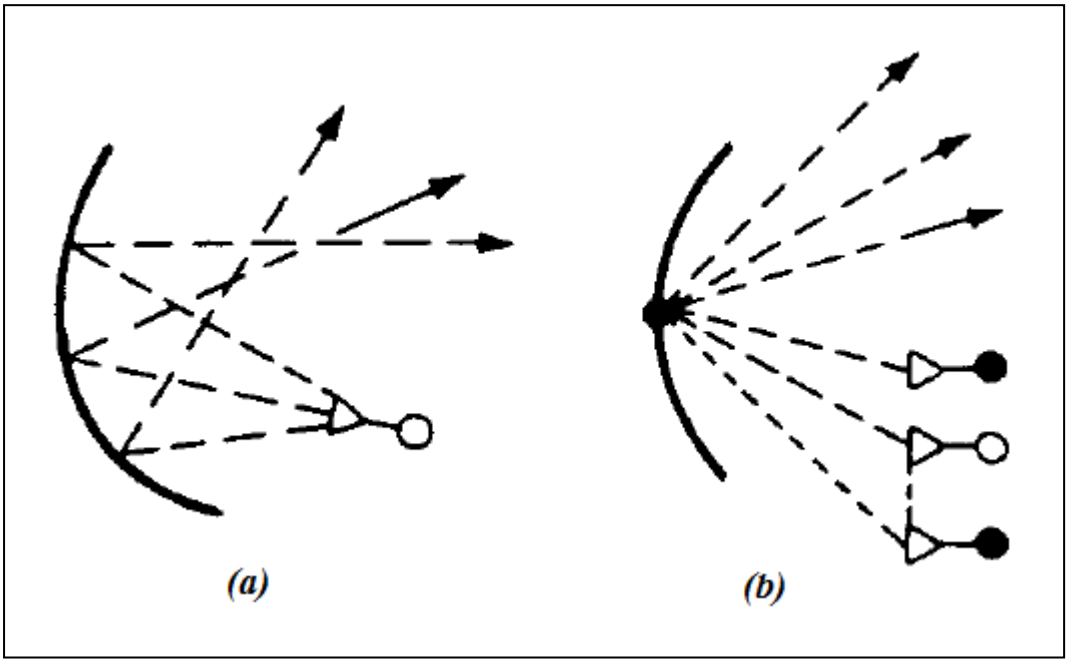

Figure 3.11. *Shaped beam reflectors [3].*

As a matter of fact, the phase of the reflected rays depend on the position of the feed: with these two arrangements, the rays coming on the antenna aperture will have different phases, allowing to achieve a beam with specified shape.

Most shaped reflectors avoid the blockage losses placing the feed outside the focus position: an example of shaped reflector with offset fed is the ASR-9

RADAR antenna (fig. 3.12). In this device, the elevation shaping, the azimuth beam skirt and side-lobes are strictly controlled using a CAD design process.

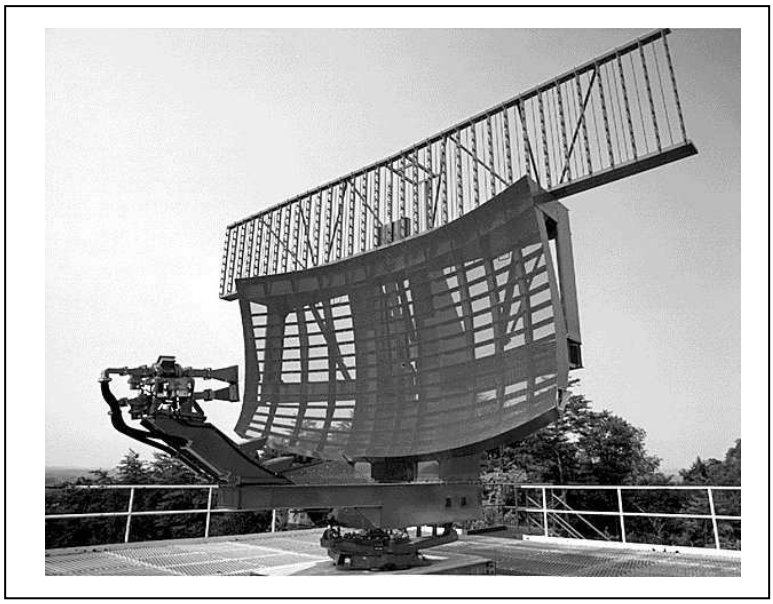

Figure 3.12. *ASR-9 shaped beam radar antenna.*

An alternative way to obtain a shaped beam keeping the single fed configuration (with or without offset) is to shape the reflector (figure 3.13): starting from the desired beam configuration, it is possible, with numerical techniques to modifies the reflecting dish surface, in order to achieve the desired radiated beam.

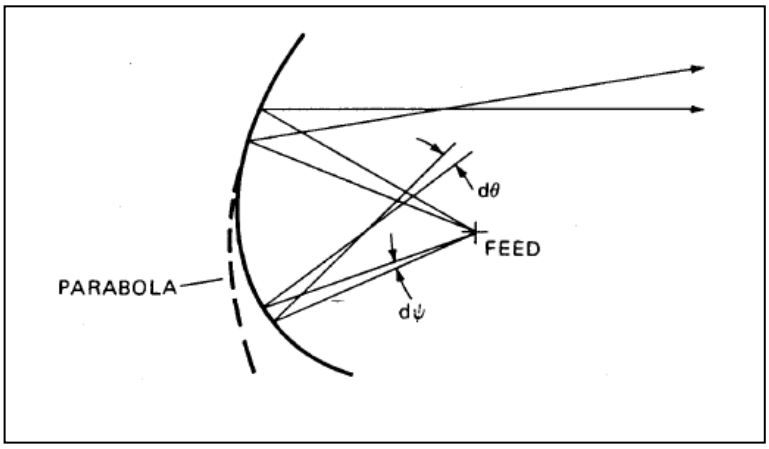

Figure 3.13. *Reflector shaping [3].*

3.7. Short description of parabolic cylinder reflectors [3] .

The parabolic cylinder reflector antenna is an alternative configuration for the parabolic reflector, widely used in RADAR applications. In this configuration, the reflecting surface is a portion of inner lateral surface of a cylinder, and the focus is the axis of the cylinder. In applications, the sources employed to illuminate the reflector surface are linear and usually consist of linear dipoles, linear arrays or slotted waveguides.

The equation of reflector shape in rectangular coordinates is:

$$z = \frac{y^2}{4f} \tag{3.19}$$

Where *f* is the focal length.

In figure 3.14 a typical geometry of a cylinder reflector is shown:

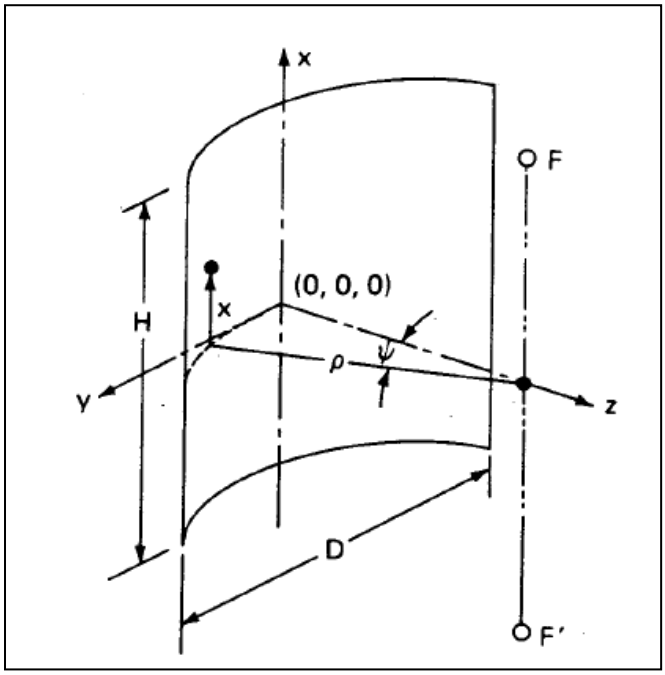

Figure 3.14. *Cylinder reflector geometry [3].*

In most cases, the feed line is placed in the focal line *F-F'* , although offset configuration are possible in order to avoid blockage losses. Depending of

applications, this reflector configuration allows to obtain a steerable or shaped beam in the elevation or azimuth plane with modest cost.

An example of parabolic cylinder reflector antenna for RADAR applications is shown in figure 3.15.

Figure 3.15. *AN/TPS-63 radar antenna.*

Chapter 4.

Feed for reflector antennas.

4.1 Introduction [2].

As mentioned in chapter 3, parabolic reflector antennas are widely used in radio-astronomy applications, communications, remote sensing and radar.
A critical point in the design of reflector antennas is the choice of the feed: as a matter of fact, the feed must be a point source radiator, because the reflecting surface of the dish converts incoming plane waves into spherical fronts centered at the focus and vice-versa. The feed must also provide an adequate illumination of the reflector with minimum spill-over and cross-polarization, and it must also be able to handling the average power levels required by the system without break-down.
For these reasons, open rectangular or circular waveguides are frequently used as the primary feed to illuminate a reflector antenna.

4.2 Open Waveguides Feeds [2].

Let us consider an electromagnetic field propagating inside a rectangular waveguide (figure 4.1) of dimensions *axb* : if we "cut" the waveguide with a transverse plane, the field radiates in the space through the aperture.

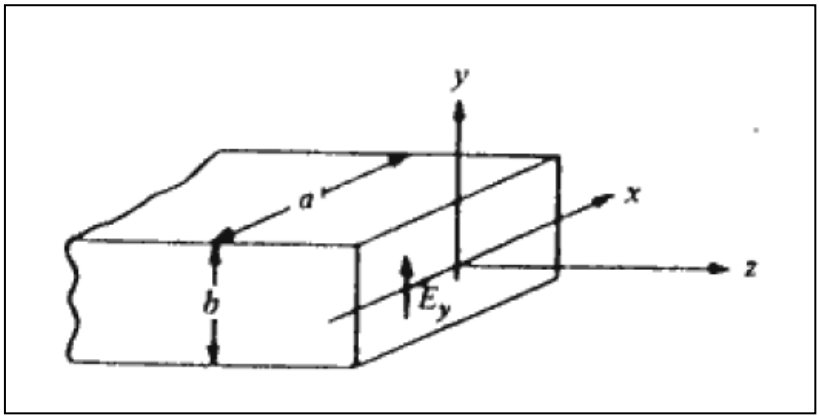

Figure 4.1. *Open rectangular waveguide [2].*

The dominant propagating mode in the rectangular waveguide is the TE_{10} (transverse electric) mode; placing the origin of the coordinate system in the center of the aperture, the *x* component of the magnetic field and the *y* component of the electric field are given by:

$$\underline{E} = V^+ \sqrt{\frac{2}{ab}} \cos\frac{\pi x}{a} \cdot \underline{i}_y$$

$$H = -\frac{V^+}{Z_{10}} \sqrt{\frac{2}{ab}} \cos\frac{\pi x}{a} \cdot \underline{i}_x \tag{4.1}$$

If we neglect the reflected dominant mode and the small amplitude higher mode excited in the open end of the waveguide, and suppose that outside the aperture both the *x* and *y* component of the field are negligible on the *z=0* plane, the equation (4.1) may be considered to specify the aperture fields on the *z=0* plane.

In practice, this approximation provides a reasonably good estimate of the main lobe. In applications where waveguides are utilized as feed for reflector antennas, these assumptions are usually acceptable because we focus on the characteristics of the main lobe.

The field radiated by the aperture can be evaluated considering the magnetic current M_s on the open end of the waveguide:

$$\underline{M}_s = -i_z \times \underline{E} = -i_z \times E_0 \cos\frac{\pi x}{a} \underline{i}_y = E_0 \cos\frac{\pi x}{a} \underline{i}_x \tag{4.2}$$

Where $E_0 = V^+ \sqrt{\frac{2}{ab}}$

Using the field equivalence principle, it is possible to compute the radiated far field in the yz and xz plane (E_θ and E_φ component respectively) which are proportional to:

$$E_\theta \propto \frac{2}{\pi} ab \cdot E_0 \frac{\sin[k_0 (b/2) \sin\theta]}{k_0 (b/2) \sin\theta} \tag{4.3}$$

$$E_\theta \propto \frac{\cos[k_0 (a/2) \sin\theta]}{[k_0 (a/2) \sin\theta]^2} \cos\theta \tag{4.4}$$

Where $k_0 = \frac{2\pi}{\lambda_0}$.

Using equations (4.1), (4.2), (4.3), (4.4), after some considerations the power radiated by the open waveguide can be written as the maximum of the Poynting vector:

$$|S_{MAX}| = \frac{|V^+|^2}{\zeta \cdot r^2} \frac{ab}{4\pi^2} (\beta_{10} + k)^2$$

(4.5)

Where $\beta_{10} = \frac{\omega\mu}{Z_{10}}$

Starting from this expression we find that the directivity of the structure is equal to:

$$D = \frac{Z_{10}}{\zeta}\frac{2ab}{\pi}\left(\frac{\beta_{10}+k}{\pi}\right)^2 \tag{4.6}$$

By replacing *ab* with πr^2, equation (4.6) provides a good estimate of the directivity for the circular truncated waveguide.

Typical values of directivity for the truncated waveguides are very low (usually about 4 dBi) because they depend by the physical dimensions, much smaller than the wavelength.

4.3. Horn Feeds [2].

The solution to obtain high values of directivity in equation (4.6) is to modify the sizes *a* and *b* in order to increase the product *ab*. For this reason, and in order to avoid the problems due to reflection, the width *a* is tapered to *a′* (with *a′>a*) by flaring the waveguide in the H-plane. The obtained structure, shown in figure 4.2, is called *H-Plane horn*.

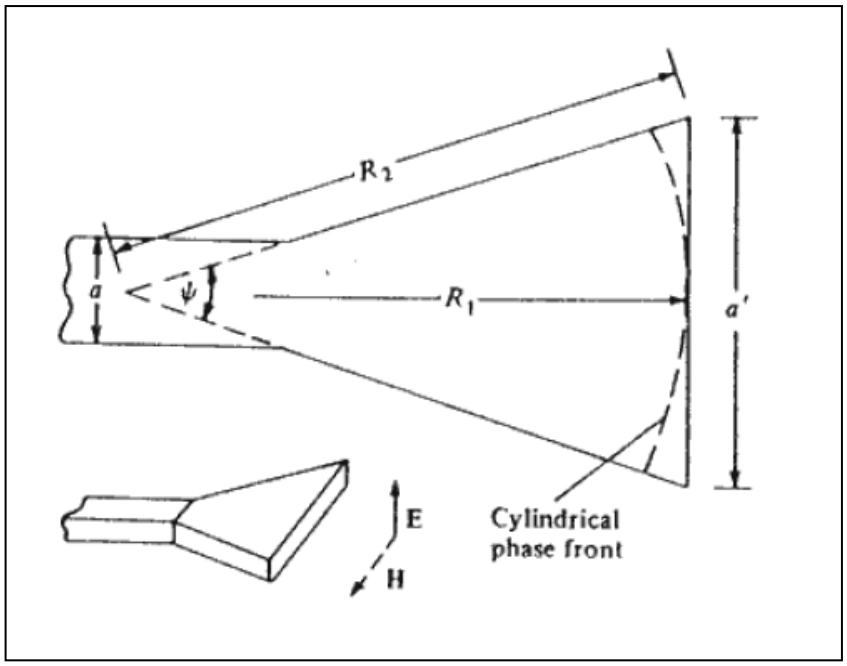

Figure 4.2. *H-Plane horn [2].*

The field propagating inside the horn and coming from the input waveguide is a cylindrical wave with a circular constant-phase front, and it is nearly in-phase with the aperture field if the flare angle ψ is small. If the phase error does not exceed $\pm\pi/4$ at the side of the aperture, the gain and the radiation pattern are very close to the values obtained for a constant-phase aperture field. By referring to figure 4.2, the condition on phase error can be expressed as:

$$k_0(R_2 - R_1) \leq \frac{\pi}{4} \tag{4.7}$$

After some considerations, equation (4.7) gives:

$$\tan\frac{\psi}{4} \leq \frac{\lambda_0}{4a'} \tag{4.8}$$

Plotting the previous equation as a function of a'/λ_0, we obtain that it is possible to achieve large apertures, and consequently high gains, if the values of the flare angle ψ are small (figure 4.3), resulting in very long and bulky horns.

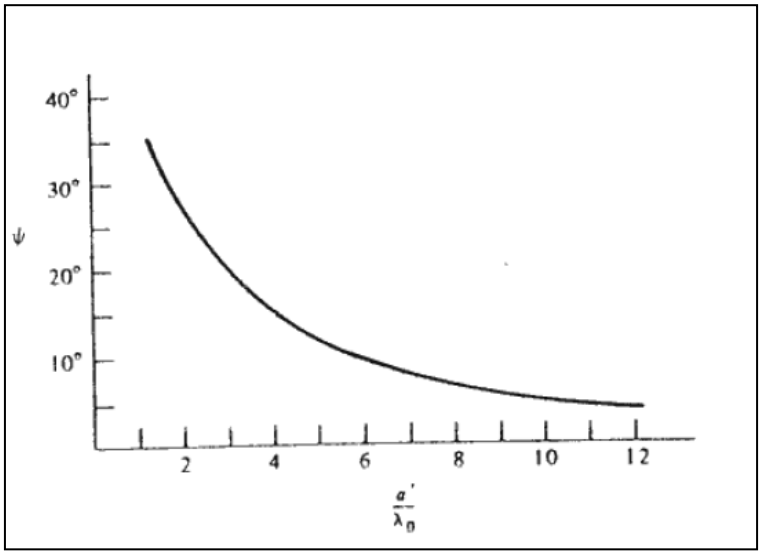

Figure 4.3. *Flare angle ψ as a function of ratio a'/λ_0. [2]*

The directivity of an H-plane horn antenna is given by the expression:

$$D = \frac{10.2}{\lambda_0} \cdot a'b \tag{4.9}$$

The value of the gain for this structure is almost equal to the directivity, due to very small losses and reflections of waveguide structures. By analyzing the effects of the phase error on the antenna gain, it is found that, for a fixed length, the maximum gain is obtained by increasing the aperture width a' until a phase error of around $3/4\pi$ occurs.

It is also possible to obtain an E-Plane horn (figure 4.4), by increasing the height b of the waveguide instead of the width a.

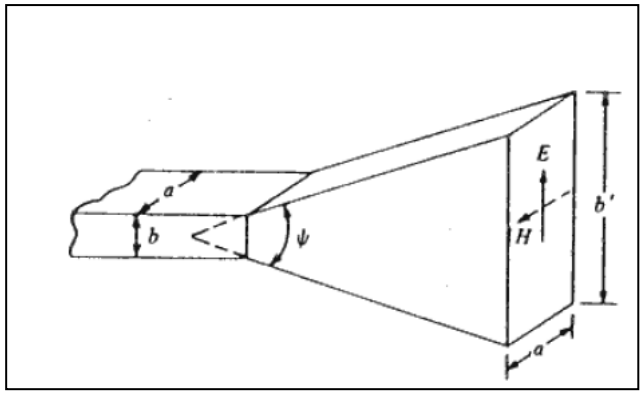

Figure 4.4*. E-Plane horn [2].*

The theoretical considerations regarding the directivity of the E-plane horn are the same of the H-plane horn, providing to replace in equation (4.9) b and a' with b' and a respectively.

For an E-Plane horn, it is possible to achieve the maximum gain by increasing b' until a phase error of $\pi/2$ occurs.

By comparing the E-Plane and H-plane horn we notice that the tolerable phase error for the H-plane horn is larger: as a matter of fact, in the H-plane the aperture field goes to zero at both sides of the aperture, while for the E-plane horn the aperture field is constant in the E-plane.

A further increase of gain for these structures it is possible by using the pyramidal horn: in this device, shown in figure 4.5, the waveguide is flared both in E-plane and H-plane, acting on a and b sides at the same time.

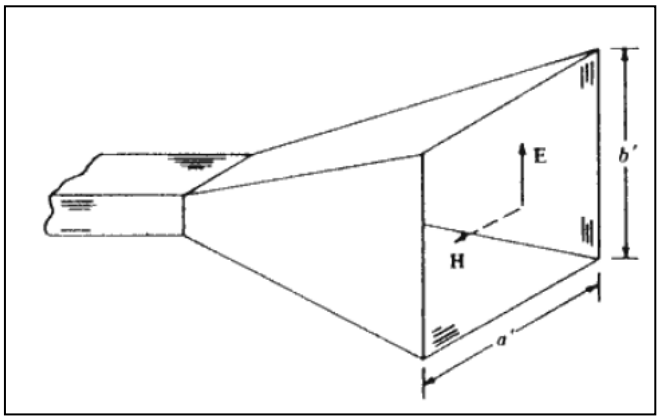

Figure 4.5. *Pyramidal horn [2].*

For a pyramidal horn of fixed length, the maximum gain is obtained by increasing the flare angles to allow a phase error of around $3\pi/4$ and $\pi/2$ in the H-plane and E-plane respectively. The directivity of pyramidal horns is expressed by:

$$D = \frac{6.4}{\lambda_0} \cdot a'b' \tag{4.10}$$

Due to their characteristics of radiation (reasonable gain, low cross-polar component of radiated field, low reflection coefficient), horn antennas are widely used as feed for reflector antennas. In the last years a large number of technical papers (i.e. [9] - [13]) and book chapters ([1], [14] - [17]) are dedicated to design and improve the radiation characteristics of the horn antennas.

4.4. Microstrip printed feeds.

Microstrip printed antennas, with their small weight and size, low cost and ease of fabrication and integration with other devices, represent an alternative to feed reflectors. Despite these advantages, single microstrip antennas are not widespread in reflector applications, due to their high level of cross polarization in the radiated field and to the difficult in shaping their radiation pattern [14].

To overcome these problems, an array configuration can be used: in [18] and [19] a series of 2x2 patch array are used to feed reflectors and, with an adequate element spacing, a good gain and a -20 dB side lobe level are obtained.

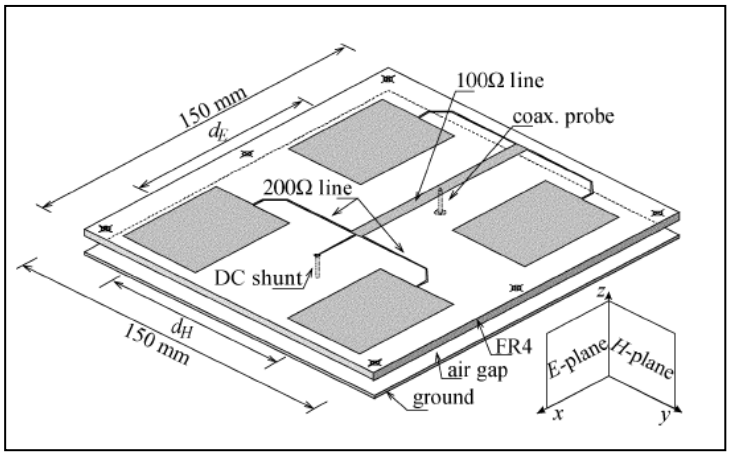

Figure 4.6. *2x2 printed patch array feed [19].*

Small linear arrays are also employed [20] in a multifunctional reflector antenna system.

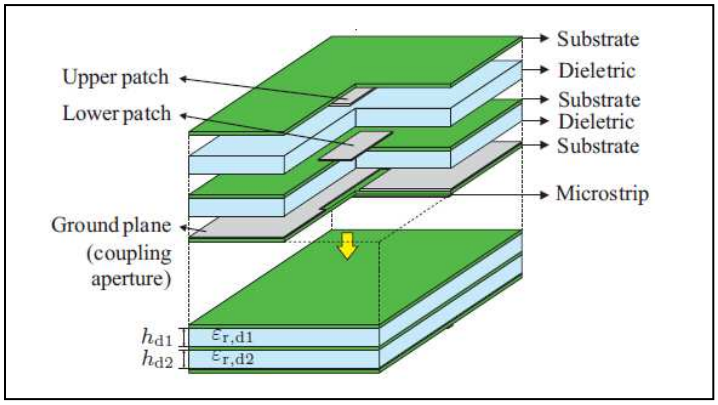

Figure 4.7. *Stacked patch antenna [21].*

In [21] a broadband stacked patch antenna is used to feed an ellipsoidal reflector, obtaining a gain of 18.1 dB. The stacked configuration in microstrip patch arrays is useful in reflector feeds for space-craft applications, where the low cost and reduced sizes are desirable characteristics: in [22],

an hexagonal array of seven elements and a square array of nine elements are presented, with results similar to an horn feed operating in the same frequency band with a gain of 15 dBi and a -20 ÷ -25 dB side lobe level.

Multilayered patch arrays are also employed in the design of dual polarized reflector feeds [23].

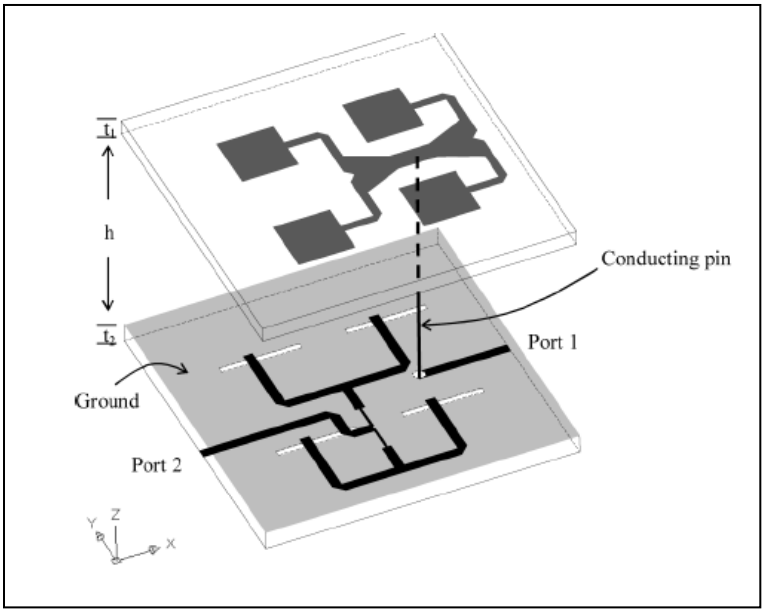

Figure 4.7. *Dual polarized suspended patch array [23].*

In reflector antennas operating in modern communications systems and in some radar applications (i.e. weather radar), in addition to constraints regarding the high gain and low side lobe level, the requirement of wide operating band is very important [24]: in telecommunication system broadband characteristics allow to carry a greater amount of information with high data rate; in weather radar the heterogeneity of hydrometeors requires that the antenna operates at different frequencies. All of these applications involve reflector antennas with feeds capable to operate in a broad frequency range: the log-periodic dipole arrays (LPDA), with their very large bandwidth (up to a decade) and their reasonable gain, are excellent candidates for broadband reflector feed systems [25].

In the last years, a large number of LPDA (wired or printed) feeds have been proposed, and their characteristics as feed have been extensively investigated by Duhamel and Ore in [26].

Due to their asymmetric radiation pattern, in order to obtain a symmetrical radiated field, often a LPDA feed consists of two or more antennas: in [27] and [28] feeds based on two LPDA with a wide operating bandwidth (from 1 to 10 or 20 GHz) have been proposed.

Multiple log periodic antennas also allow to design feeds operating at different polarization: in [29], a cryogenically cooling feed system for the VLBI (Very Long Baseline Interferometry 2010) and

SKA (Square Kilometers array) is able to receive both the dual linearly and circularly polarized field [30].

Another LPDA feed for the dual-reflector antenna of US-SKA is proposed in [31].

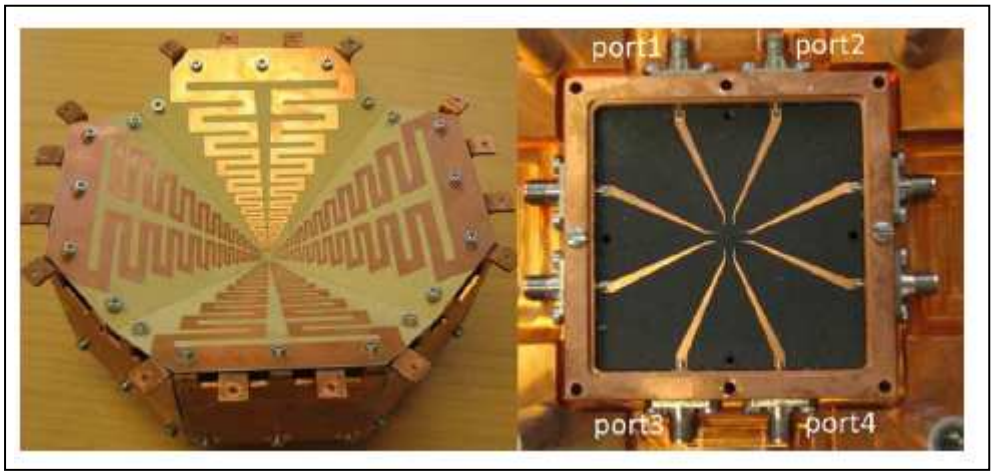

Figure 4.8. *Multiple log periodic antennas feed [29].*

Chapter 5.

Printed Log-Periodic Feeds

5.1. Introduction.

A printed log periodic feed is a broadband directional antenna, whose properties are regularly repetitive as a logarithmic function of the excitation frequency. Even the length and spacing of the elements of a log-periodic antenna increase logarithmically from one end to the other. This kind of antenna is useful in all the applications requiring a wide range of frequencies to be covered with a reasonable gain. The log-periodic concept has been implemented using different elements, but the most popular, by far, is the log-periodic dipole array (LPDA) [32]. In an LPDA, alternating elements must be driven with 180° of phase shift from one to another. This phase shift, in a wire LPDA, is normally implemented by connecting individual elements to the wires of a balanced transmission line in an alternate way. LPDAs using cylindrical dipoles have been proposed by Du Hamel in the 1957 [32]. They are extensively used as wideband antennas, and their design can be performed following the suggestions given by Carrel and Isbell [33]–[35]. Wire LPDAs can be designed with a bandwidth up to a decade, and with a typical gain around 10 dBi in air [36], and realized at VHF and UHF frequencies, with a standard and cost-effective technology. Unfortunately, such advantages are lost in the SHF band, where the dipoles become so short and tiny that they can be realized only by specialized technologies [37].

On the other hand, printed LPDAs are very promising, due to their low production cost and weight. However, their realization can be difficult since all elements must be fed (and with alternate sign) by a paired strip (PS) [38]. Therefore, an appropriate feeding network must be designed in order to excite each element with the requested phase. As a matter of fact, the design and modeling of this feeding network has been the most critical task in the different printed LPDAs that have been proposed in the literature [39]–[43].

The feeding network can be divided into two parts: the printed dipoles feeding line, and the external feeding structure. In the antenna simulation, the LPDAs external feeding is modeled as a differential port placed at the narrow end of the antenna, providing the necessary wideband matching. However, this is an ideal device because it does not physically incorporate the actual external feeding line and the geometry of the SMA connector. In practice, the wideband matching of a LPDA can be obtained with an infinite balun [44]. In the wire LPDA antennas employed for TV receivers, this infinite balun is realized with a coaxial cable passed through one of the antenna booms and connected to the narrow side of the antenna. In the printed LPDA this infinite balun has been obtained soldering the

outer conductor of a coaxial cable to the bottom layer of the LPDA, and connecting the inner conductor to the top layer of the antenna using a via-hole inside the substrate [45]. This allows an antenna with a reasonably large matching and gain bandwidth, but destroys the antenna symmetry.

In this chapter we will propose two new methods to overcome the problems due to the printed log periodic feeding network: in paragraph 5.2 we will show [46] that the insertion of an additional mirror coaxial cable, soldered in the top layer of the array, allows to obtain not only an excellent input matching and a very good radiation pattern over the whole frequency band, but also the stabilization of the antenna phase center; after these considerations, in paragraph 5.3 [47], because the additional coaxial cable is not simple to realize since printed LPDAs at microwaves frequencies can be very small, a fully planar feeding network without any shorting pins is proposed. These two solutions have been tested in the design of two printed LPDA antennas operating respectively in the range 4-18 GHz and 3-6 GHz. Both the proposed configurations have been employed as feeds for reflector antennas. The obtained results provided the starting point for the design of a high gain log-periodic feed for weather radar applications, operating in S and C band and described in paragraph 5.4.

All the proposed structures have been designed and optimized using CST Microwave Studio 2012, a general-purpose software for the 3-D electromagnetic simulation of microwave components. The analysis of the performance of the reflector configurations have been performed using TICRA GRASP 8W, an integrated tool for reflector antenna analysis.

5.2. Design of printed log periodic array working in C, X and Ku band.

The concept of log-periodic wire-antennas is applied to microstrip printed technology, to get the antenna layout shown in figure 5.1. The array dipoles are fed (in an alternate way) with two microstrip lines printed on the opposite sides of a dielectric slab (as in Figure 5.2a). As a consequence, the standard approach for the design of LPDAs proposed by Carrel [33] can be used, but with some modifications.

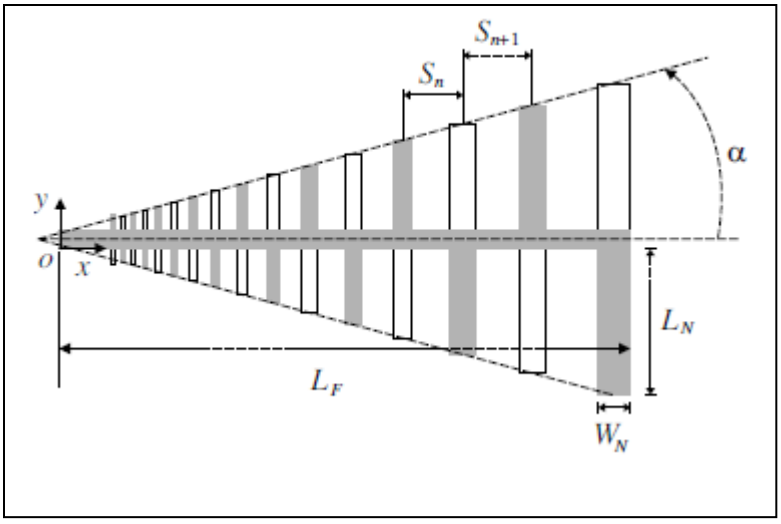

Figure 5.1 *Antenna layout: dark lines on the upper side of the dielectric slab, transparent ones on the bottom.* L_F*=56.92mm.*

Starting from the required bandwidth (4-18 GHz), and following the design rules given in [33], we get the following antenna parameters: number of dipoles $N = 15$, aperture angle $2\alpha = 30°$, log-period $\tau = 0.85$ for an average directivity of 8.5 dB. The wideband matching of the printed LPDA is obtained with an infinite balun, realized with a coaxial cable. The outer conductor of the coaxial cable is soldered to the bottom layer of the LPDA, and the inner conductor is connected to the top layer of the antenna using a via-hole inside the substrate.

In order to improve the antenna performances, an additional mirror coaxial cable, soldered in the top layer of the array, can be used. We have selected the characteristic impedance of the feeding line equal to 50 Ω, so as to obtain an easy matching with the coaxial cable. Since the feeding line (figure 5.2a) has an anti-symmetric field configuration, its corresponding width can be computed by inserting a dummy ground plane in the middle of the substrate (figure 5.2b) [48, 49].

As a consequence, we can simply design a 25 Ω standard microstrip (with $h=2$ slab thickness) and evaluate its corresponding width W by assuming a quasi-static propagation.

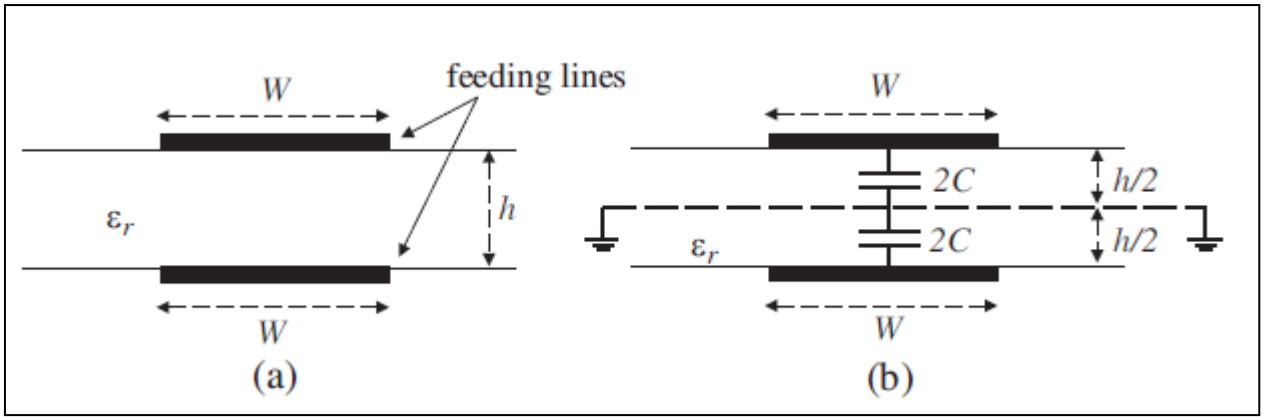

Figure 5.2. *(a) Section of the antenna feeding line. (b) Equivalent circuit for the computation of the line parameters.*

Since the printed LPDA lies on a dielectric substrate, the geometric parameters of this antenna cannot be computed as in the case of a standard wire-LPDA [33], which radiates in free space. In our prototype we have used a Arlon AD 250 substrate (with $\varepsilon_r = 2.5$ and $h = 0.51\ mm$), for which the width of the 50 Ω feeding lines is $W = 1.91\ mm$. For this specific substrate, the resonant length $2L_N$ of the largest dipole (see Figure 5.1) at the lowest operating frequency (4 GHz) is computed by using CST Microwave Studio, and is equal to 14.665 mm. The length of the other dipoles is computed according to:

$$\frac{L_{n+1}}{L_n} = \frac{1}{\tau} \qquad n = 15,...,1 \tag{5.1}$$

Now, we must compute the width W_N of the largest dipole. Let us consider the following expression:

$$Z_n = \frac{\eta_0}{\pi}\left[\ln\left(\frac{L_n}{a_n}\right) - 2.25\right] \tag{5.2}$$

Which was derived by Carrel [35] as the average characteristic impedance of a cylindrical dipole, wherein a_n is the radius of the dipole, and L_n its half-length. We select the radius a_n of the largest dipole in order to give a 50 Ω average characteristic impedance. Then, we compute W_N by the requirement of equivalent perimeter [50]:

$$W_N = \pi \cdot a_n \tag{5.3}$$

The width of the others dipoles (see figure 5.1 and equation 5.4) are summarized in table 5.1, and their spacing are computed accordingly to [33].

$$\frac{W_{n+1}}{W_n} = \frac{1}{\tau} \qquad n = 15,...,1 \tag{5.4}$$

Dipole	L_n [mm]	W_n [mm]	S_n [mm]
1	1.507	0.33	
2	1.773	0.39	0.99
3	2.086	0.45	1.17
4	2.454	0.54	1.38
5	2.887	0.63	1.62
6	3.397	0.74	1.90
7	3.996	0.88	2.24
8	4.701	1.03	2.63
9	5.531	1.21	3.10
10	6.507	1.42	3.64
11	7.655	1.67	4.28
12	9.006	1.97	5.04
13	10.595	2.32	5.93
14	12.465	2.72	6.98
15	14.665	3.20	8.21

Table 5.1. *Geometry of the designed printed LPDA.*

The coupling between the coaxial feeding network and the radiating dipoles degrades the antenna matching, especially in the upper frequency band, where the dipoles are very small. In order to improve the antenna performances at high frequencies, a further dipole is inserted immediately before the dipole 1, with the same width and length, and with a spacing equal to the one between dipole 1 and dipole 2. The inclusion of this further dipole does not imply any change in the overall size of the antenna, but is able to lower the return loss below -10 dB in the whole operating bandwidth, as we will show later.

However, the a-symmetric fed configuration due to single coaxial cable utilized, shows a significant drift of the phase center with the frequency. Therefore, to overcome this problem, the insertion of an additional mirror coaxial cable, soldered in the top layer of the array, has been investigated. The simulations have shown that the latter has significantly better radiation performances, and therefore the designed antenna has been manufactured with the mirror coaxial cable (see figure 5.3). Figure 5.4 shows both the simulated and measured frequency responses of the input reflection coefficient.

We have found that the additional mirror coaxial cable does not modify the antenna input matching, therefore this case is not reported in figure 5.4. As apparent, the broadband specification between 4 and 18 GHz is fulfilled with a good agreement between simulation and measurement.

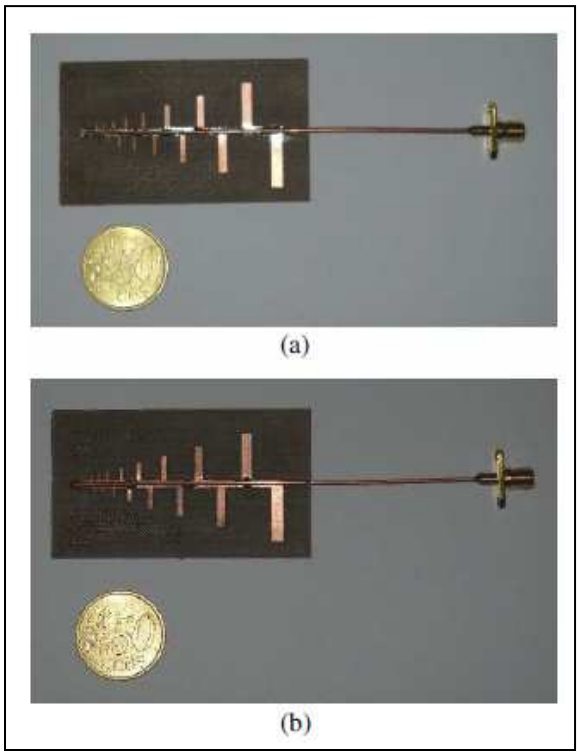

Figure 5.3. *Photo of 4-18 GHz LPDA antenna. (a) Front. (b) Back.*

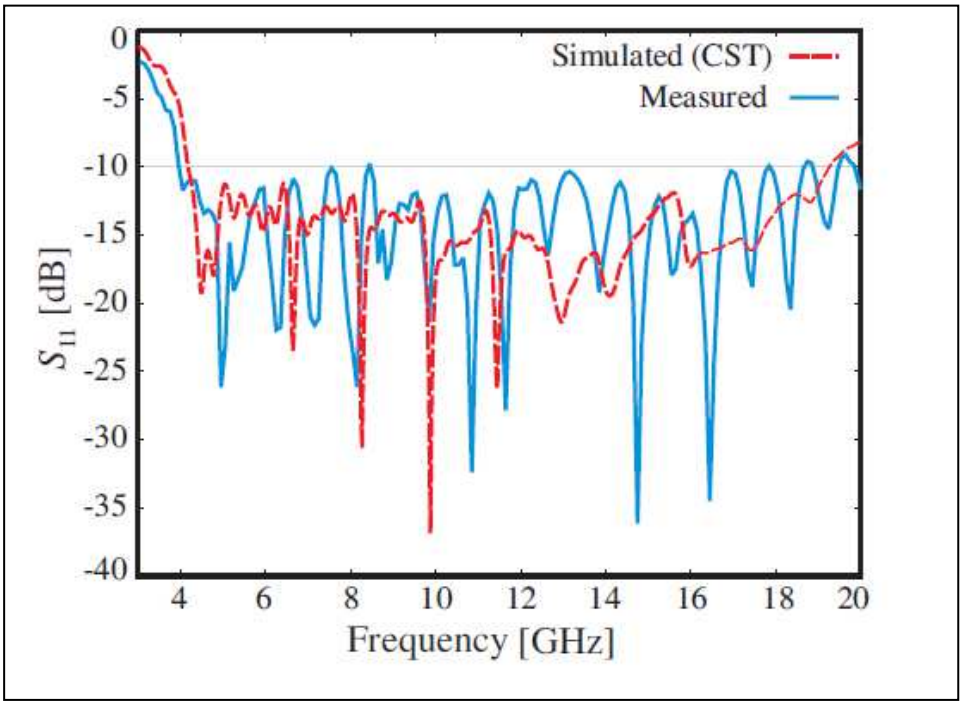

Figure 5.4. *Reflection coefficient of the 4-18 GHz LPDA antenna.*

In figure 5.5 the antenna gain (evaluated by CST) with respect to frequency is reported, both for the configuration with or without mirror coaxial cable. The antenna gain is quite stable over the required bandwidth.

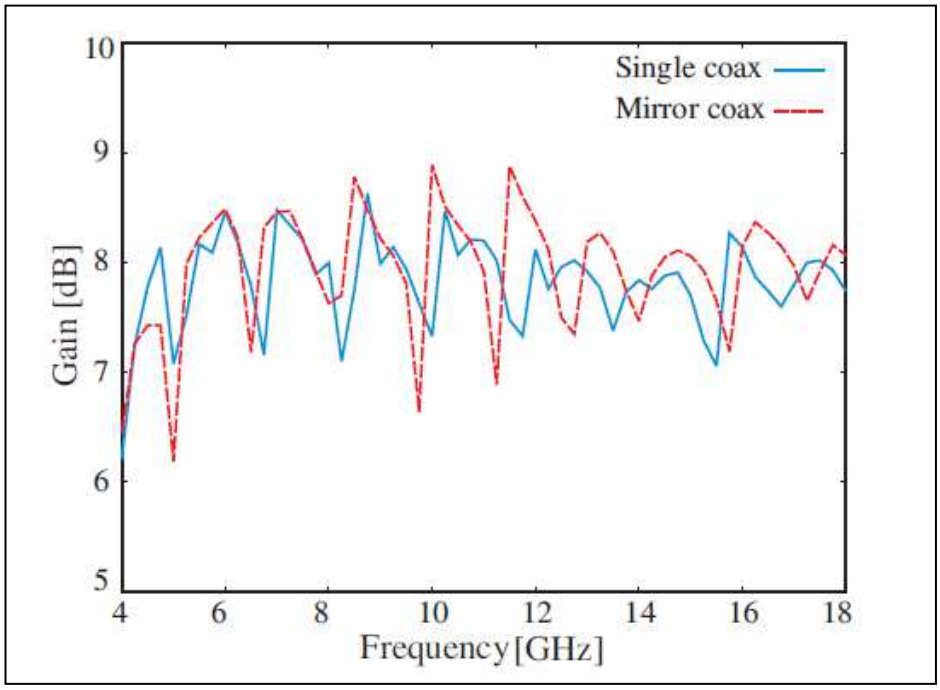

Figure 5.5. *Gain of the 4-18 GHz LPDA antenna.*

The phase center variation as a function of the frequency is computed by using CST Microwave Studio and is reported in figure 5.6, where Delta is the distance between the phase center and the origin *O* of the coordinate system in Figure 5.1. The comparison with the feeding configuration using a single coaxial cable is also shown. Using a single coaxial cable in the implementation of the feeding network, the phase center remains almost constant in the frequency band 5.5-11.25 GHz, wherein it varies from *30 mm* to *50 mm* (with a maximum variation equal *to ±10 mm*, i.e., ±0.25 λ_0, being $\lambda_0 = 40$ *mm* the free-space wavelength at the center frequency of 8.375 GHz). From the results shown in figure 5.6, it appears that the presence of the mirror coaxial cable allows to stabilize the phase center up to 13 GHz. As a matter of fact, in the configuration with the mirror coaxial cable the phase center is stable in the frequency band 4.25-13.25 GHz, with a relative bandwidth greater than 100%, with a maximum variation equal to *28 mm*. It is worth noting that, if we limit ourselves to a 30% smaller frequency band, namely 4.25-10.75 GHz, the phase center variation halves to *15 mm.*

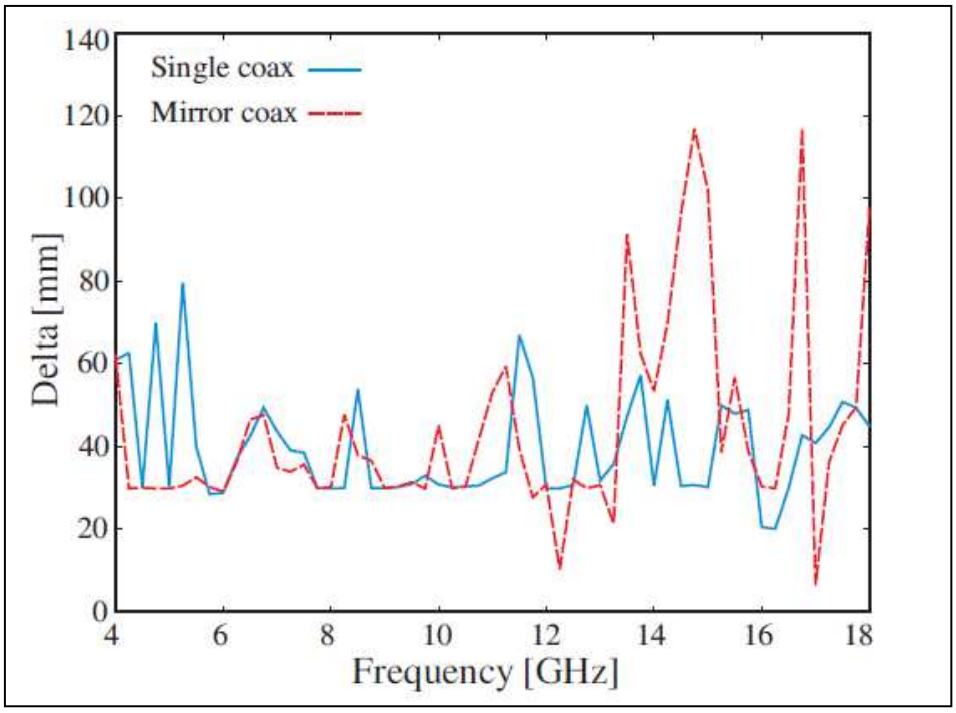

Figure 5.6. *Variation of phase center.*

In figures 5.7 and 5.8, the simulated and measured E-Plane and H-Plane radiation patterns are reported, respectively.

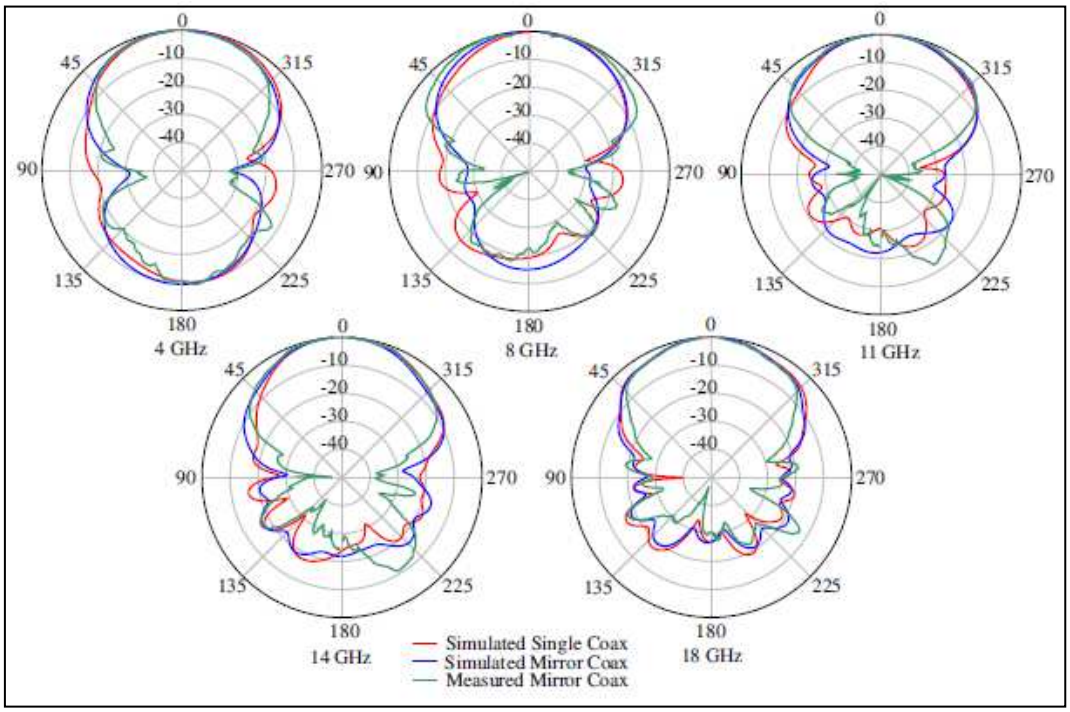

Figure 5.7. *Simulated and measured E-plane far field.*

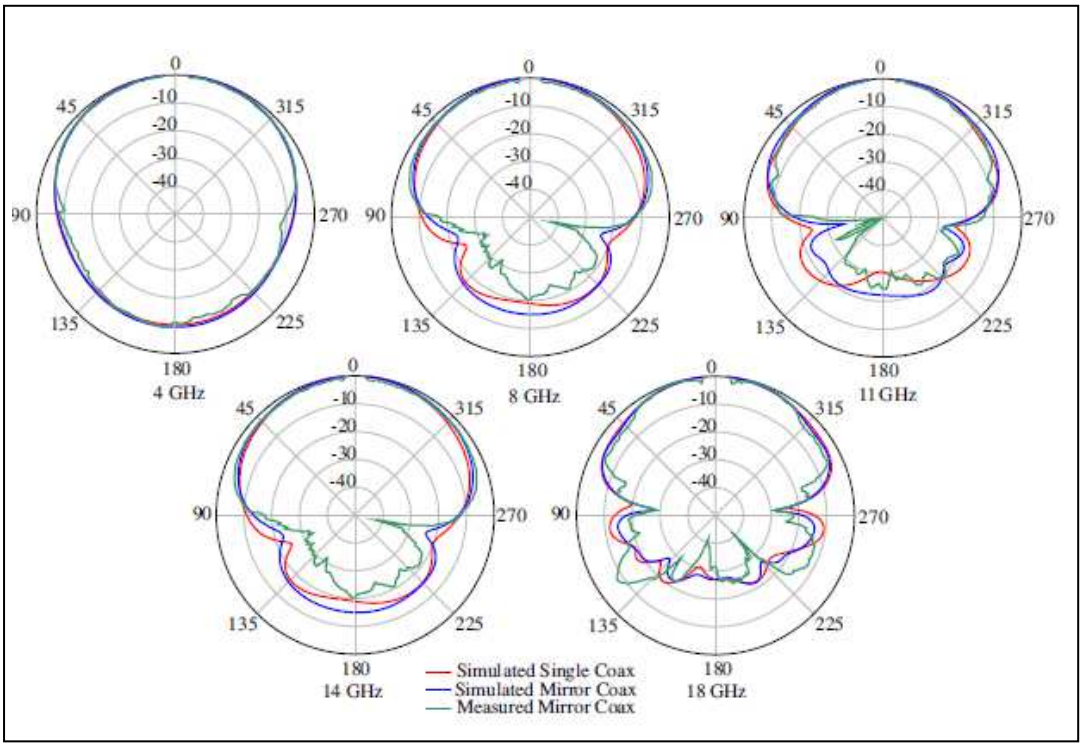

Figure 5.8. *Simulated and measured H-plane far field.*

The comparison between the simulated far field of the configuration with and without the mirror coaxial cable shows that the last configuration allows a significant improvement on the radiated field, which is in this case more symmetrical and with a lower side lobe level. The measured far field pattern, reported only for the configuration with the mirror coaxial cable, is in very good agreement with the simulations.

After these considerations, the configuration with mirror coaxial cable has been employed as feed for a parabolic reflector with *d=8 m* diameter, in order to obtain a *47 dBi* gain at 4 GHz.

As mentioned in chapter 3, all parabolic dishes have the same curvature, but some are shallow dishes while others are much deeper, and more are like a bowl. A convenient way to choose the size of the dish is the desired gain (see equation 3.18) and the *f/d* (focus to diameter) ratio (see chapter 3), which is related to the feed beamwidth and to the angular reflector aperture: as *f/d* becomes smaller, the feed pattern illuminating the reflector surface becomes broader.

A way to match the feed pattern radiated field with the angular aperture ψ_r is described by equation [51]:

$$\psi_r = 4 \cdot arctg\left(\frac{d}{4f}\right) \tag{5.5}$$

In equation (5.5), by setting the diameter *d* of the reflector, it is possible to achieve the optimal *f/d* by imposing the angular aperture ψ_r equal to 10 dB feed beamwidth [52].

Frequency (GHz)	E-Plane 3dB Beamwidth (degree)	H-Plane 3dB Beamwidth (degree)
4	68.4	118.5
8	66.4	113.3
11	60.7	94.3
14	55.5	85.3
18	54.6	82.6
Mean value	61.12	98.8
M_T	80	

Table 5.2*. 3dB 4-18 GHz printed LPDA feed beamwidth.*

In our case (see table 5.2), for the 4-18 GHz LPDA printed feed, the beamwidth of E-plane and H-plane radiated field is different (see figures 5.7 and 5.8), and choosing the angular aperture ψ_r equal to 10 dB feed beamwidth will result in a not satisfactory illumination of the reflector surface, especially in the central region. Therefore, the *f/d* ratio is computed by choosing ψ_r equal to mean value M_T of 3 dB antenna beamwidths in E-plane and H-plane. As indicated in table 5.2, ψ_r is equal to *80*°, and from equation (5.5) the corresponding value *f/d* is equal to 0.*678.*

According with the obtained *f/d* ratio, the focal length *f* for a 8 meters diameter reflector is equal to 5.244 meters. In figures 5.9-5.13 the $\theta=0°$ normalized simulated radiated far field cuts for such reflector antenna at 4, 8, 11, 14, 18 GHz are shown. The result obtained exhibit a side lobe level equal to about -17 dB and a good gain (see table 5.3) over the whole operating bandwidth, allowing the use of 4-18 GHz LPDA printed feed with mirror coaxial cable in reflector antennas for wide band communication systems.

Frequency	Gain
4	46.72
8	53.35
11	56.30
14	58.03
18	60.76

Table 5.3. *Reflector antenna gain.*

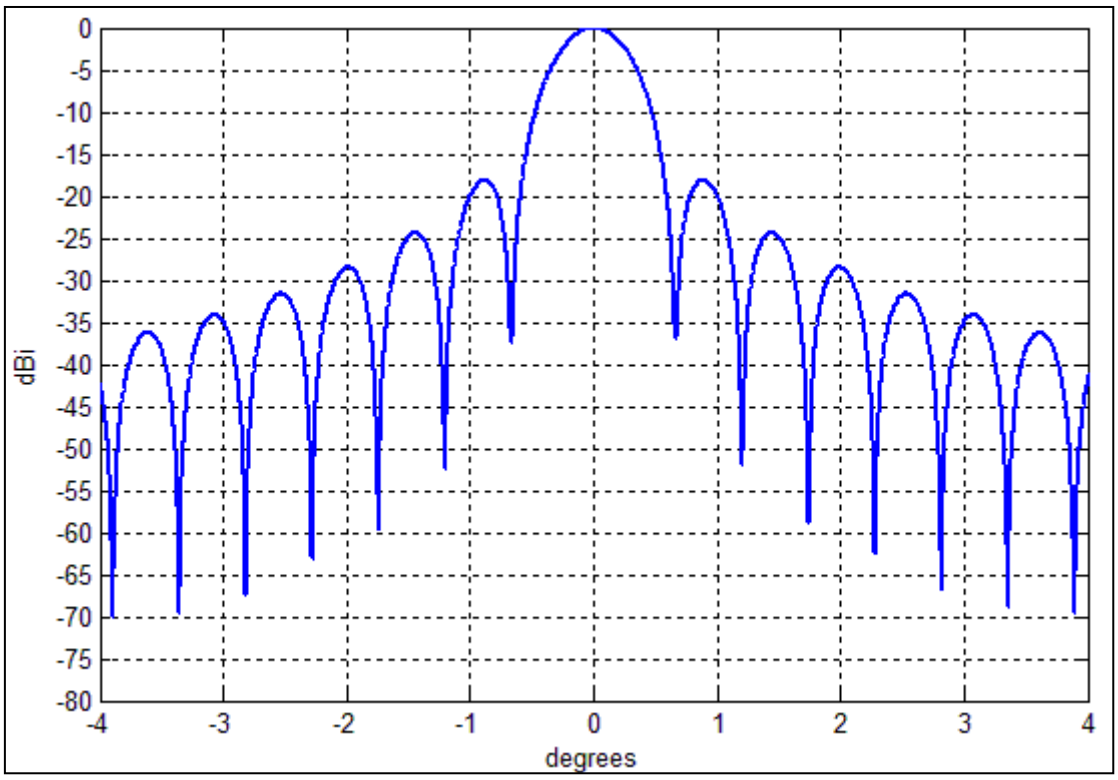

Figure 5.9. *4 GHz reflector radiated far field.*

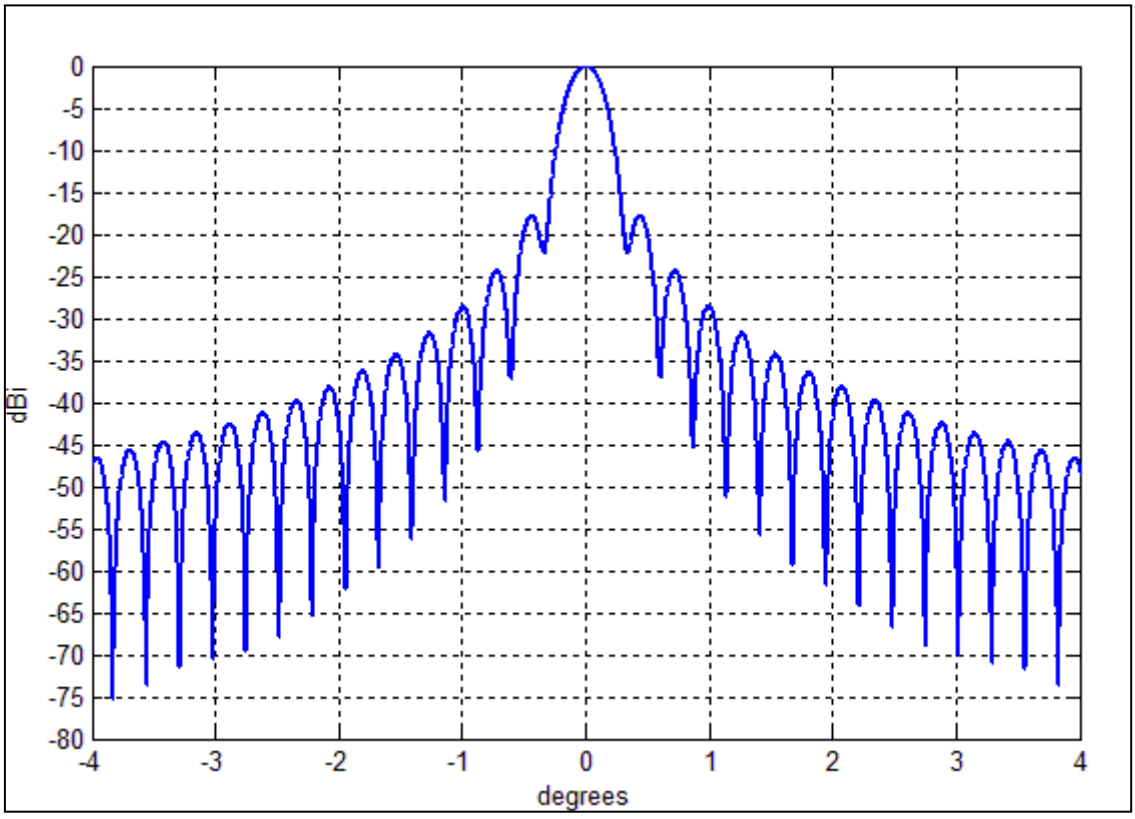

Figure 5.10. *8 GHz reflector radiated far field.*

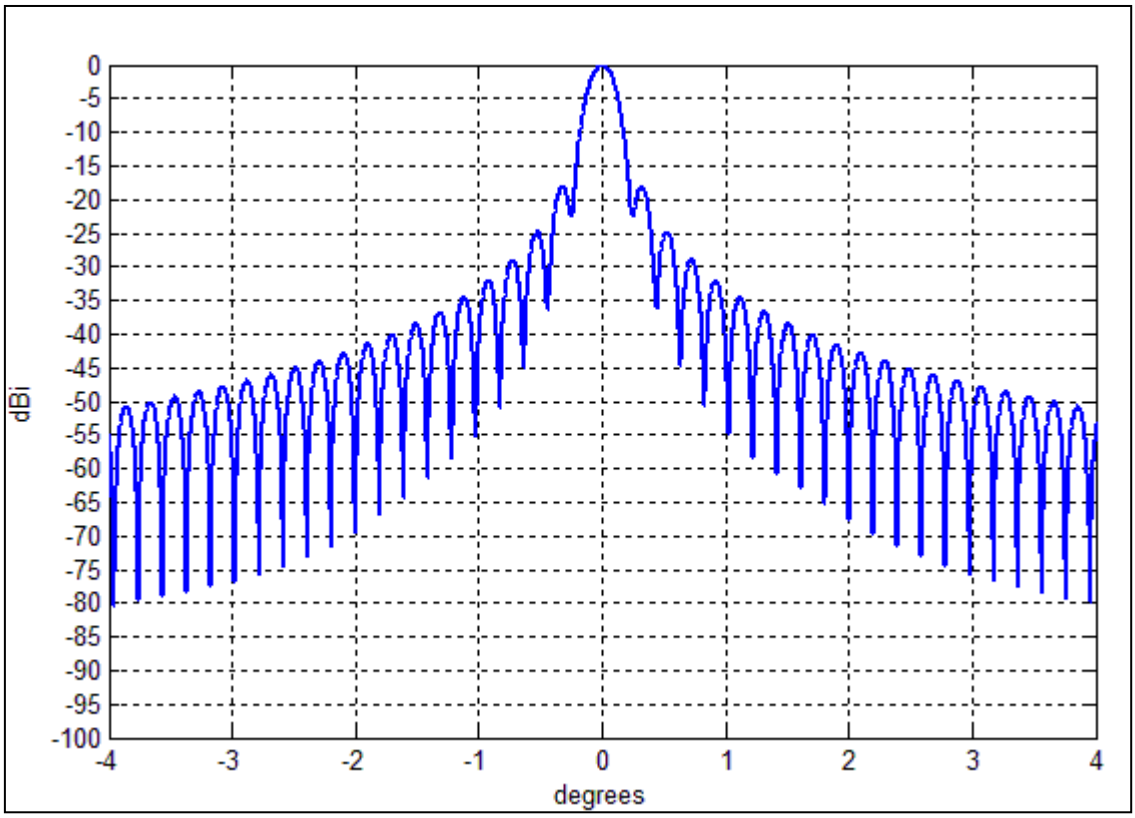

Figure 5.11. *11 GHz reflector radiated far field.*

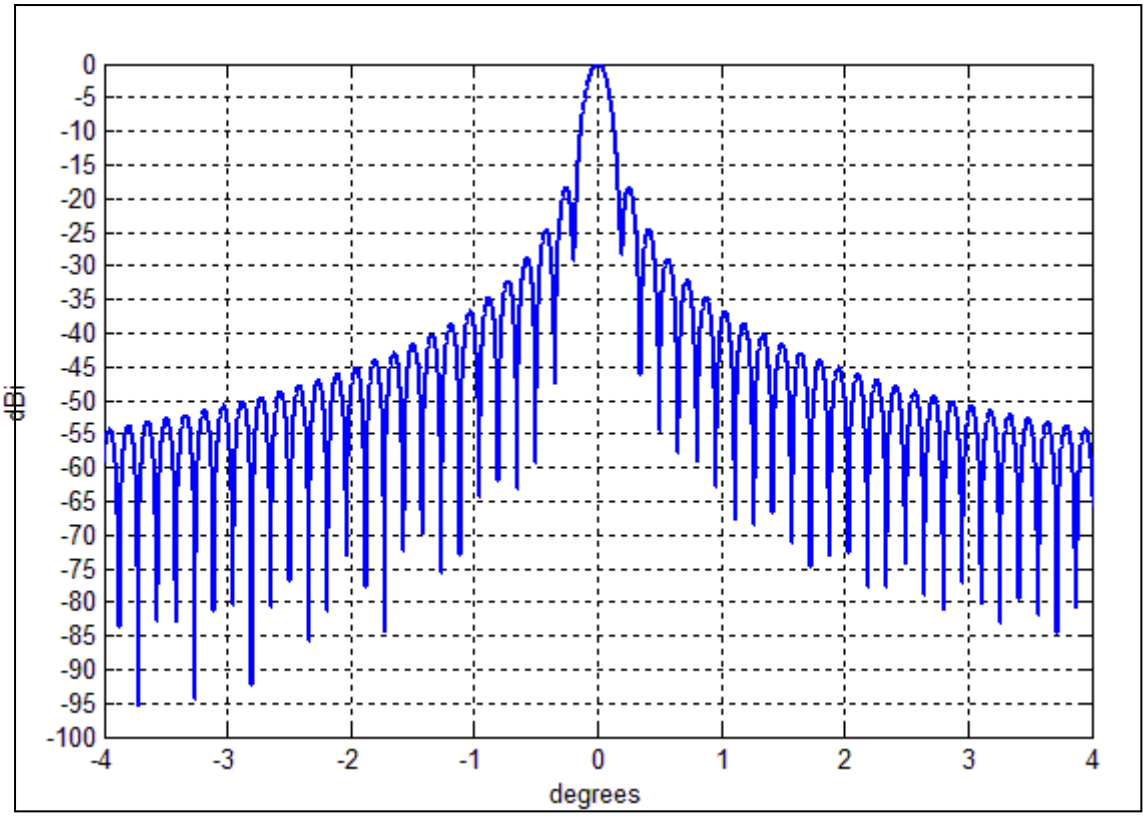

Figure 5.12. *14 GHz reflector radiated far field.*

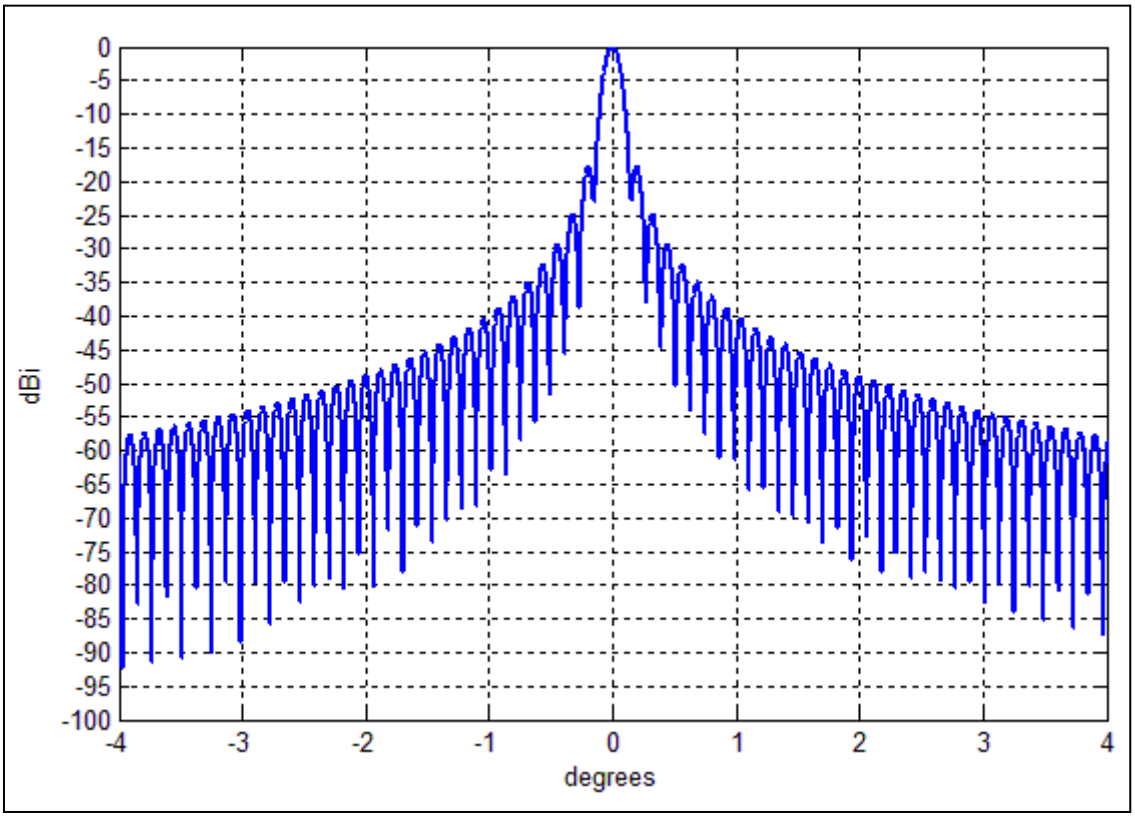

Figure 5.13. *18GHz reflector radiated far field.*

5.3. Design of a printed log periodic array with CPW feed line working in S and C band.

The feeding technique described in previous paragraph is not simple to realize since printed LPDAs at microwave frequencies can be very small, and the coaxial cable can affect the radiation pattern. To overcome such problems, the solution is a fully planar feeding network without any shorting pins. Thus, we present in this section a new feeding technique, based on a coplanar waveguide (CPW) cut into one of the paired strip while the other paired strip is floating. Some preliminary results on the same topic have been presented (for the first time, to the best of our knowledge) in [52], but without any experimental verification.

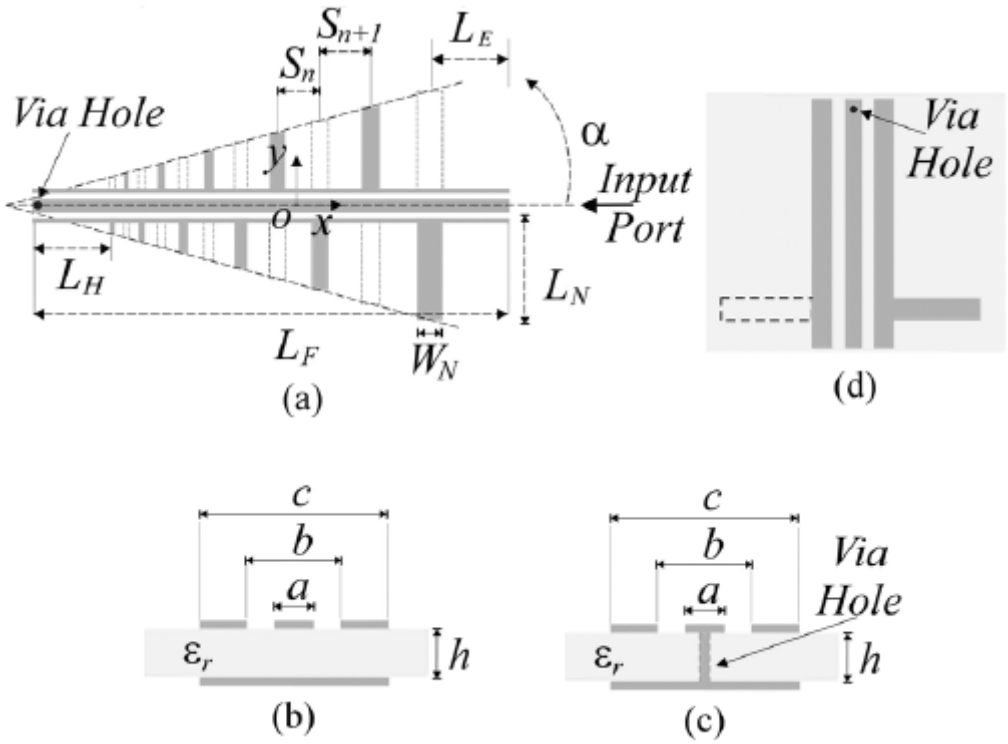

***Figure 5.14**. (a) 3-6 GHz Antenna Layout (top layer) not in scale. L_F=117.15 mm, L_H=22.97, L_E=26.44. (b) Coplanar waveguide transverse section at the input port: a = 1.05, b = 1.5 mm, c = 3.9. (c) Coplanar waveguide view at the via-hole section. (d) Top view of the coplanar waveguide, at the via-hole section, for the configuration with CPW ground lines left open.*

Coplanar waveguides have already been employed to feed printed antennas [53]–[55]. In this section we will create a sort of "flat" coaxial cable in one of the LPDA layers and a balun at its end. The balun is obtained using a via-hole between the CPW and the strip on the other side of the slab and an "open" termination of the two ground conductors of the CPW. In this way, the backward waves have an opposite current on the two sides of the PS, thus exciting only the correct mode, and so correctly feeding the dipoles. Moreover, we have found that no air-bridges are required on the

CPW, so that the realization is fully planar, but for the via-hole. Therefore, our solution fully shares all the advantages of the printed technology.

The dipoles of the printed LPDA, shown in figure 5.14, are alternately connected on the two lines of the paired strips, fed by a coplanar waveguide printed within one strip. The structure is very close to a standard (namely, wire) LPDA, and therefore the standard strategy to design an LPDA can be used [33], though with some modifications.

The design specifications of the proposed LPDA antenna are its operating bandwidth (3-6 GHz) and directivity. The design parameters are the spacing factor σ (see [33]) and the log-period τ (see figure 5.14(a) and equation (5.1)) which are selected by using Carrel design curves for the specified bandwidth and directivity [33].

In our case, we require an average directivity of 9 dBi in the bandwidth 3-6 GHz, therefore we set the log-period and the spacing factor to the values of $\tau = 0.88$ and $\sigma = 0.16$, respectively.

The number N of elements of the LPDA antenna, is given by the expression [33]:

$$N = 1 + \frac{\ln\left(B \cdot B_{AR}\right)}{\ln\left(\frac{1}{\tau}\right)} \tag{5.6}$$

Wherein B is the operating bandwidth, and B_{AR} is the bandwidth of the active region. In our case

$$B = \frac{f_{MAX}}{f_{MIN}} = \frac{6}{3} = 2 \tag{5.7}$$

$$\alpha = \arctan\left(\frac{1-\tau}{4 \cdot \sigma}\right) = \arctan\left(\frac{1-0.88}{4 \cdot 0.16}\right) = 10.62° \tag{5.8}$$

$$B_{AR} = 1.1 + 7.7\left(1-\tau\right)^2 \cdot \cot\alpha = 1.691 \tag{5.9}$$

Where α is the log-periodic antenna aperture angle, so that $N = 10.53$. Since N must be integer, we need 11 elements in order to fulfill the requirements on directivity and bandwidth.

We have chosen the characteristic impedance of CPW feeding line equal to 50Ω, so as to obtain an easy matching with the standard SMA connectors.

Choosing ARLON AD450 as dielectric substrate, a low-loss material (whose dielectric loss tangent is δ = 0.0035) with a dielectric permittivity ε_r = 4.5 and a thickness of 1.524 mm, the CPW parameters are computed using the following design equations [52][56] and imposing Z_0 = 50Ω.

$$Z_0 = \frac{\eta_0}{2\sqrt{\varepsilon_{eff}}} \frac{1}{\frac{K(k_1)}{K(k_1')} + \frac{K(k_2)}{K(k_2')} + \frac{2 \cdot t}{(b-a)}} \tag{5.10}$$

Where:

$$\varepsilon_{eff} = \frac{\frac{K(k_1)}{K(k_1')} + \frac{\varepsilon_r K(k_2)}{K(k_2')} + \frac{2 \cdot t}{(b-a)}}{\frac{K(k_1)}{K(k_1')} + \frac{K(k_2)}{K(k_2')} + \frac{2 \cdot t}{(b-a)}} \tag{5.11}$$

$$k_1 = \frac{c}{b} \cdot \sqrt{\frac{b^2 - a^2}{c^2 - a^2}} \tag{5.12}$$

$$k_2 = \frac{\tanh\left(\frac{\pi \cdot a}{4 \cdot h}\right)}{\tanh\left(\frac{\pi \cdot b}{4 \cdot h}\right)} \tag{5.13}$$

$$k_n' = \sqrt{1 - k_n^2}, \quad n = 1,2 \tag{5.14}$$

The term η_0 = 377Ω in (5.10) is the characteristic impedance of free space, t = 0.035 mm is the thickness of metallizations and $K(k_1)$, $K(k_2)$ are complete elliptic integral of the first kind where the integration parameters k_1 and k_2 depend by CPW parameters (i.e: a, b, c). Choosing the total width c of the CPW feeding line equal to the width of paired strips corresponding to an equivalent impedance of 50Ω, the resulting CPW parameters are a = 1.05 mm, b = 1.5 mm, c = 3.9033 mm.
The length L_N and the width W_N of the largest dipole, in this case have been evaluated using a more efficient cut-and try procedure on CST microwave studio [57] obtaining L_N = 17.5 mm and W_N = 2.87 mm.

The length and widths of the other dipoles are computed by using the expressions (5.1) and (5.4). In table 5.4, the geometry of the dipoles (see figure 5.14) is reported: the spacing S_N are computed in according to [33].

Dipole	L_n [mm]	W_n [mm]	S_n [mm]
1	4.87	0.80	
2	5.54	0.91	3.54
3	6.30	1.03	4.03
4	7.15	1.17	4.58
5	8.13	1.33	5.20
6	9.24	1.52	5.91
7	10.50	1.72	6.72
8	11.93	1.96	7.63
9	13.55	2.23	8.67
10	15.40	2.53	9.86
11	17.50	2.87	11.20

Table 5.4. *Geometry of the designed printed LPDA.*

The aim of coplanar waveguide is to implement a flat coaxial cable as feeding network of a printed log-periodic antenna. Therefore, the central conductor of the coplanar waveguide must be connected, through a via hole, to the bottom layer of paired strips (as indicated in figure 5.14), so that a single progressive wave propagates on the paired strips itself toward the largest dipole. In this way, the CPW termination acts as a balun, as long as the two ground lines of the CPW end abruptly (as in Fig. 5.14(d)). The starting length L_H of the final termination of the CPW [see Fig. 1(a)] has been chosen equal to half a wavelength at the central frequency of 4.5 GHz. This value has been then optimized, and the best input matching has been obtained for L_H = 22.97 mm.

The LPDA antenna has been manufactured (figure 5.15) and fully characterized. In figure 5.16 the simulated and measured frequency responses of the input reflection coefficient are shown, and the broadband input matching specification between 3 and 6 GHz is fulfilled, with a very good agreement between simulation and measurement. As a matter of fact, the input matching range extends well beyond 6 GHz, and the 10-dB antenna bandwidth approximately extends from 2.5 to 7.5 GHz, as shown in figure 5.16. On the other hand, the antenna gain rapidly decreases, and the radiated far-field pattern deteriorates out of the design bandwidth (3–6 GHz).

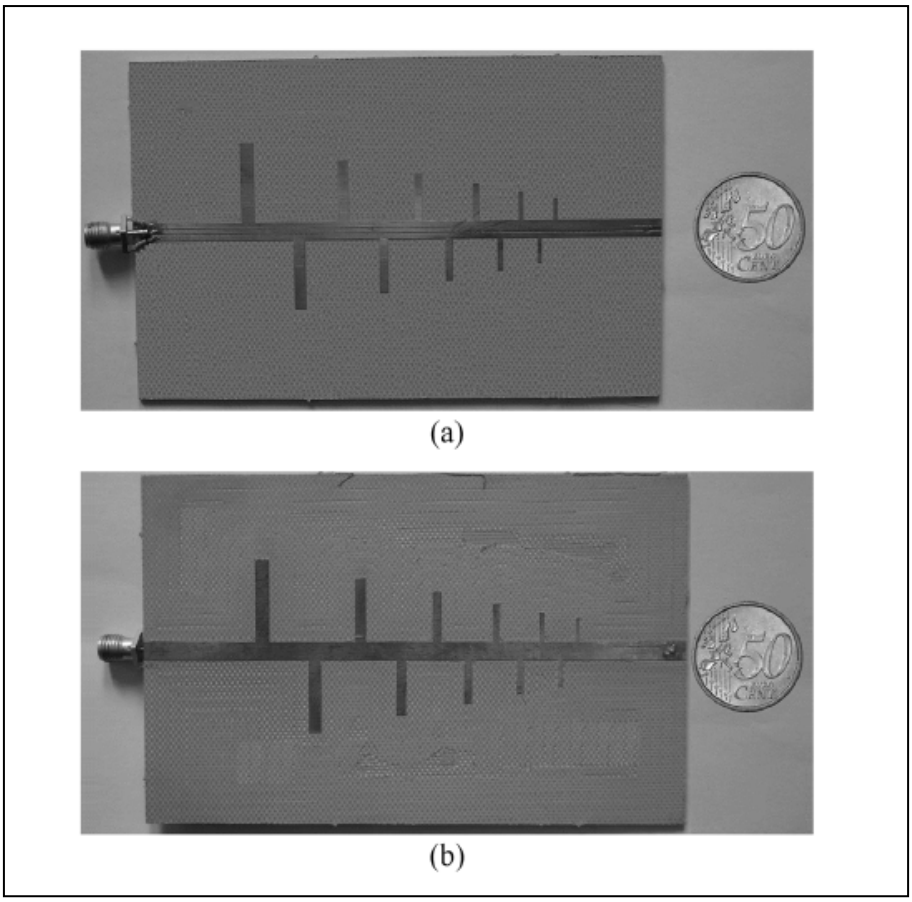

***Figure 5.15**. Photograph of the LPDA antenna: (a) front; (b) back. On the back side, there is no connection between the SMA connector and the strip.*

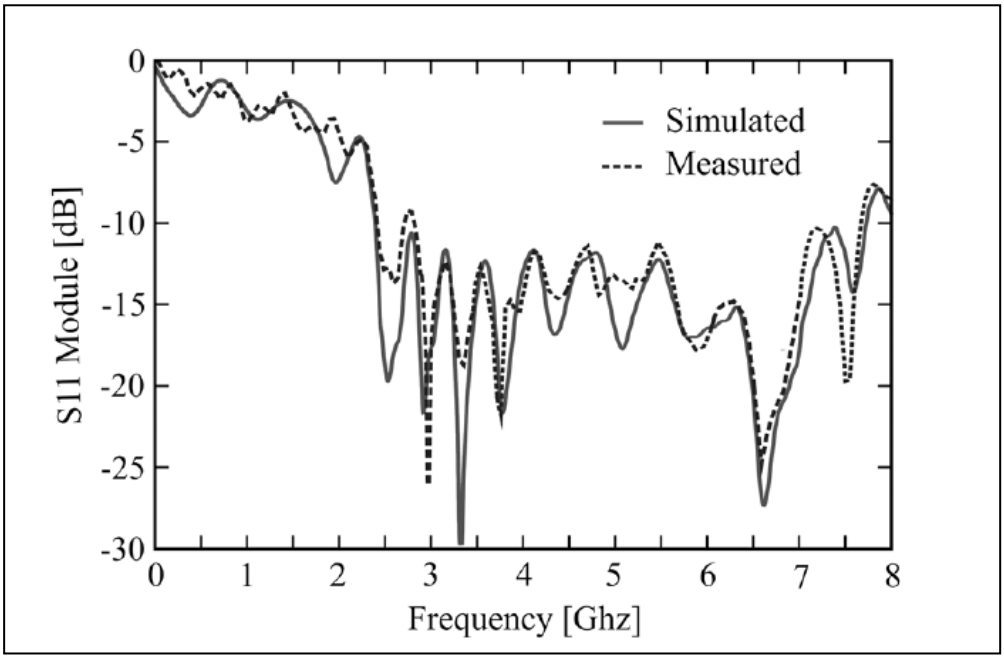

***Figure 5.16.** Reflection coefficient of the 3-6 GHz LPDA antenna.*

In figure 5.17, the antenna gain (both evaluated by CST and measured) as function of the frequency is reported. The antenna gain is quite stable over the required frequency range, with an average value equal to 6.85 dB. On the other hand, it drops to about 4 dB at 2.5 and 6.5 GHz.

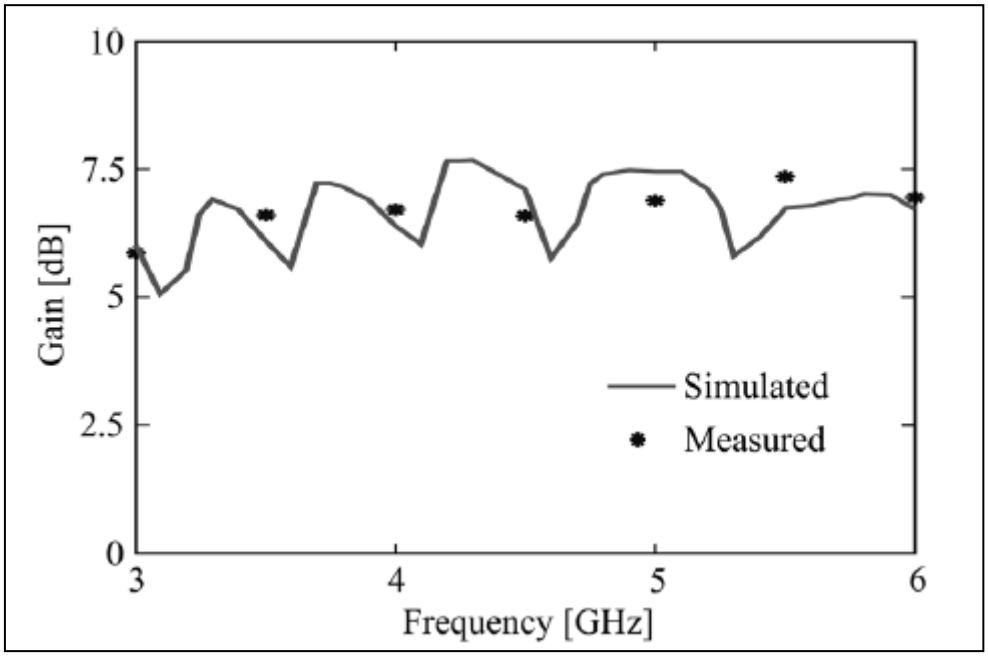

Figure 5.17. *Gain of the 3-6 GHz LPDA antenna.*

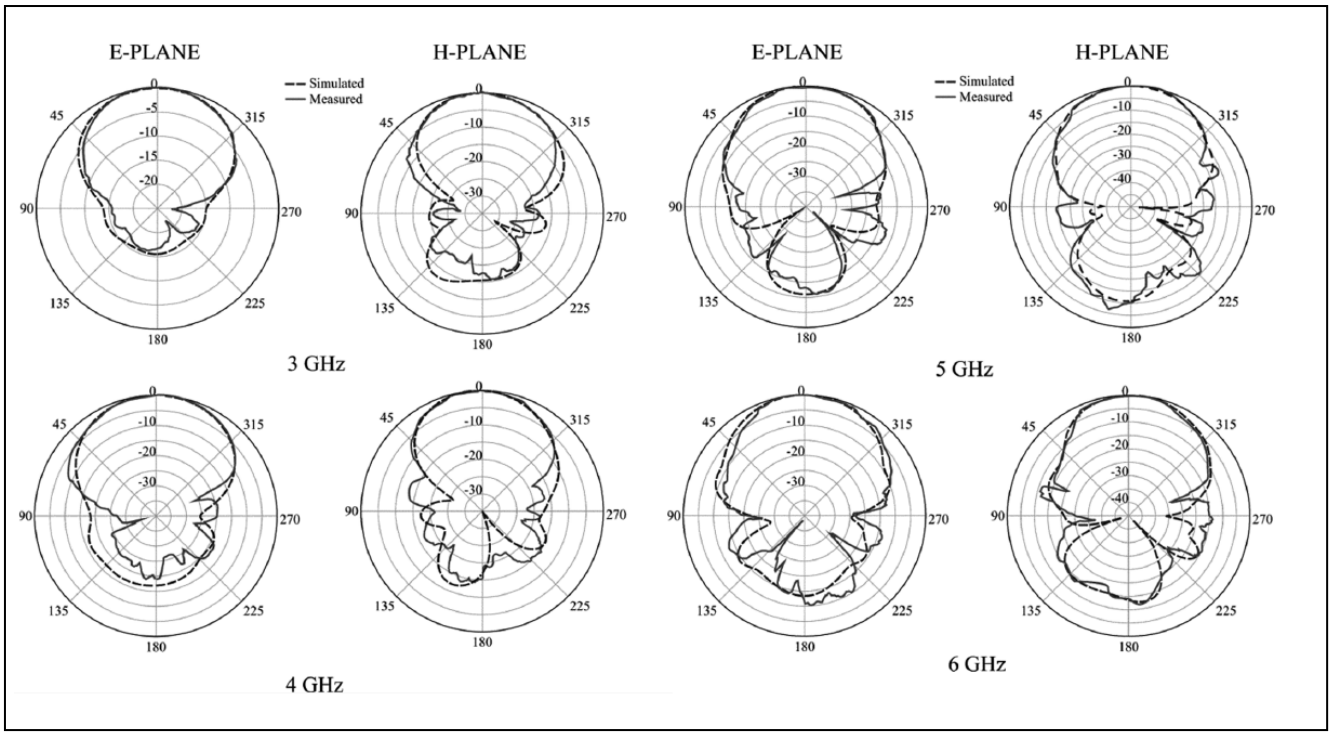

Figure 5.18. *Simulated and measured E-plane and H-plane radiation pattern of the 3-6 GHz LPDA antenna.*

Figure 5.18 reports the simulated and measured E-plane and H-plane radiation patterns. The cross-polar component is not shown since it is always below 25 dB with respect to the co-polar component of the radiated field. The measured far-field pattern is in very good agreement with the simulations, showing the endfire behavior in the whole operating frequency band.

Therefore, the proposed LPDA can be successfully used as a broadband antenna in the frequency range 3–6 GHz, with a relative bandwidth greater than 33%.

This LPDA antenna has been used as feed for a reflector antenna: also in this case, the choice of an optimal *f/d* ratio, due to the strong asymmetry of the radiated fields in E-Plane and H-Plane, has been performed by the mean value 3dB feed beamwidth in E-Plane and H-Plane (see paragraph 5.2).

Frequency (GHz)	**E-Plane 3dB Beamwidth (degree)**	**H-Plane 3dB Beamwidth (degree)**
3	65.9	90.5
4	56.7	73.4
5	57.5	74.3
6	55	70
Mean value	58.77	77.05
M_T	67.91	

Table 5.5*. 3dB 3-6 GHz printed LPDA feed beamwidth.*

Setting the diameter of the reflector equal to 8 meters, in order to obtain a gain of 45 dBi at 3 GHz, and using the M_T value indicated in table 5.5, by equation (5.5) we obtain the focal length of the reflector f = 6.551 m.

In figures 5.19-5.22 the $\theta=0°$ normalized simulated radiated far field cuts for such reflector antenna at 3, 4, 5, 6 GHz are shown. The result obtained exhibit a side lobe level equal to about -17 dB and a good gain (see table 5.6) over the whole operating bandwidth, allowing the use of 3-6 GHz LPDA printed feed with coplanar waveguide in reflector antennas for wide band communication systems.

Frequency	**Gain**
3	44.03
4	47.36
5	49.68
6	50.91

Table 5.6*. Reflector antenna gain*

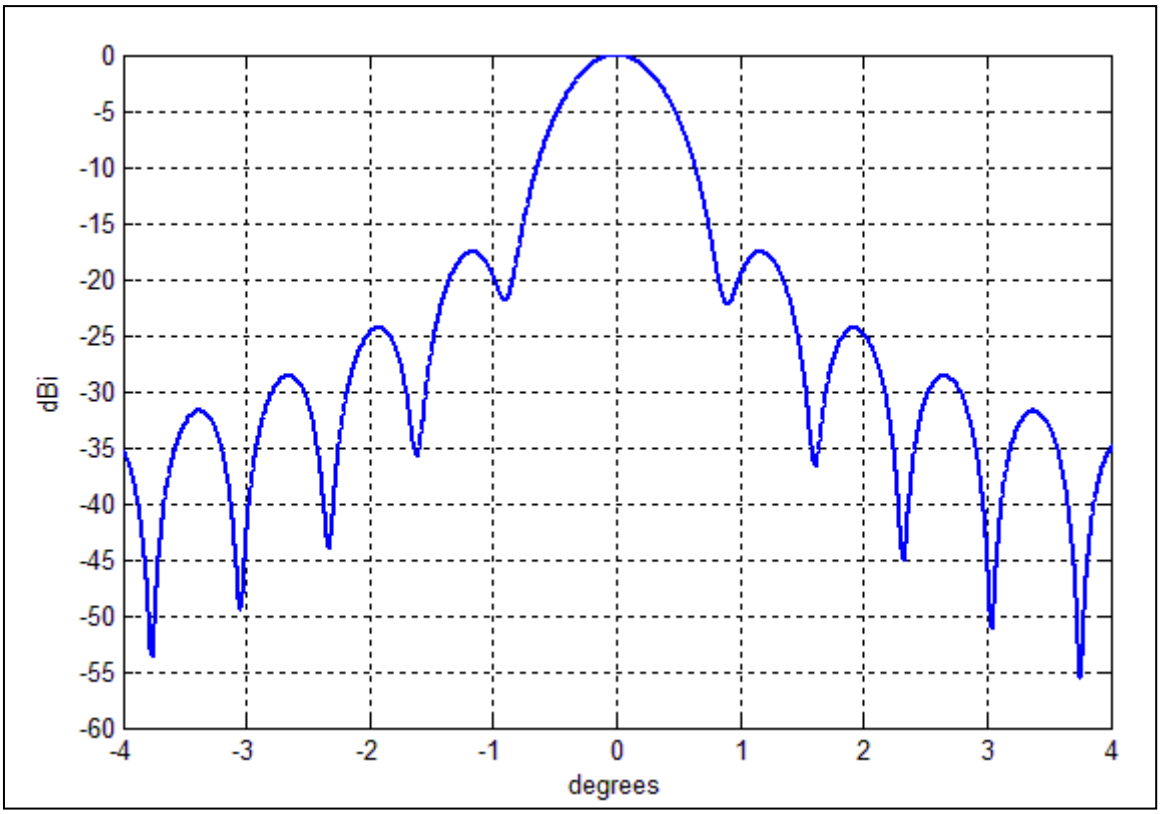

***Figure 5.19**. 3 GHz reflector radiated far field.*

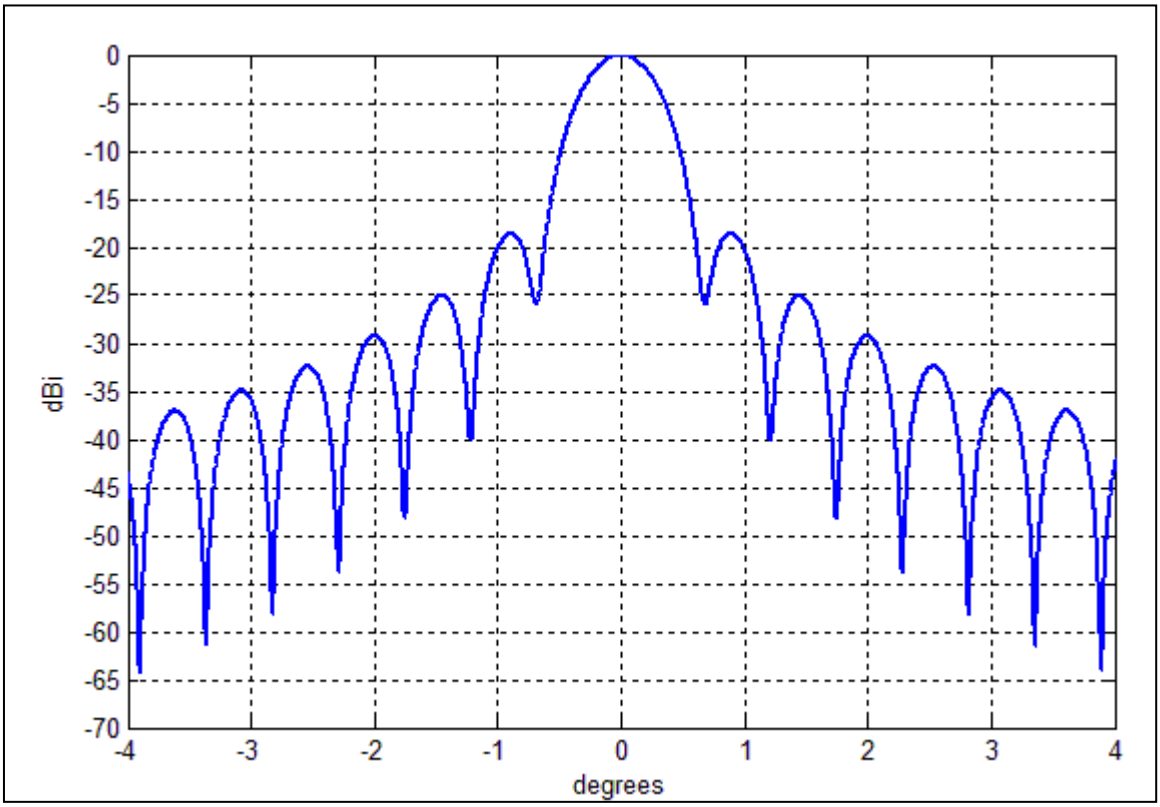

***Figure 5.20**. 4 GHz reflector radiated far field.*

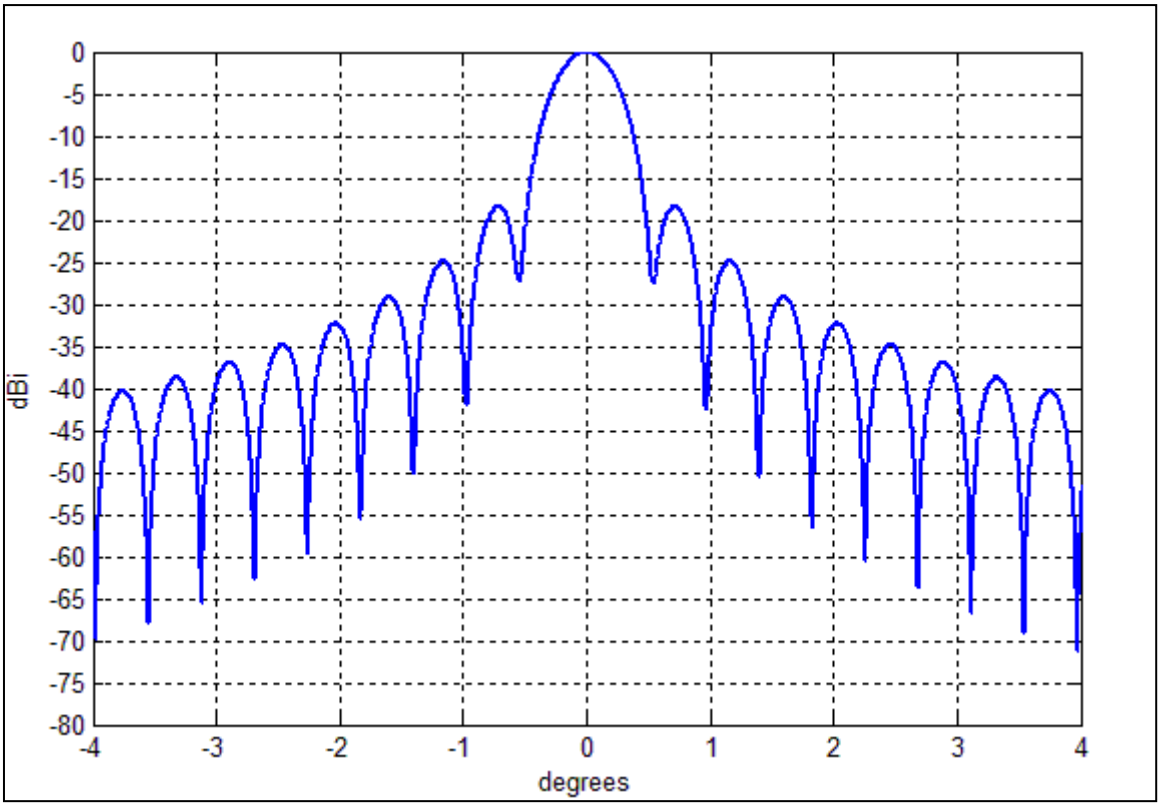

Figure 5.21. *5 GHz reflector radiated far field.*

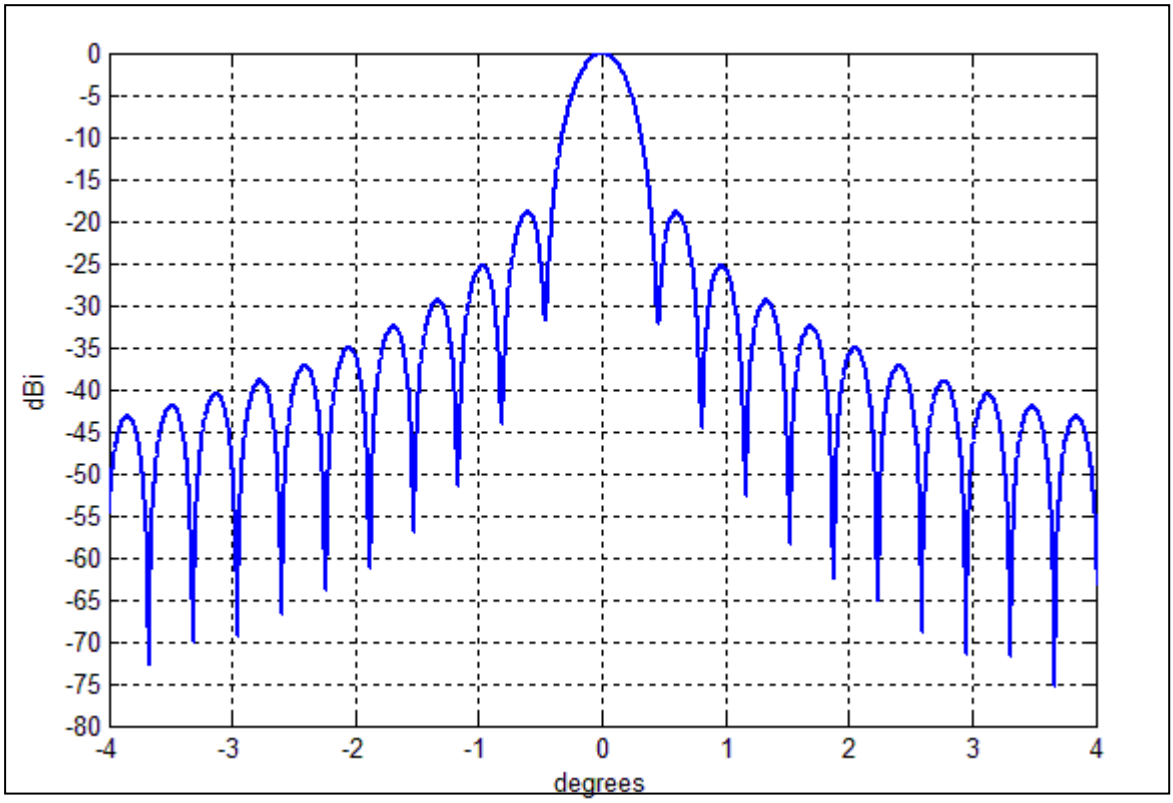

Figure 5.22. *6 GHz reflector radiated far field.*

5.4. "V" Shaped S-C band log-periodic feed for weather radar applications.

In this section the design of a high gain feed for weather radars applications is presented.
The choice of the frequency range is one of the main features of weather radars: the S-band (2.7-3.0 GHz) is well-suited for detecting heavy rains at very long ranges (up to 300 kilometers); usually, the S-band weather radars are typically employed in severe weather regions, where extreme rainfalls pose a challenge to precise measurements and long range surveillance [3]. The C-band (5.4-5.8 GHz) represent instead a good compromise between range and cost of the system and provides the detection of rain up to 200 kilometers. Weather radars also operate in X-band (9.3-9.5 GHz) but, due to high attenuation of the hydrometeors at these frequencies, they are used only for detection of storm at short range (up to 70 kilometers).
The S and C band are therefore the most widely used in long range weather radars, and, for this reason, we introduce the design of a high gain printed log periodic feed able to work both in S and C band.
The concept of log-periodic printed antennas described in the previous paragraph is applied to two different groups of dipoles designed to operate each in a specific frequency band, in order to get the feed shown in figure 5.23.

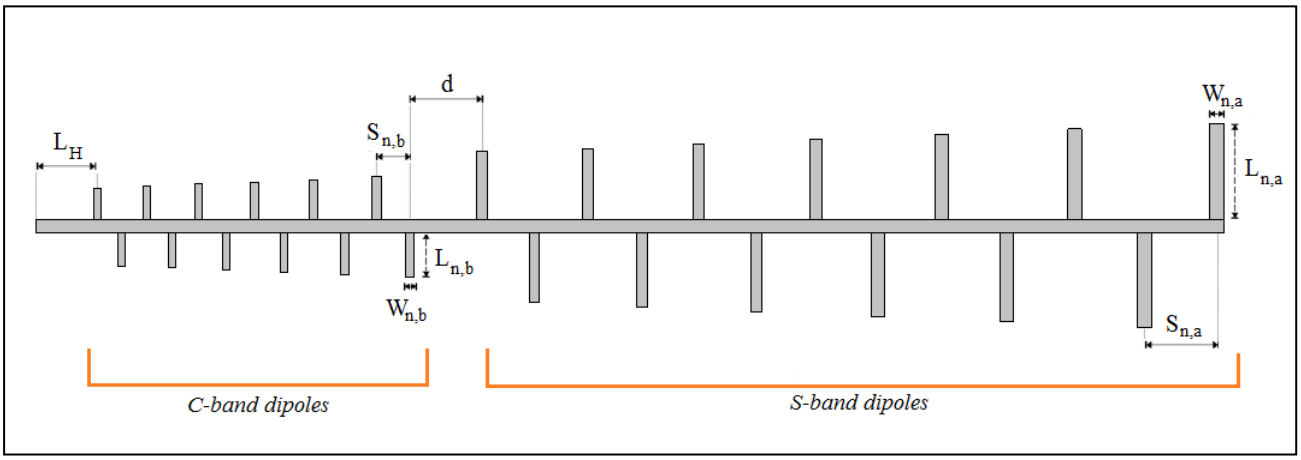

***Figure 5.23**. S-C band feed layout.*

This solution allows to obtain a log periodic antenna with a reduced size, operating only in the range 2.7-3.0 GHz and 5.4-5.8 GHz instead of a complete printed LPDA array working between 2.7 and 5.4 GHz.
For each group, the number of dipoles and the scaling factor τ must be defined. Even though both parameters can be different for each group of dipoles, as a design rule we choose to use the same values for both groups [41].

As mentioned in previous paragraphs, the number of dipoles of each group is determined by the design specifications (i.e. the bandwidth and directivity requirements). In our case, for the proposed printed LPDA feed, we require an average directivity of 12 dBi (the maximum directivity available in the Carrel design curves), and therefore we set the log period τ and the spacing factor σ of both groups of dipoles to the value $\tau = 0.97$ and $\sigma = 0.185$.

The chosen dielectric substrate is the TACONIC TSM-DS3, a material developed for high power applications [59], with low losses (dielectric loss tangent $\delta = 0.0011$) and a dielectric permittivity ε_r=3. The substrate thickness and metallizations are respectively $h = 0.887$ mm, $t = 0.070$ mm.

In order to tolerate the high power levels required by a weather radar system (i.e. [60], [61]), the feeding network selected for the feed is the dual coaxial cable configuration described in paragraph 5.2: as a matter of fact, the CPW feeding technique allows a more simple realization with low cost, compact size and is easy to connect with the SMA connectors but, due to dielectric breakdown of the air between the metallic strips, it is capable to handle only low power levels.

The characteristic impedance Z_0 of the printed feeding lines (paired strips) of the two groups of dipoles has been selected in order to obtain an easy matching with the UT-085 coaxial cables [64] employed : by choosing $Z_0 = 50\Omega$ we obtain (see paragraph 5.2) $W = 2.8864$ mm.

The number N of elements of each group of dipoles is computed by using expressions (5.6)-(5.9); starting from the required bandwidths, we get: number of dipoles $N = 12$, aperture angle $2\alpha = 4.65°$.

The length $L_{N,ab}$ and the width $W_{N,ab}$ (where a, b indicate respectively the group of dipoles working in S and C band) of the longest dipole of each group have been evaluated using the cut-and-try procedure described in paragraph 5.3, obtaining $L_{n,a} = 20.74$ mm, $W_{n,a} = 3.09$ mm and $L_{n,b} = 9.50$ mm and $W_{n,b} = 1.92$ mm.

The length and widths of the other dipoles of each group are computed by using expressions (5.1) and (5.4). In table 5.7 the geometry of the dipoles (see figure 5.23) is reported.

The length of the final termination L_H of the paired strips has been chosen equal to half a wavelength at the highest operating frequency (i.e. $L_H = 25.85$ mm).

In figures 5.24 and 5.25 the reflection coefficient for each group of dipoles is reported. In order to improve the performance of S-band dipole group, a further dipole is inserted immediately before the dipole 1, with the same width and length and with spacing equal to the one between dipole 1 and dipole 2 of the S-band dipole group [46],[65]. As mentioned in paragraph 5.2, this solution is able to lower the reflection coefficient below -10 dB in the whole operating bandwidth.

In figure 5.26 the reflection coefficient for the complete antenna is shown: in order to obtain a good input matching both in S and C band, we performed simulations varying the distance d between the two groups of dipoles from 11.28 mm to 33.86 mm. As reported in figure 5.26, the best S_{11} is

obtained for d = 11.28 mm. the final geometry of the whole antenna (figure 5.27) is reported in table 5.7.

Dipole	*Ln*[mm]	*Wn*[mm]	*Sn*[mm]
a1	14.84	2.21	
a2	15.30	2.28	11.33
a3	15.77	2.35	11.67
a4	16.26	2.42	12.03
a5	16.76	2.50	12.40
a6	17.28	2.58	12.78
a7	17.81	2.66	13.18
a8	18.36	2.74	13.59
a9	18.93	2.82	14.01
a10	19.52	2.91	14.44
a11	20.12	3.00	14.89
a12	20.74	3.09	15.35
b1	6.79	1.37	
b2	7.00	1.41	5.18
b3	7.22	1.45	5.34
b4	7.44	1.50	5.51
b5	7.67	1.55	5.68
b6	7.91	1.59	5.85
b7	8.16	1.64	6.03
b8	8.41	1.69	6.22
b9	8.67	1.75	6.41
b10	8.94	1.80	6.61
b11	9.21	1.86	6.82
b12	9.50	1.92	7.03

Table 5.7*. Geometry of S-C band printed LPDA feed.*

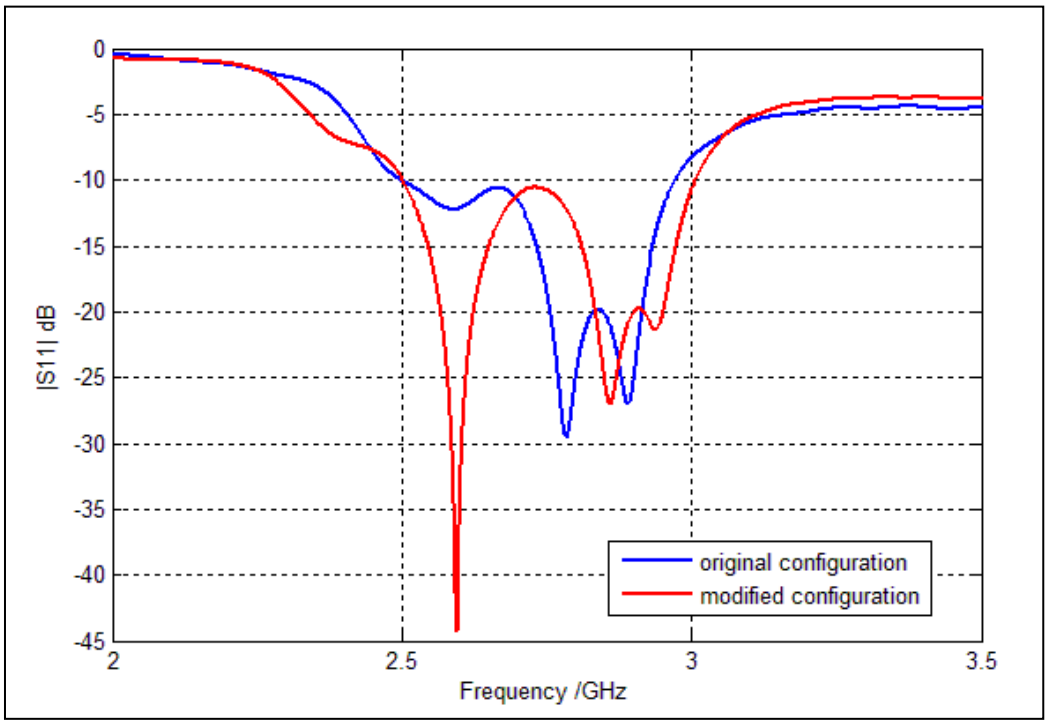

Figure 5.24. *S band dipoles group reflection coefficient.*

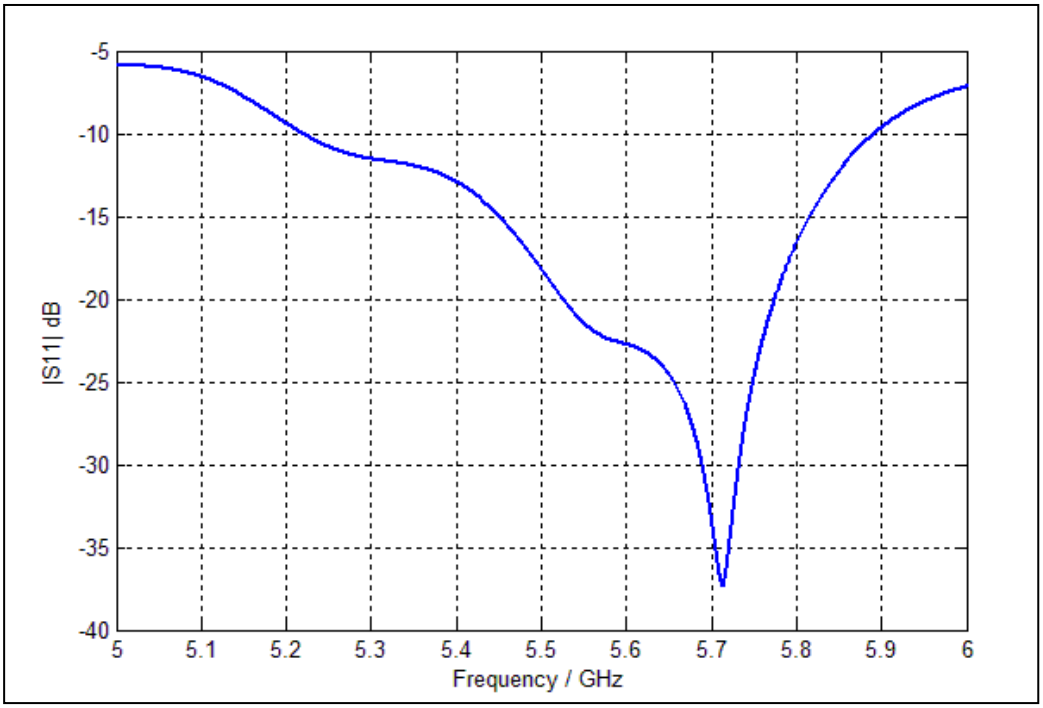

Figure 5.25. *C band dipoles group reflection coefficient.*

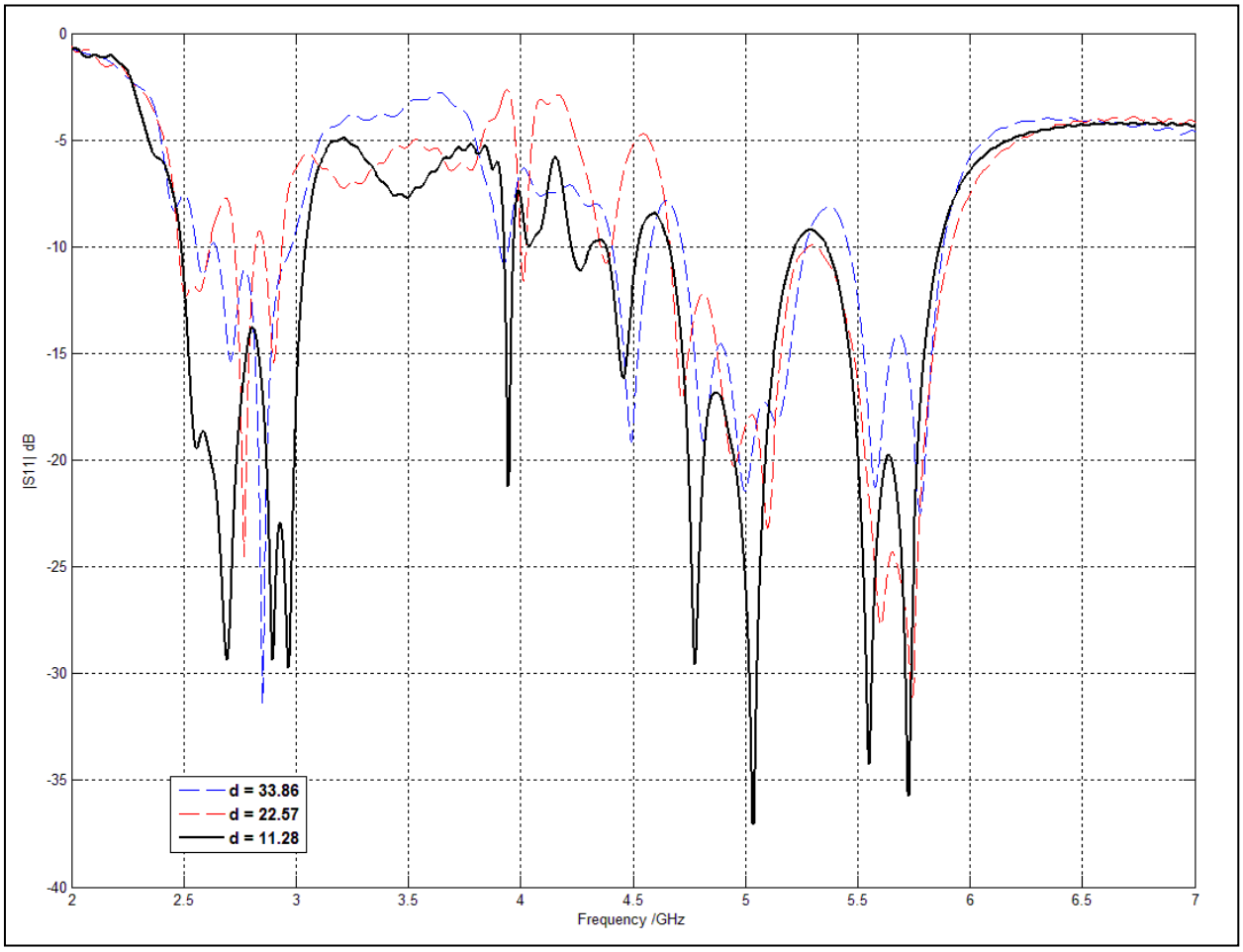

Figure 5.26. *S-C band feed reflection coefficient as a function of d parameter.*

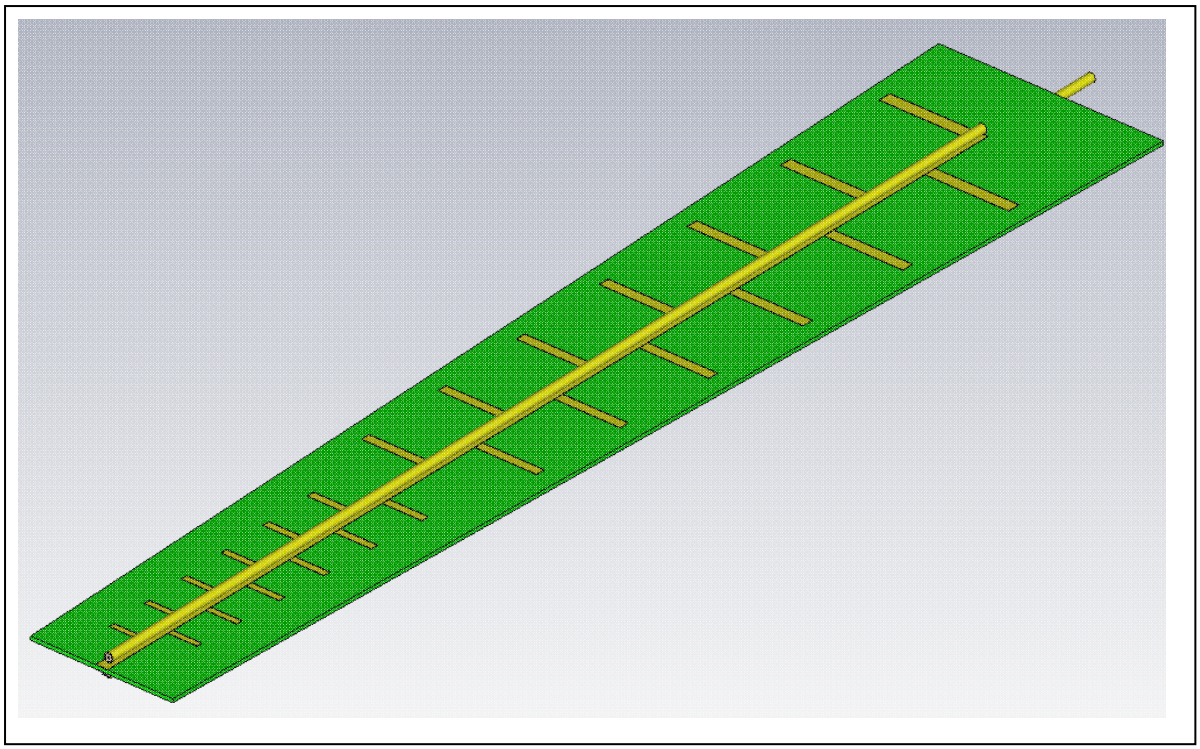

Figure 5.27. *Complete S-C band feed.*

The feed gain, evaluated by CST and shown in figure 5.28, is quite stable in both the operating frequencies with an average value equal respectively to 11.6 dBi in the S-band and 9.43 dBi in the C-Band.

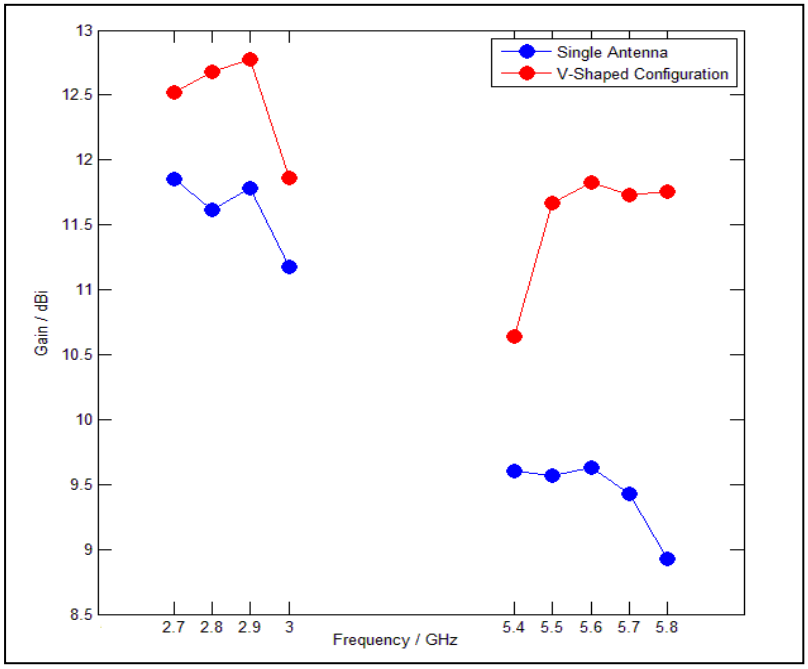

Figure 5.28. *S-C band feed gain.*

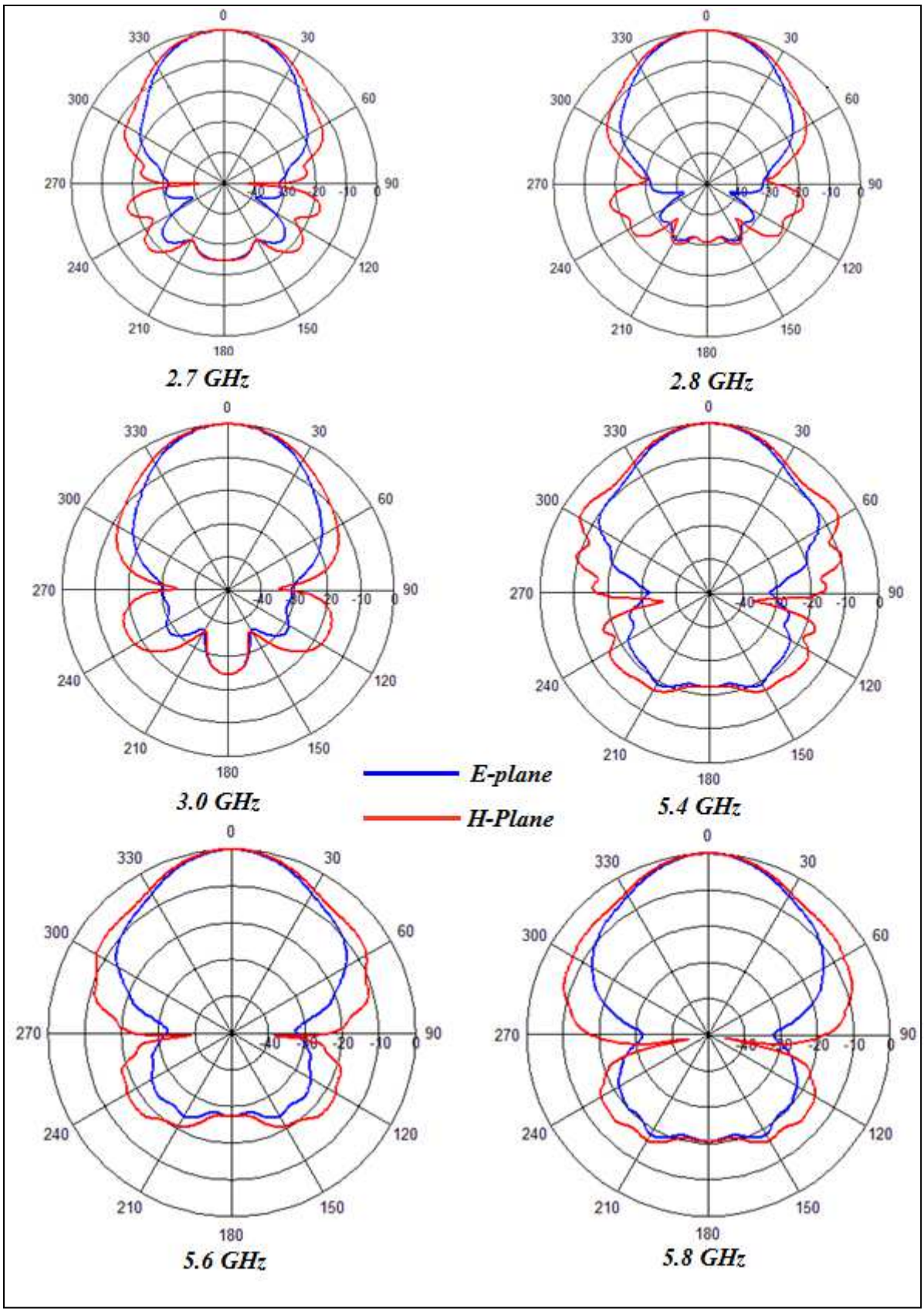

Figure 5.29. *S-C band feed E-plane and H-plane radiation patterns.*

In figure 5.29 the simulated E-plane and H-plane radiation patterns are reported: it is well know [26] that the radiation pattern in the H-plane of log-periodic antennas (wired or printed) is much more wider than in E-plane. This aspect can adversely affect the efficiency of a reflector antenna: to avoid the problem, in order to obtain a symmetrical radiated field both in E-plane and H-plane, a feed configuration with two S-C band printed LPDA antennas (figure 5.30) is introduced [62] [27].

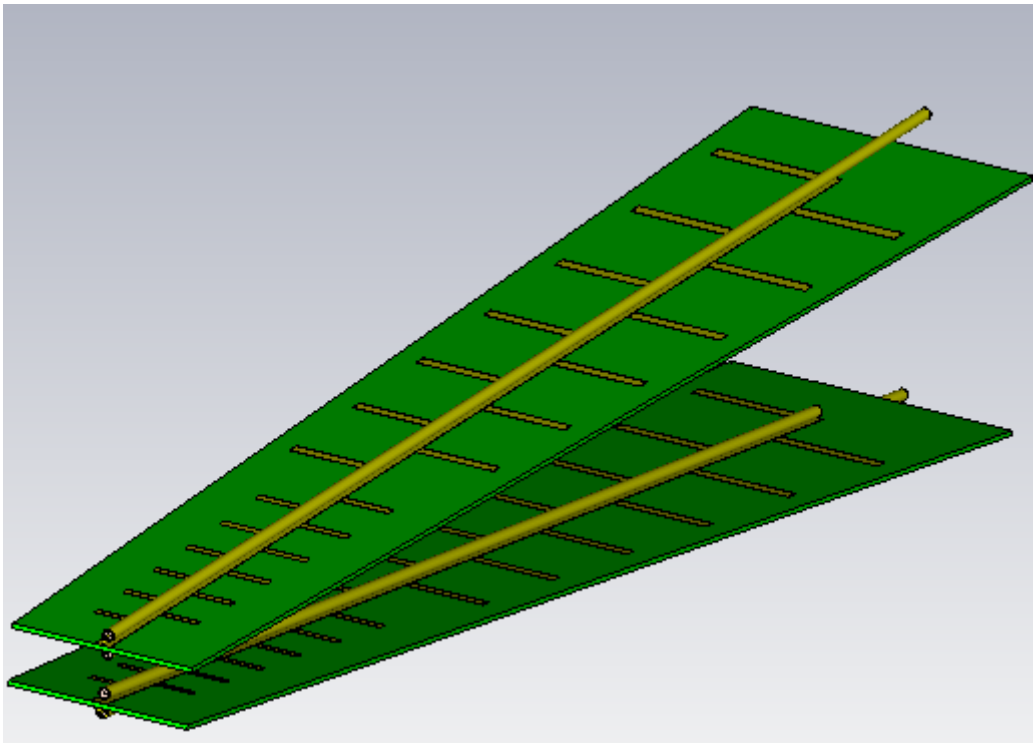

Figure 5.30. *"V" Shaped S-C band log-periodic feed.*

The obtained feed includes an additional design parameter: the angle ψ between the two printed LPDA antennas. This parameter is related to the H-plane beamwidth, which decreases rapidly with increasing ψ [26]: if ψ is much less than α, a sacrifice in gain occurs (due to a broadened H-plane beamwidth); if ψ is much greather than α, unsatisfactory front-to-back ratio has been found to occur.

A design principle for the correct choice of ψ angle is described in [63]: in case of a unidirectional log-periodic array, the optimal value of ψ angle is comprised between $0.8*2\alpha$ and $1.2*2\alpha$.

In order to obtain both a good input matching and a symmetric beamwidth in E-plane and H-plane, we performed simulations varying ψ from 3.72° to 5.64° and with simultaneous excitation of the two antennas. A summary of the results is displayed in figure 5.31: as easily observed, the best input matching is obtained for $\psi = 3.762°$.

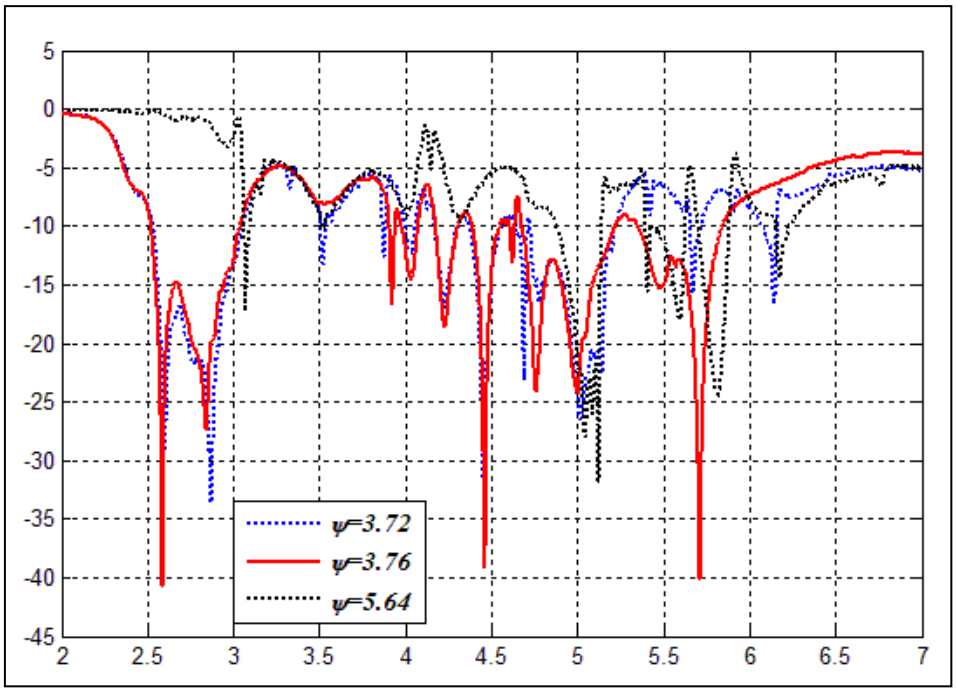

Figure 5.31. *"V" Shaped S-C band reflection coefficient as a function of ψ angle.*

In figure 5.28 is reported the gain for the structure with ψ = 3.762° compared with the single antenna configuration. As expected, the V-shaped configuration allow to obtain an improvement in the symmetry of E-plane and H-plane radiation pattern (see figure 5.32), and an increase of gain in the overall operating bandwidth.

After these considerations, the proposed structure can be successfully used as feed for a reflector antenna in the 2.7-3.0 GHz and 5.4-5.8 GHz frequency range. Using a 9 meters diameter reflector, in order to select the optimal *f/d* ratio, the 10 dB feed beamwidths and the side lobe level are reported in table 5.8.

Frequency (GHz)	Gain	E -plane 10 dB beamwidth	E -plane Side Lobe Level	H -plane 10 dB beamwidth	H – plane Side Lobe Level
2.7	12.5	75.08	-17.6	87.39	-17.6
2.8	12.7	77.31	-23.2	83.39	-23.2
2.9	12.8	73.95	-32.1	84.38	-27.8
3.0	11.9	81.04	-24.9	94.73	-21.1
5.4	10.6	104	-19.8	99.64	-11
5.5	11.7	87.38	-23.2	103.38	-16.3
5.6	11.8	85.54	-25.9	97.23	-17.3
5.7	11.7	96	-25.2	104.6	-22.3
5.8	11.8	86.15	-23.4	97.23	-20.2
Mean Value		86.16		94.69	
MT		90.42			

Table 5.8. *"V" Shaped S-C band feed gain and 10 dB beamwidth.*

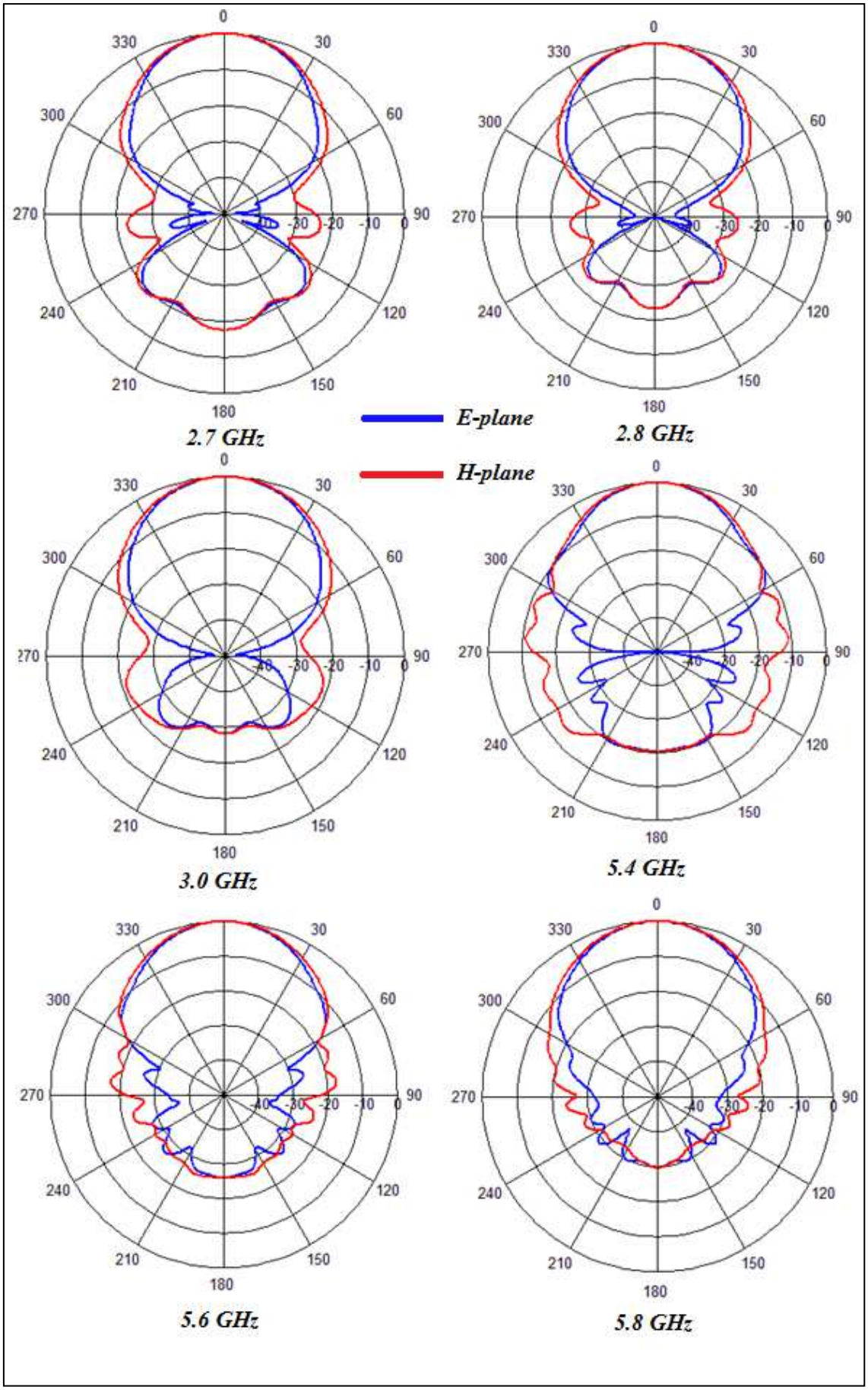

Figure 5.32. *"V" Shaped S-C band radiation patterns.*

The focal length f = 5.1255 has been obtained by equation (5.5) by substituting ψ = 90°.

In the figures 5.33-5.38 are reported the simulated θ = 0° cuts of the radiated far field of the reflector antenna, at 2.7, 2.8, 3.0, 5.4, 5.6, 5.8 GHz. The results shows side lobe level equal to -30 dB in the S-band and -25 dB in the C-band and a good gain (see table 5.9) in the whole operating bandwidth.

Frequency (GHz)	**Gain (dBi)**
2.7	46.47
2.8	46.99
2.9	47.19
3.0	47.25
5.4	50.74
5.5	51.58
5.6	52.12
5.7	52.19
5.8	52.24

Table 5.9*. S-C band reflector antenna gain.*

Finally, we calculated the theoretically minimum range for a weather radar system equipped with a reflector antenna having a 9 *m* diameter and fed by the "V-shaped" printed log periodic feed.

The theoretically minimum range can be evaluated by using the Probert-Jones equation (1.23):

$$P_R = \frac{P_T G^2 \cdot \phi\theta \cdot H \cdot \pi^3 \cdot K^2 \cdot Z}{512(2\ln 2) \cdot R^2 \lambda^2 \cdot L}$$

Where R is the range of target, $H = c\tau$, and L is the total loss factor of a radar system: typically L= 21.1 dB [66].

Because of the large range of magnitudes involved in the (1.23), it is convenient to employ the logarithmic units and write the equation (1.21) in this form [67]:

$$10\log P_{MDS} = 10\begin{cases}\log P_{TX} + \log h + 2\log G - 2\log\lambda + 2\log\theta_{RAD} + \log K^2 \\ +3\log\pi - 10\log 2 - \log(\ln 2) - 2\log R + \log Z - \log L\end{cases} \quad (5.15)$$

Where θ_{RAD} is the 3 dB beamwidth in radians and P_{MDS} is the minimum discernible signal: typical radar values [66] lie in the range of -104 dBm to -115 dBm [60].

By substituting in equation (5.15) G = 46.47 (gain at 2.7 GHz), $\theta = \varphi$ = 0.95° (reflector radiated field beamwidth at 3 dB), K^2=0.93, H = 3.3 μsec [60], λ = 0.112 m (wavelength at 2.7 GHz), Z = 20 dBz (typical value of reflectivity for rain), P_T = 320 KW and P_{MDS} = -115 dBm we obtain R = 371.67 Km.

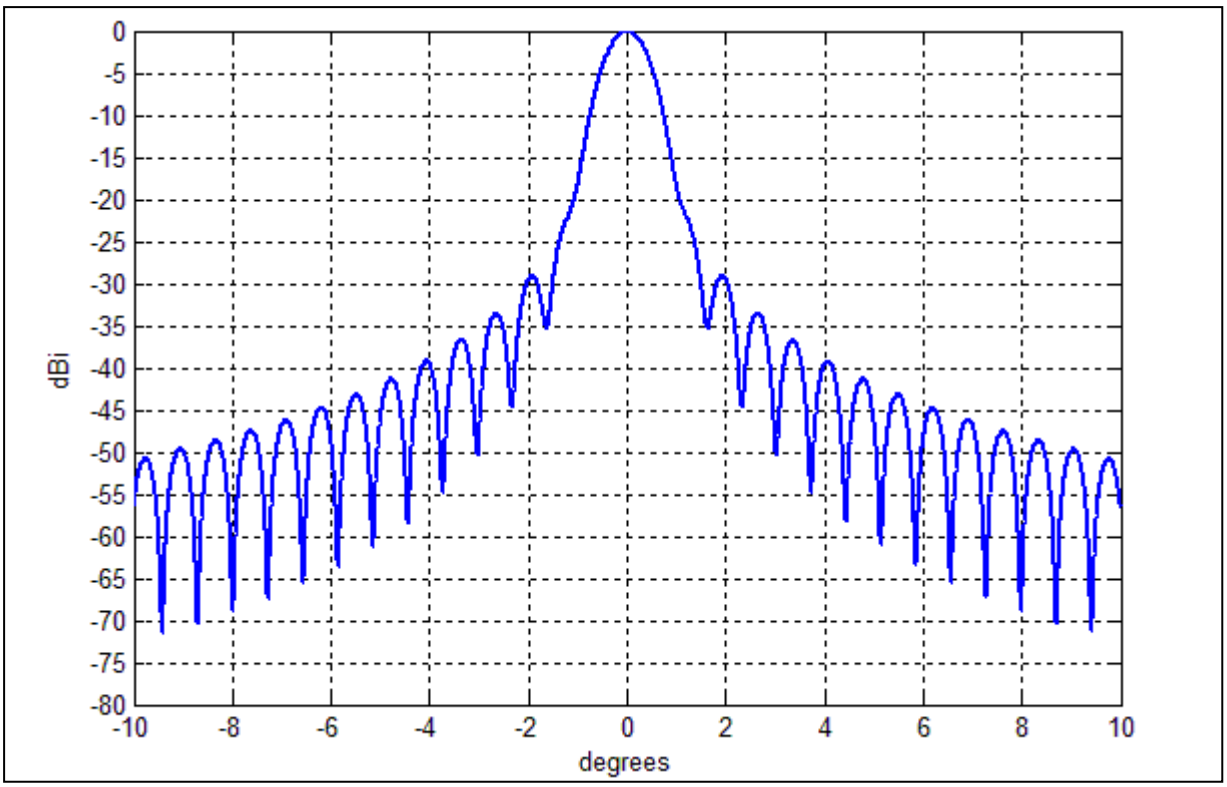

***Figure 5.33**. 2.7 GHz reflector radiated far field.*

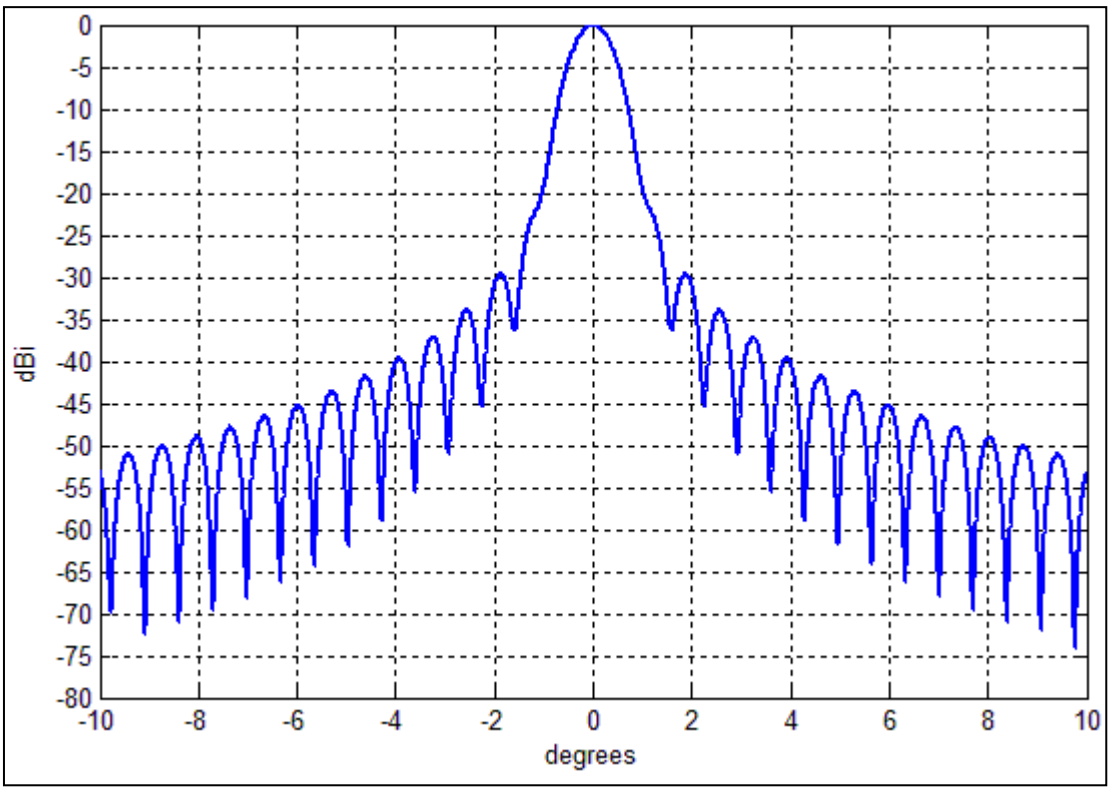

Figure 5.34. *2.8 GHz reflector radiated far field.*

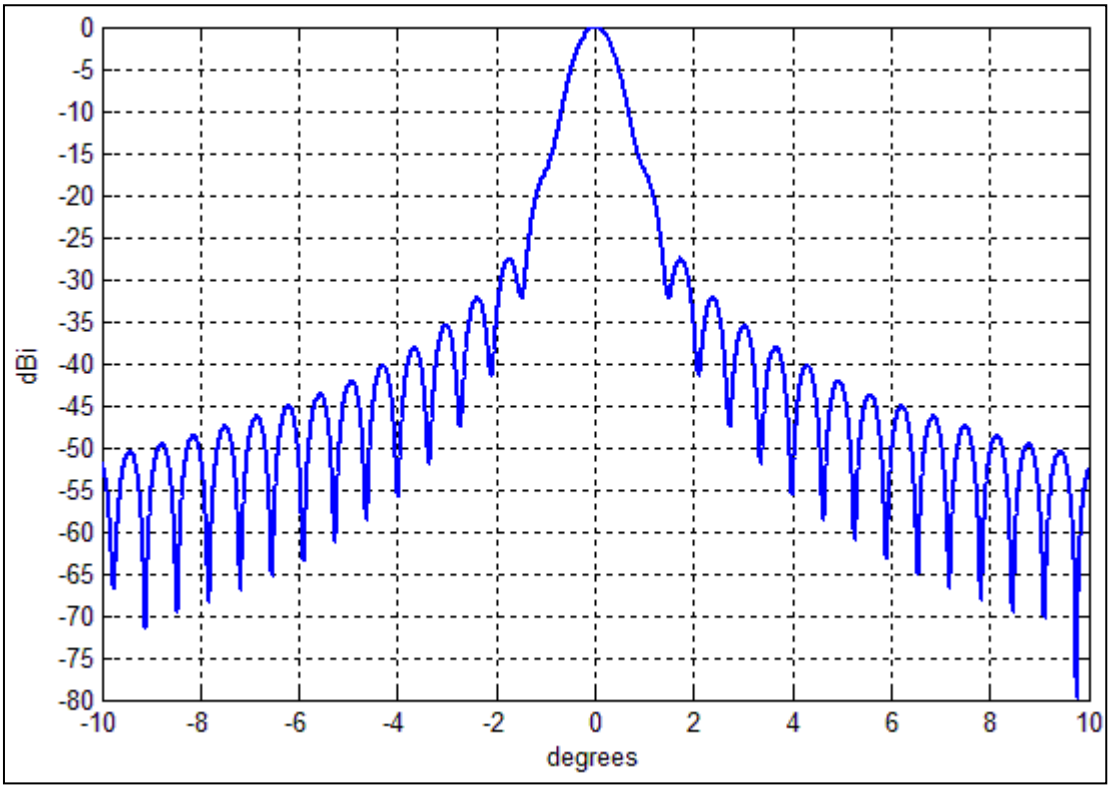

Figure 5.35. *3.0 GHz reflector radiated far field.*

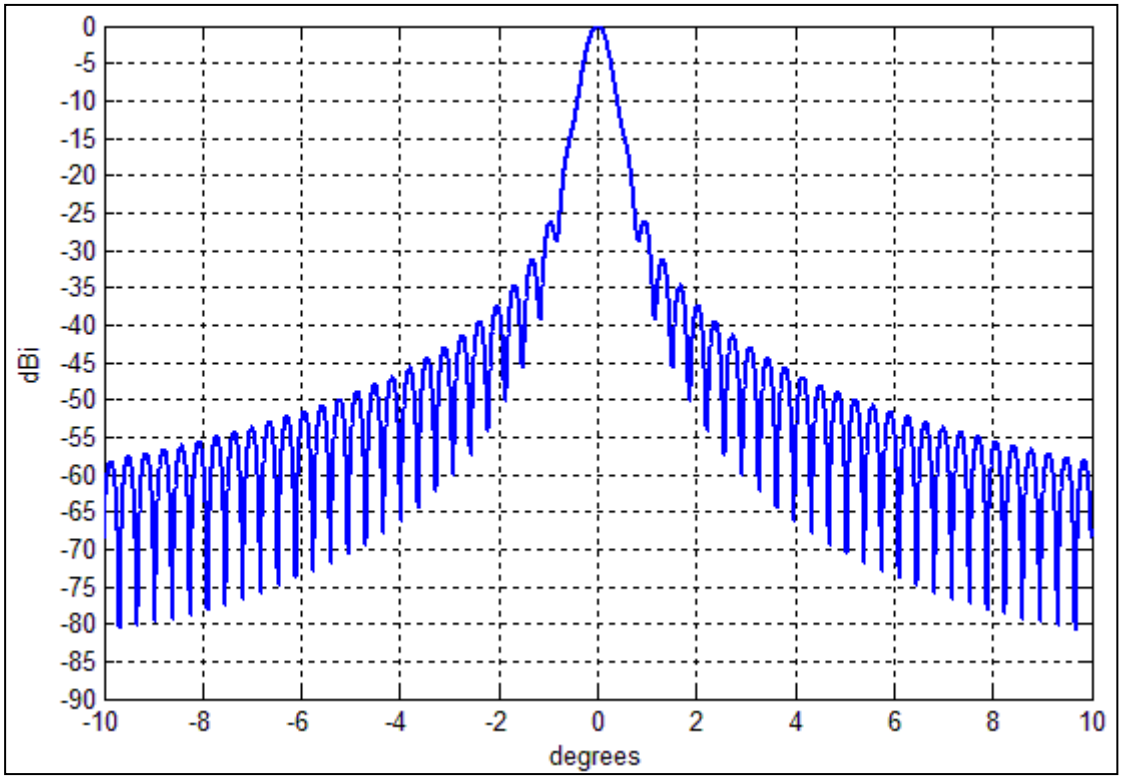

Figure 5.36*. 5.4 GHz reflector radiated far field.*

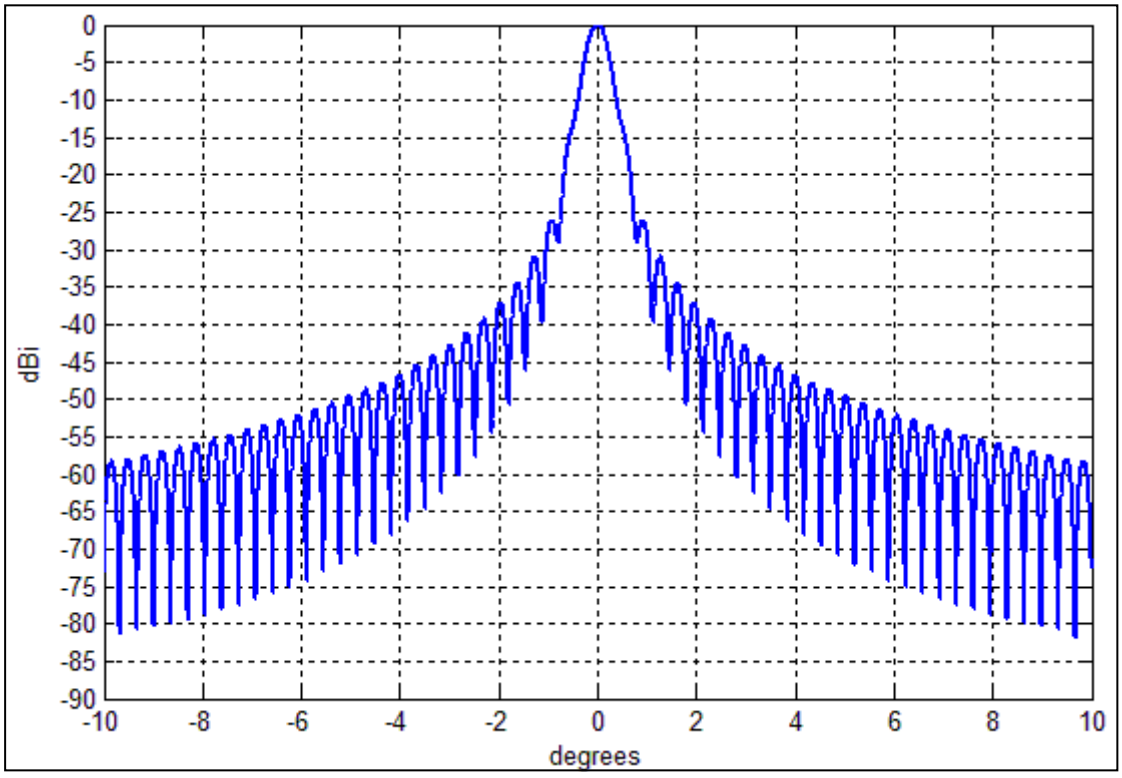

Figure 5.37. *5.6 GHz reflector radiated far field.*

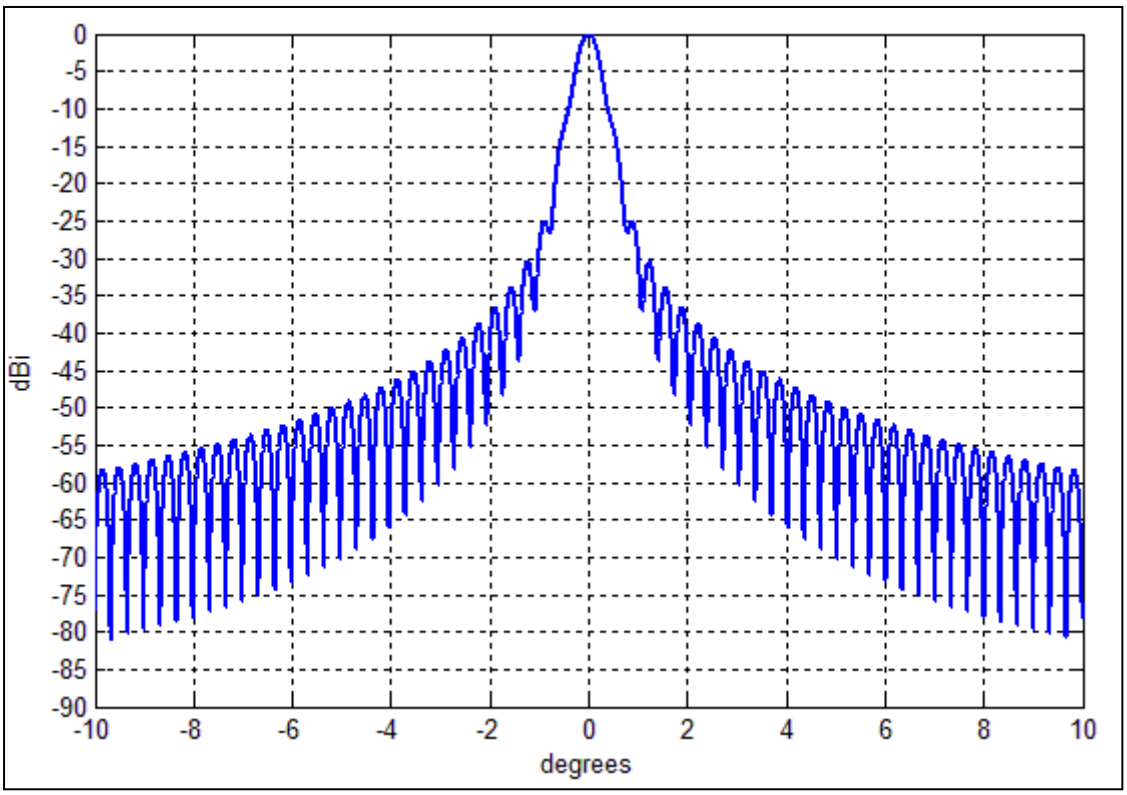

Figure 5.38. *5.8 GHz reflector radiated far field.*

Conclusions.

In this Phd thesis a study of new feeding techniques for the log-periodic printed feeds has been presented. The first proposed technique has been applied to a printed LPDA operating over the C, X and Ku band and has been analyzed using CST MICROWAVE STUDIO 2012: the antenna is fed using two coaxial cables, which provide the required broadband input matching, stabilize the antenna phase center, and improve the far field pattern when compared with an antenna fed with a single coaxial cable. The second proposed technique, based on a coplanar feeding waveguide, is able to avoid manufacturing problems due to the soldering, typical of the coaxial cable configuration, allows to obtain a simple realization, with low cost and compact size, and is easy to connect with the external SMA connectors.

Finally, a “V-Shaped” S-C band printed log-periodic feed has been designed. In the 2.7-3.0 GHz and 5.4-5.8 GHz frequency bands, the developed feed provides a S_{11} < -10 dB and a symmetric radiation pattern both in E-plane and H-plane, with a gain greater than 10.5 dBi over the whole operating bandwidth. This feed may be recommended for usage in weather radar systems having a transmitting power less than 400 KW, allowing a discrete operational range.

References.

[1] C.A. Balanis, “Antenna Theory, Analysis and design”, John Wiley & Sons, 1997
[2] R. E. Collin, “Antennas and Radiowave Propagation”, Mc Graw Hill, 1985.
[3] M. I. Skolnik, “RADAR Handbook”, Mc Graw Hill, 1990.
[4] Naval Education and Training – Program Development Center, “Shipboard Electronics Material Officer”, Department of the Navy – USA 1982.
[5] www.radartutorial.eu
[6] L.J. Battan, “Radar Observation on the atmosphere”, University of Chicago Press, 1973.
[7] J.R. Probert Jones, “The Radar Equation in Meteorology”, Q. J. R. Meterological Society, vol. 88, pp. 485-495, 1962.
[8] T. Ulaby, R. K. Moore, A. K. Fung, “Microwave Remote Sensing, Active and Passive”, vol. 2, Artech House, 1986.
[9] J. M. Rathod and Y. P. Kosta, "Low cost design & development of conical horn feed for parabolic reflector antenna," in Recent Advances in Microwave Theory and Applications, 2008. MICROWAVE 2008.International Conference on, 2008, pp. 775-777.
[10] B. Shahnaz, et al., "Analysis of Low Side Lobe Reflector Antenna," in Multitopic Conference, 2006. INMIC '06. IEEE, 2006, pp. 383-388.
[11] A. A. Kishk and L. Shafai, "Small reflector antenna with low sidelobes," Antennas and Propagation, IEEE Transactions on, vol. 51, pp. 2907-2912, 2003.
[12] S. B. Sharma, et al., "Cross-Polarization Cancellation in an Offset Parabolic Reflector Antenna Using a Corrugated Matched Feed,"Antennas and Wireless Propagation Letters, IEEE, vol. 8, pp. 861-864,2009.
[13] Z. A. Pour and L. Shafai, "A Simplified Feed Model for Investigating the Cross Polarization Reduction in Circular- and Elliptical-Rim Offset Reflector Antennas," Antennas and Propagation, IEEE Transactions on, vol. 60, pp. 1261-1268, 2012.
[14] L.Shafai, S.K.Sharma, S.Rao:"Handbook of Reflector Antennas and Feed Systems", Vol.II, Artech House, 2013.
[15] R. C. Johnson, H. Jasik, " Antenna Engineering Handbook", McGraw-Hill,1993.
[16] T. A. Milligan, "Modern Antenna Design", John Wiley & sons, 2005.
[17] W.L. Stutzmann, "Antenna Theory and design", John Wiley & sons, 1981.
[18] S.Yang, S.Lee, A.E.Fathy:"Patch Antennas: an Alternative Feed to Reflectors", Antennas and Propagation Society Internationa Symposium, 3-8 July 2005.
[19] R.Gardelli, G.La Cono, M.Albani: "A Low-Cost Suspended Patch Antenna for WLAN Access Point and Point-to-Point Links", IEEE Antennas and Wireless Propagation Letters, Vol 3, pp. 90-93, 2004.

[20] J.Huang, Y. Rahmat-Samii: "Fan Beam Generated by a Linear-Array Fed Parabolic Reflector", IEEE Transactions on Antennas Propagation, vol 38, No.7, July 1990.
[21] C.Schulz, C.Baer, T.Musch, I Rolfes:"A broadband stacked patch antenna with enhanced antenna gain by an optimized ellipsoidal reflector for X-band applications," Proceedings of 2011 IEEE International Conference on Microwaves, Communications, Antennas and Electronics Systems (COMCAS), pp. 1-7.
[22] K.S.Kona, K.Bahadori, Y.Rahmat-Samii:"Stacked Microstrip-Patch Arrays as Alternative Feed for Spaceborne Reflector Antennas", IEEE Antennas and Propagation Magazine, Vol.49, No.6, December 2007.
[23] T.L.Chen, H.S.Wu: "Dual-Polarized Planar Reflector Feed for Direct Broadcast Satellite Systems", IEEE Antennas and Wireless Propagation Letters, vol.9, 2010.
[24] S.M.Ali, M.A.Zakariya, Z.Baharudin, M.H.M.Khir, A.A.Baba: "Recent Advances in Microwave Reflector Antenna Technology", 2012 IEEE Asia-Pacific Conference on Applied Electromagnetics (APACE 2012), December 11 - 13, 2012, Melaka, Malaysia.
[25] Chao, Y., Y. Chen, H. Wei, Q. K. Zhen, and Q. Wei, "Band-notched UWB printed log-periodic dipole antenna fed by half mode substrate integrated waveguide," International Symposium on Antennas and Propagation, Bangkok, Thailand, 2009.
[26] R.H. Duhamel, F.R. Ore, "Log Periodic Feed for Lens and Reflectors", IRE International Convention Record, vol.7, pp.128-137, 21-25 March, 1966.
[27] F.F. Dubrovka, D.Dolzhenko,"An UltraWideband 1-20 GHz Modified Log-Periodic Feed", Proceedings of Ultrawideband and Ultrashort Impulse Signals, 6-10 September, 2010, Sevastopol, Ukraine pp. 230-232.
[28] F. F. Dubrovka, M.M. Lytvyn, S.M.Lytvyn, P.Y. Stephanenko, V.M.Tereshenko, V.I.Huz, V.P.Lipatov, M.I.Andrushenko, H.O. Yena,"A novel ultra-wideband offset-fed reflector antenna system with main lobe selection," Proceedings of Ultrawideband and Ultrashort Impulse Signals, 2004 Second International Workshop, 2004,pp. 67-70.
[29] Jian Yang, Miroslav Pantaleev, Per-Simon Kildal, Benjamin Klein,Yogesh Karandikar, Leif Helldner, Niklas Wadefalk, Christopher Beaudoin,"Cryogenic 2–13 GHz Eleven Feed for Reflector Antennas in Future Wideband Radio Telescopes", IEEE Transaction on Antennas and Propagation, VOL. 59, NO. 6,pp. 1918-1933, June 2011.
[30] L.Shi, H. Sun, X. Lu, "A Study of Log Periodic Feeds Multiple-BeamAntenna: Offset Parabolic Reflector Antenna", Proceedings of Global Symposium on Millimeters Waves, pp.303-305, 21-24 April 2008, Nanjing.
[31] R. Olsson, P. Kildal, S. Weinreb, "A novel low-profile log-periodic ultra wideband feed for the dual-reflector antenna of US-SKA," in Antennas and Propagation Society International Symposium, 2004. IEEE, 2004, pp. 3035-3038.Vol.3.
[32] R. H. DuHamel and D. E. Isbell, “Broadband logarithmically periodic antenna structures,” in IRE Nat. Conv. Rec., 1957, pp. 119–128, part I.

[33] R. Carrel, “The design of log-periodic dipole antennas,” in IRE Int.Conv. Rec., Mar. 1961, vol. 9, pp. 61–75.
[34] D. E. Isbell, “Log periodic dipole arrays,” IRE Trans. Antennas Propag., vol. AP-8, no. 3, pp. 260–267, May 1960.
[35] R. Carrel, “Analysis and design of the log-periodic dipole antenna”, Ph.D. dissertation, University of Illinois, Urbana, IL, USA, 1961.
[36] R. C. Johnson and H. Jasik, Antenna Engineering Handbook—Second Edition. New York, NY, USA: McGraw-Hill, 1984.
[37] H. Zhou, N. A. Sutton, and D. S. Filipovic, “Surface micromachined millimeter-wave log-periodic dipole array antennas,” IEEE Trans. Antennas Propag., vol. 60, no. 10, pp. 4573–4581, Oct. 2012.
[38] H. A. Wheeler, “Transmission-line properties of parallel strips separatedby a dielectric sheet,” IEEE Trans. Microw. Theory Tech., vol. MTT-13, no. 2, pp. 172–176, Feb. 1965.
[39] E. Avila Navarro, J. M. Blanes, J. A. Carrasco, C. Reig, and E. A.Navarro, “A new bi-faced log periodic printed antenna,” Microw. Opt. Technol. Lett., vol. 48, no. 2, pp. 402–405, Feb. 2006.
[40] R.R. Pantoja,A.R. Sapienza, and F. C.Medeiros Filho,, “A microwave printed planar log-periodic dipole array antenna,” IEEE Trans. Antennas Propag., vol. AP-35, no. 10, pp. 1176–1178, October 1987.
[41] E. A. Navarro, J. A. Carrasco, and C. Reig, “Dual printed antenna for Wi-Fi applications,” IEEE Antennas Wireless Propag. Lett., vol. 8, pp.596–598, 2009.
[42] D. Kim, Q. Chen, and K. Sawaya, “Microstrip log-periodic dipole antenna array,” in Proc. ISAP, Fukuoka, Japan, 2000, pp. 1–4.
[43] A. A. Gheethan and D. E. Anagnostou, “The design of reconfigurable planar log-periodic dipole array using switching elements,” in Proc. IEEE Antennas Propag. Soc. Int. Symp., June 2009, pp. 1–4.
[44] Feng, C. and Q. Jian, "A novel infinite balun used in folded dipole", IEEE Antennas and Propagation Society International Symposium, Vol. 1, 547-548, 1990.
[45] D. E. Anagnostou, J. Papapolymerou, M. M. Tentzeris, and C. G. Christodoulou, “A printed log-periodic Koch-dipole Array (LPKDA)”, IEEE Antennas Propag. Lett., vol. 7, pp. 456–460, 2008.
[46] G. A. Casula, P. Maxia, G. Mazzarella, G. Montisci, “Design of a Printed Log-Periodic Dipole Array for Ultra-Wideband Applications”, Prog. Electromagn. Res. C, vol 38, pp. 15-26, 2013.
[47] G.A. Casula, P. Maxia, G. Montisci, G. Mazzarella, F. Gaudiomonte, “A Printed LPDA Fed by a Coplanar Waveguide for Broadband Applications”, IEEE Antennas Wireless Propag. Lett., vol. 12, pp.1232–1235, 2013.
[48] Pozar, D. M., Microstrip Antennas: The Analysis and Design of Microstrip Antennas and Arrays, IEEE Press, New York, USA, 1995.
[49] Mazzarella, G., "CAD modeling of interdigitated structures", IEEE Transactions on Education, Vol. 42, No. 1, 81-87, 1999.

[50] Gheethan, A. A. and D. E. Anagnostou, "Reduced size planar log-periodic dipole arrays using rectangular meander line elements", IEEE Antennas and Propagation Society InternationalSymposium, 1-4, 2008.
[51] S. J. Orphanidis, "Electromagnetic Waves and Antennas", www.ece.rutgers.edu/~orfanidi/ewr2008.
[52] G. A. Casula, P. Maxia, G. Montisci, "Design of a printed wide band log-periodic antenna dipole array with a new feeding technique", in Proc. 6th EuCAP, Prague, Czech Republic, Mar. 2012, pp 1882-1884.
[53] S. Y. Chen, P. H. Wang, and P. Hsu, "Uniplanar log-periodic slot antenna fed by a CPW for UWB applications," IEEE Antennas Wireless Propag. Lett., vol. 5, pp. 256–259, 2006.
[54] S. H. Kim, J. H. Choi, J. W. Baik, and Y. S. Kim, "CPW-fed log periodic dumb-bell slot antenna array," Electron. Lett., vol. 42, no. 8, pp. 436–438, Apr. 2006.
[55] G. Montisci and G. Mazzarella, "An alternative layout for CPW-fed printed antennas with low back radiation,"Microw. Opt. Technol. Lett., vol. 36, no. 6, pp. 481–483, Mar. 2003.
[56] B. C. Wadell, Transmission Line Desing Handbook. Norwood, MA, USA: Artech House, 1991.
[57] C. K. Campbell, I. Traboulay, M. S. Suthers, and H. Kneve, "Design of a stripline log-periodic dipole antenna," IEEE Trans. Antennas Propag., vol. AP-25, no. 5, pp. 718–721, Sep. 1977.
[58] V. N. Bringi, V. Chandasekar, "Polarimetric Doppler Weather Radar", Cambridge University Press, 2001.
[59] Taconic TSM-DS3 datasheet, http://www.taconic-add.com/pdf/tsm-ds.pdf.
[60] Selex System Integration, METEOR 1600S Weather Radar datasheet, http://www.gematronik.com/fileadmin/media/pdf/ProductDatasheet/METEOR_1600S_engl_1907154812.pdf
[61] Selex System Integration, METEOR 1700C Weather Radar datasheet, http://www.gematronik.com/fileadmin/media/pdf/product-Information/Datenblatt.1700C.13.engl.pdf.
[62] A. Mulyanto, R. J. Vernon,"A V-Shaped Log-Periodic Printed-Circuit Antenna Array for the 1-10 GHz Frequency Range" Antennas and Propagation Society Simposium, June 1979.
[63] R. Justice, "Catenary Supported Log Periodic Antenna", US Patent 3271774 A, Sept. 6, 1966.
[64] Micro-coax, "Semi Rigid Coaxial Cable" datasheet, pag.10.
[65] G.A. Casula, P. Maxia, G. Mazzarella, "A Printed LPDA with UWB Capability", International Workshop on Antenna Technology (IWAT), March 2010, Lisbon.
[66] www.radartutorial.eu: "Book1-Radar Basis".
[67] S. Raghavan, "Radar Meteorology", Kluver Academic Publishers, 2003.

List of figures.

List of tables.

List of publications related to the thesis.

Journal articles.

G. Andrea Casula, Paolo Maxia, Giuseppe Mazzarella, Giorgio Montisci, "Design of a Printed Log-Periodic Dipole Array for Ultra-Wideband Applications", Prog. Electromagn. Res. C, vol 38, pp. 15-26, 2013.

G. Andrea Casula, Paolo Maxia, Giorgio Montisci, Giuseppe Mazzarella, Francesco Gaudiomonte, "A Printed LPDA Fed by a Coplanar Waveguide for Broadband Applications", IEEE Antennas Wireless Propag. Lett., vol. 12, pp.1232–1235, 2013.

Proceedings of international conferences.

G. Andrea Casula, Paolo Maxia, Giorgio Montisci, "Design of a printed wide band log-periodic antenna dipole array with a new feeding technique", in Proc. 6th EuCAP, Prague, Czech Republic, Mar. 2012, pp 1882-1884.

G.Andrea Casula, Paolo Maxia, Giuseppe Mazzarella, "A Printed LPDA with UWB Capability", International Workshop on Antenna Technology (IWAT), March 2010, Lisbon.